Design and commissioning of a Laser Doppler Velocimetry seeding system for non-ideal fluid flows

S I M O N E   G A L L A R I N I

816805

POLITECNICO

MILANO 1863

SIMONE GALLARINI
816805

SUPERVISOR:
Prof. Andrea Spinelli
ASSISTANT SUPERVISORS:
Prof. Fabio Cozzi and Prof. Alberto Guardone

Politecnico di Milano
Dipartimento di Energia
via Lambruschini 4 – 20156 Milano

Laurea Magistrale in Ingegneria Energetica – Anno accademico 2014/2015
April 2016

Dedicated to all the passionate people.

ABSTRACT

The design, the construction and the commissioning of a seeding system for Laser Doppler Velocimetry operating in non-ideal conditions, namely in the close proximity of the liquid-vapor saturation curve and critical point, is presented. The system is implemented in the Test Rig for Organic VApors (TROVA), a facility built at the CREALab (Politecnico di Milano) with the aim of characterizing non-ideal gas flows representative of those occurring in Organic Rankine Cycle turbine passages. The tested fluid is the siloxane MDM (Octamethyl-trisiloxane – $C_8H_{24}O_2Si_3$), a silicon oil of particular interest for high temperature ORC applications.

Depending on the test operating conditions, the fluid under scrutiny expands in a convergent-divergent nozzle from total pressure and total temperature ranging from $4\,bar$ to $25\,bar$ and from $253.2\,°C$ to $310.3\,°C$ respectively, therefore the seeding has to be injected in a high temperature and high pressure environment, without altering the thermo-fluid dynamic behavior of the fluid. A suspension of the tracer particles (titanium dioxide, TiO_2 or silicon dioxide, SiO_2) in the working fluid is atomized into the flow, within a plenum ahead of the nozzle inlet. Since the surrounding fluid is in superheated vapor (or supercritical) conditions, the spray then evaporates leaving the solid particles free to follow the flow. The designed system consists of a tank, pressurized with nitrogen and containing the MDM–seeding suspension, of a jet mixing system, to maintain the suspension stirred, and of a drawing line ending with the atomizing nozzle. During normal operation, the tank is pressurized at a pressure higher than the plenum one and the fluid flows naturally through the atomizer.

The system has been commissioned and validated through the verification of its operation. The presented work is the initial part of an optimization process, and the implemented tests show the developments that have to be carried out to perform a reliable LDV measurement. The system is suitable for all cases where optical measurements (LDV, PIV, etc.) have to be applied in high temperature, high pressure conditions similar to those occurring in the TROVA and whenever the use of auxiliary fluids different from the working one is not feasible. The reported test proves the suitability of the system in properly seeding the flow.

SOMMARIO

Negli ultimi anni, l'interesse nella gasdinamica non ideale è cresciuto, grazie al grande numero di applicazioni industriali in cui tali correnti si possono incontrare. Nei codici CFD sono presenti modelli termodinamici per la previsione delle proprietà dei fluidi non ideali e il loro utilizzo risulta abbastanza consolidato. Tuttavia, in letteratura non sono ancora presenti risultati sperimentali in grado di validare i suddetti modelli per fluidi non ideali.

Tra le applicazioni principali in cui si possono incontrare correnti non ideali vi sono gli ORC, Organic Rankine Cycles, la cui popolarità è molto cresciuta negli ultimi anni, per applicazioni a bassa e media temperatura e potenza. I fluidi comunemente utilizzati in applicazioni ORC sono fluidi ad alta complessità e massa molecolare, quindi i flussi nei turboespansori sono, normalmente, fortemente supersonici e le non idealità non sono trascurabili.

Per sopperire alla mancanza di dati sperimentali riguardanti il comportamento termo-fluidodinamico dei flussi non ideali, al CREALab del Politecnico di Milano, è stato costruito un impianto di prova chiamato Test Rig for Organic VApors (TROVA). Per caratterizzare completamente il flusso, sono necessarie delle misure indipendenti di temperatura, velocità e pressione. La misura di velocità deve essere necessariamente una misura diretta, data l'assenza di gallerie di calibrazione per sonde di pressione per flussi non ideali. Per realizzare misure dirette di velocità, è stata scelta la tecnica LDV, in quanto permette di effettuare una misura senza bisogno di calibrazione, puntuale e non intrusiva. Il fluido testato nel TROVA è il silossano MDM (Ottametiltrisilossano – $C_8H_{24}O_2Si_3$), un fluido tra i più diffusi per applicazioni ORC ad alta temperatura. L'impianto è una galleria del vento blow down, basata su un ciclo ORC (si veda la Figura 1), dove la turbina è sostituita da un ugello convergente-divergente.

Seguendo il ciclo termodinamico, il fluido viene scaldato, e quindi pressurizzato, in un volume chiuso da opportune valvole, fino a condizioni surriscaldate o supercritiche ($2 \rightarrow 4$). All'avvio della prova, il vapore viene fatto fluire dal serbatoio in un plenum, attraverso una valvola che ne regola la pressione ($4 \rightarrow 6$). Il valore di pressione assunto dal fluido nel plenum corrisponde alla pressione totale a ingresso ugello. Dato che la corrente nell'asse dell'ugello si può considerare isentropica, tale pressione corrisponde alla pressione totale dell'ugello, almeno finchè l'ugello opera in regime adattato o sottoespanso. Nel plenum, vengono dunque misurate la pressione e la temperatura totali dell'ugello. A valle del plenum, il flusso espande nell'ugello ($6 \rightarrow 7$), dove vengono misurate le pressioni statiche in corrispon-
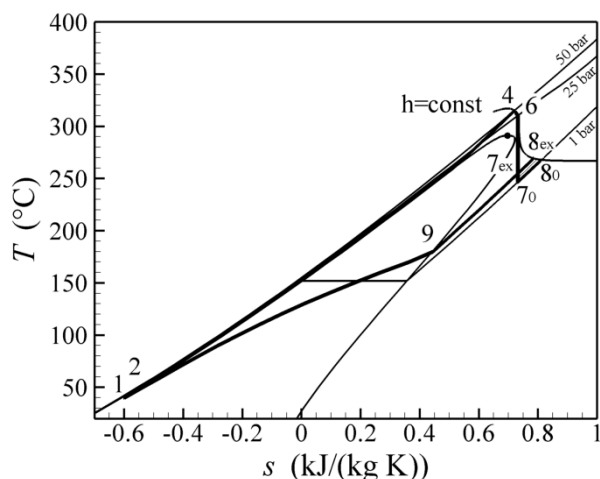
Figura 1: Ciclo termodinamico implementato nel TROVA.

Tabella 1: Condizioni operative per i primi test sul TROVA, dove p_{Tn} e T_{Tn} sono la pressione e temperatura totali dell'ugello, e Z_{Tn} è il fattore di comprimibilità del fluido.

Test	p_{Tn} [bar]	T_{Tn} [°C]	Z_{Tn}
MDM_1	25	310.3	0.31
MDM_2	10	276.9	0.62
MDM_{1st}	4	253.15	0.86

denza dell'asse. La sezione di prova possiede un accesso ottico che permette la misura della velocità con tecnica LDV e la visualizzazione delle strutture di flusso a elevato gradiente di densità mediante tecnica Schlieren. Il fluido viene poi scaricato in un serbatoio di bassa pressione dove viene condensato ($7_0 \rightarrow 1$). Il circuito è completato da un pompa dosatrice che pressurizza il fluido dal serbatoio di bassa pressione al serbatoio di alta pressione ($1 \rightarrow 2$). I test per cui il TROVA è stato progettato sono rappresentativi delle condizioni operative delle attuali e probabilmente future turbine ORC (si veda la Tabella 1).

L'inseminazione del flusso all'interno del TROVA non è banale: il flusso deve essere inseminato ad alta temperatura (tra 253.2 °C e 310.3 °C) e alta pressione (tra 4 bar e 25 bar). Tra le varie possibilità d'inseminazione, gocce liquide non possono essere utilizzate, dato che esse tendono ad evaporare e a contaminare il fluido che si intende testare. Inoltre, a causa della variazione di pressione durante l'espansione, la dimensione delle gocce varierebbe considerevolmente. Sul fronte dei sistemi di inseminazione con particelle solide, il ciclone, il letto fluidizzato e l'inseminatore a spazzola rotante non possono essere utilizzati, a causa delle complicazioni derivanti dalla necessità di

utilizzare vapori ad alta temperatura e pressione. Per questi motivi, è stato necessario progettare un sistema di inseminazione innovativo, basato sull'atomizzazione di una sospensione di MDM e particelle traccianti.

Le particelle inseminanti devono possedere un indice di rifrazione n sufficientemente diverso da quello del fluido in cui sono immerse, una densità ρ_p e un diametro d_p adeguati a tracciare la corrente.

Il rapporto $\zeta = \rho_p/\rho_f$ (dove ρ_f è la densità del fluido) gioca un ruolo importante nella dinamica della particella. Per $\zeta = 1$, l'energia viene trasferita adeguatamente dal flusso alla particella, lungo tutto il range di numero di Stokes $St = \tau_p/T_{flow}$, dove τ_p è il tempo caratteristico della particella e T_{flow} è il tempo caratteristico del flusso. La dimensione ottimale della particella è un compromesso tra la necessità di un piccolo diametro, per seguire adeguatamente il flusso, e un diametro grande, per avere uno scattering maggiore.

Nel TROVA, non vi è il bisogno di risolvere completamente le fluttuazioni turbolente, ma è sufficiente tracciare il flusso medio sull'asse. Questo rilassa notevolmente i vincoli sul diametro e la densità della particella da utilizzare.

Risolvendo l'equazione del moto della particella immersa nel flusso che deve tracciare, con l'ausilio di dati provenienti da simulazioni CFD delle prove programmate per il TROVA (Tabella 1) si trova che, per materiali traccianti di uso comune (TiO_2 e SiO_2), le particelle devono avere un diametro d_p minore o uguale a $0.5\,\mu m$, per poter seguire adeguatamente il flusso.

Rispettando questi vincoli, sono state selezionate due diverse polveri traccianti: il biossido di titanio e l'Aerosil 200, a base di biossido di silicio. Sono entrambi ossidi metallici, quindi hanno densità molto maggiori rispetto a quelle del vapore da tracciare. Il diametro delle particelle è di $200\,nm$ per il TiO_2 e di $125\,nm$ per l'Aerosil 200.

La prima parte del progetto del sistema riguarda la determinazione delle proprietà principali del sistema d'inseminazione, che sono la portata di particelle da iniettare e il volume totale di sospensione da iniettare. La portata di particelle da iniettare dipende dalla concentrazione media di particelle che si deve avere nella corrente. La concentrazione di particelle dipende caratteristiche dell'ottica del sistema LDV (in particolare dalla dimensione del volume di misura) e viene determinata in modo che la probabilità di realizzazioni multiple (ossia di avere più di una particella contemporaneamente nel volume di misura) sia minore dello 0.5%. Nota la concentrazione media di particelle e la portata volumetrica del flusso da inseminare, si possono calcolare la portata e il volume totale da iniettare durante una prova, che dipendono dalla concentrazione massica delle particelle nella sospensione di MDM e particelle traccianti. Con una concentrazione di particelle in sospensione compresa tra 5×10^{-5} e 10^{-7}, risultano portate volumetriche da iniettare dell'ordine di $50\,ml/min$ e $300\,ml/min$
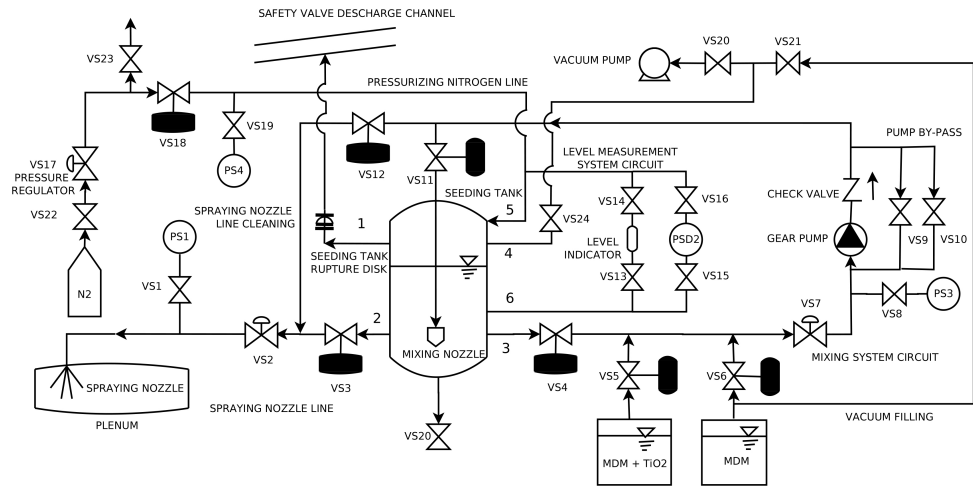
Figura 2: Schema del sistema d'inseminazione progettato.

e volumi totali per prova da iniettare da 50 a 300 ml.

Seguendo i vincoli citati, è stato progettato un sistema composto da un serbatoio per la sospensione di MDM e inseminante, da un sistema di pressurizzazione, da uno di misurazione del livello, uno di miscelamento e un atomizzatore (Figura 2). Il serbatoio è riempito parzialmente dalla sospensione e ha un volume di circa 3 l. Il serbatoio è pressurizzato attraverso il sistema di pressurizzazione, che utilizza azoto gassoso. Durante un test, il serbatoio è pressurizzato ad una pressione maggiore di quella del punto di iniezione, all'interno del plenum antecedente l'ugello di prova. Quando la valvola VS3 viene aperta, la sospensione fluisce naturalmente attraverso l'ugello atomizzatore. La portata atomizzata dipende dalla differenza di pressione Δp sull'atomizzatore, che è regolata finemente dalla valvola a spillo VS2 e controllata dal misuratore di pressione PS1. L'atomizzatore sfrutta l'instabilità di Rayleigh e dato che non vengono utilizzati fluidi ausiliari, il fluido da testare non viene contaminato. Il sistema di pressurizzazione è composto da una bombola di azoto a 220 bar con un regolatore di pressione e il misuratore di pressione PS4. Le particelle in sospensione tendono a sedimentare, quindi un sistema di miscelazione preleva la sospensione dal serbatoio e la ricircola attraverso la pompa e l'ugello di miscelazione. Il sistema di misura del livello è composto da un indicatore di livello visivo e da un misuratore differenziale di pressione. Il sistema è protetto dalle sovrapressioni con un disco di rottura dimensionato per una pressione massima di 50 bar. Il sistema può funzionare sia in condizioni subcritiche che supercritiche, quindi il dimensionamento di una valvola di sicurezza sarebbe stato molto incerto, data l'ampia variazione delle possibili condizioni termodinamiche del fluido alle condizioni di apertura. Per questo motivo, è stato selezionato un disco di rottura.

Il sistema è stato costruito e testato. Un importante aspetto è legato all'atomizzatore: i dati resi disponibili dal costruttore sono relativi al suo funzionamento con acqua. Una misura sperimentale della curva caratteristica dell'ugello è quindi necessaria. Per ottenerla è sufficiente imporre il salto di pressione a cavallo dell'ugello, misurare la portata atomizzata e interpolare i dati con una legge del tipo $\Delta p = K \dot{V}^{\alpha}$.

La capacità del sistema di eseguire le operazioni per cui è stato progettato è stata testata. Sono state eseguite molte prove sul TROVA, per verificare la capacità di inseminazione corretta del flusso. Le prove hanno portato alla conclusione che l'evaporazione dello spray avviene correttamente prima della sezione di prova e che il sistema è in grado di inseminare la corrente, anche se la scelta dell'inseminante e la configurazione dell'atomizzatore possono essere migliorate.

Il presente lavoro è la parte iniziale del processo di ottimizzazione del sistema e i test effettuati, anche se non hanno prodotto una misura di velocità affidabile, hanno fornito indicazioni preziose riguardo alle modifiche da effettuare al sistema per raggiungere l'obiettivo per cui è stato progettato, quali l'adozione di un diverso atomizzatore (o una diversa configurazione dello stesso), l'adozione di particelle inseminanti di dimensioni maggiori e la sostituzione della pompa di miscelamento. Il sistema realizzato costituisce, dunque, l'impianto di base per l'inseminazione della corrente all'interno del TROVA; le modifiche richieste per il suo affinamento (precisate nell'ambito del presente lavoro) sono infatti relativamente limitate. La loro implementazione costituisce il prosieguo a breve termine del presente lavoro, insieme alla realizzazione di misure di velocità affidabili.

PUBLICATIONS

Some ideas and figures have appeared previously in the following publications:

1. Gallarini S., Spinelli A., Cozzi F. and Guardone A., Design and Commissioning of a Laser Doppler Velocimetry Seeding System for Non-ideal Fluid Flows, *12th International Conference on Heat Transfer, Fluid Mechanics and Thermodynamics*, 2016.

Acqua perenne, ottima e pessima, ora
morte ora vita, acqua, diventa luce!
acqua, diventa fiamma! acqua, lavora!

— Giovanni Pascoli

Learn from yesterday,
live for today,
hope for tomorrow.
The important thing
is not to stop questioning.

— Albert Einstein

ACKNOWLEDGEMENTS

CONTENTS

LIST OF TABLES

INTRODUCTION

1.1 CONTEXT

The interest in non-ideal fluid dynamics has grown in recent years, due to the variety of fields where such flows are encountered, such as transonic and hypersonic wind tunnels operating in the dense gas regime, transportation of high-pressure fuels and chemicals, pharmaceutical applications and Organic Rankine Cycle turbines. In these applications, the fluid crosses the so called *dense gas region*, near the saturation curve in the vicinity of the critical point, resulting in strongly non-ideal flows. Thermodynamic models for non ideal fluids are currently embedded in simulation codes and their use is relatively straightforward. However, experimental results validating non-ideal thermodynamic models are still lacking in literature.

Among the aforementioned industrial applications, Organic Rankine Cycles (ORC) gained a relevant role in power production from low to medium temperature sources and for low to medium power applications, especially when a high reliability is required. The turbine efficiency plays an important role in the plant thermodynamic efficiency, but it is now limited to values of about $80 - 85\%$ for machines of the MW scale [19], since the turbine expansion occurs mainly in the dense gas region (where the flow behavior is not accurately modeled by current design tools, which are not experimentally validated). The fluids usually employed in ORCs feature a high molecular complexity and high molecular weight, thus resulting in highly supersonic flows where real gas effects are not negligible.

In order to provide accurate measurements for the validation of non-ideal thermo-fluid dynamic models, a wind tunnel called Test Rig for Organic VApors (TROVA) has been constructed at CREALab (Politecnico di Milano) [24]. To fully characterize the thermo-fluid dynamics of the expanding flow, independent measurements of temperature, pressure and velocity are required. In particular, a direct velocity measurement is needed, due to the lack of non-ideal gas pressure probe calibration wind tunnels. To this purpose optical techniques are preferred and, in the considered application, Laser Doppler Velocimetry (LDV) was chosen. The tested fluid is the syloxane MDM (Octamethyltrisiloxane – $C_8H_{24}O_2Si_3$), a silicon oil of particular interest for high temperature ORC applications.

The TROVA has been commissioned and some preliminary tests with air and MDM as working fluid have been carried out (see [20],

[28] and [5]) by means of pressure and temperature measurements and Schlieren visualizations.

1.2 OBJECTIVES

The objective of this work is the design of a LDV seeding system to be applied to the TROVA facility, in order to perform velocity measurements in non-ideal supersonic flows. Therefore, the system has to be tested in its normal operating. A first velocity measurement in a MDM supersonic flow has to be performed and compared with theoretical results.

This work aims at setting the basis for direct velocity measurements and future analysis in non-ideal supersonic flows behavior.

1.3 STRUCTURE OF THIS WORK

The present work is divided in three main parts. The first part deals with topics considered fundamental for the understanding of the reasons of this work: a brief explanation of the main features of Organic Rankine Cycles and an overview of the topics related to the seeding particle properties and to the LDV measurement principles are given.

The second part treats the design of the seeding system: an overview of the TROVA facility is given firstly and the design and the system components selection is deeply discussed.

The third part deals with the commissioning and test of the seeding system: the test results are reported and commented. Finally, the conclusions of the whole work are summarized and future developments are suggested.

Within the two appendixes, is reported an overview of thermodynamic properties and models of the fluids under study.

Part I

FUNDAMENTALS

The first part of this work deals with topics that are of fundamental importance to understand the motivations of the research project and the design of the LDV seeding system, treated in Part ii. In Chapter 2 the features and peculiarities of ORCs are explained, to give a perspective of the direct industrial application for which the TROVA was conceived. In Chapter 3 the selection of the tracer is discussed, referring to particle dynamics and optical properties. Moreover, flow seeding techniques and the Laser Doppler Velocimetry measurement principle are reported.

ORGANIC RANKINE CYCLES

2.1 WHY ORGANIC RANKINE CYCLES?

In power production, there are many different systems that convert primary energy into electric or mechanical power. Depending on the specific application, they may be Rankine cycles, Joule-Bryton gas cycles, Otto and Diesel engines, Stirling engines and so on. When dealing with large scale electric power production, steam Rankine cycles are the most common, for their consolidated technology, relatively simple construction and low cost, low environmental impact, non toxicity and well known behavior of the working fluid. However, when designing a new plant, the fluid can also be considered a degree of freedom in the techno-economical optimization of the system. Thus, depending on the specific application, the fluid that better matches the heat source and sink, that leads to cheaper machinery and heat exchangers could be used. Organic Rankine Cycles (ORC) originate from this idea and came out since the first decades of the nineteenth century, but the first commercial applications became reality only in the sixties of the twentieth century.

Organic Rankine Cycles originate from the idea that also the working fluid is a degree of freedom in the cycle design.

2.2 FUNCTIONING AND FEATURES

2.2.1 *Thermodynamic cycle*

Organic Rankine Cycles are, conceptually, very simple: they are Rankine cycles that use an organic compound as working fluid. A common plant layout is the one depicted in Figure 3.

ORCs are Rankine cycles using organic compounds as working fluid

The fluid undergoes the following transformations:

$1 \rightarrow 2$ the fluid in the liquid state is compressed by a pump;

$2 \rightarrow 3$ the liquid is regenerated using the vapor exiting from the turbine;

$3 \rightarrow 4$ the fluid is heated by the hot source until saturated (or slightly superheated) vapor conditions are reached;

$4 \rightarrow 5$ the vapor is expanded in a turbine;

$5 \rightarrow 6$ the vapor releases heat for the liquid regeneration;

$6 \rightarrow 1$ the vapor is then condensed releasing thermal energy to the heat sink.

(a)

(b)

Figure 3: Layout of a typical regenerative cycle (Figure 3a) and the corresponding thermodynamic cycle on the $T-s$ plane (Figure 3b), for syloxane MDM [7].

2.2.2   *Main features*

Usually, organic fluids exhibit a positive slope of the saturation curve in the $T - s$ diagram (see Section A.5). There are two main benefits associated with this behavior:

- even if the fluid at the turbine inlet is a saturated vapor, it superheats during the expansion process, thus avoiding a two-phase flow in turbine cascades, that causes blade erosion and a drop in turbine efficiency and reliability;

- the regeneration is possible without vapor extraction from the turbine, with an increase in efficiency.

The expansion, with organic fluids, takes place with small inlet-outlet temperature differences (Section A.2). Therefore, for a fixed inlet temperature, a higher outlet temperature is reached, thus permitting a great amount of regeneration and increasing the mean temperature for heat introduction. Furthermore, these fluids exhibit low enthalpy of vaporization (Section A.3), thus a major part of heat introduction into the cycle is made at a variable temperature, leading to a better matching with variable temperature sources.

For these reasons saturated vapor cycles are very common. Supercritical cycles exist, but are very rare, due to their high pump consumption and heat exchangers cost.

On the other side, the high molecular weight and complexity of organic compounds could be a problem. The speed of sound is low and the flow within turbine channels is almost always supersonic. Shock waves at the nozzle blade exit are typically present, leading to strong inefficiencies, particularly at off-design conditions.

Normally, the plant size is a major parameter in comparing steam and organic cycles. As previously seen, ORCs are quite common for low to medium power applications, and this is due to different reasons:

- a steam turbine works with large enthalpy drop, so it has a big number of stages and the first and last one have very small and high blade height respectively. The high pressure turbine has low blade height and small diameter, that leads to a great impact on efficiency of the clearance between the blade and the casing, for very low powers. For a given expansion ratio, an ORC turbine has a smaller enthalpy drop across the expansion (see Section A.4), thus a smaller number of stages is required (usually two or three). Furthermore, usually, a higher volumetric flow rate $\dot{V}$ is elaborated, that leads to an increase in turbine mean diameter and blade height, thus reducing the blade/case clearance incidence on the efficiency. This permits to decrease the size without having disastrous effects on turbine efficiency;

ORC are usually saturated cycles, since the fluid properties permit a good efficiency without superheating of the vapor.

- with a decrease in plant size, the turbine rotational speed needs to be increased, in order to keep similarity and therefore good efficiency. This leads to the need of a reduction gear ($\omega_s = \omega\sqrt{V}/\Delta h^{3/4}$). On the other hand, as stated above, in ORCs Δh_{is} is low for a given expansion ratio, so, for a given load of a turbine stage ($\psi = \Delta h_{is}/(u^2/2) \approx const$), the turbine works with low peripheral velocities, without the need of a reduction gear and low mechanical stresses;

- a steam cycle has a sub-atmospheric condensation pressure, thus a degasser is needed to remove non-condensable gases possibly intaken. This component is really expensive, for a small plant. In ORC, a fluid that has a saturation pressure at the condensation temperature higher (or slightly below) than the atmospheric pressure can be selected, thus reducing sealing issues.

There is also a motivation for which organic fluid are not suitable for large power plants. In an energy conversion system, the major costs are heat exchangers and machines. In high power energy systems, the first is predominant, since its cost is proportional to the heat exchanged, but turbines take advantage of scale economies. In smaller plants the cost of the machines is preponderant, since the thermal power exchanged reduces proportionally. It can be proved that to reduce the heat exchanger cost (e. g. the $\dot{W}_{pump}/\dot{q}$ ratio, the pumping work on the exchanged thermal power, can be taken as an index) a small molecular mass is required.

ORCs, due to their low cost and high reliability, are widely applied in low to medium temperature and power applications, such as renewable energy power plants.

In conclusion, low to medium power applications ORC turbines, due to the above motivations, have a good efficiency, a small size and a good reliability, leading to a low cost. Normally ORCs are characterized by low maximum temperatures and pressures. Furthermore many organic compound are not aggressive nor corrosive thus leading to the possibility of using cheap materials.

ORCs are well suited for renewable energy applications, so, in the contemporary world dominated by a great attention on environment, green energy and efficiency, they gained an important role. ORC showed their energy efficiency and low cost attractiveness in small to medium power-low to medium temperature applications (below $400\,°C$ and $15\,MW$) and for combined heat and power plants, in particular for renewable energy applications, such as geothermal, biomass and solar power. ORCs gained popularity also for those application requiring great reliability and availability (remote areas, space applications, etc.). Figure 4 shows the area of application of ORC versus steam cycles, in terms of source temperature and power output.

A distinction is made between:
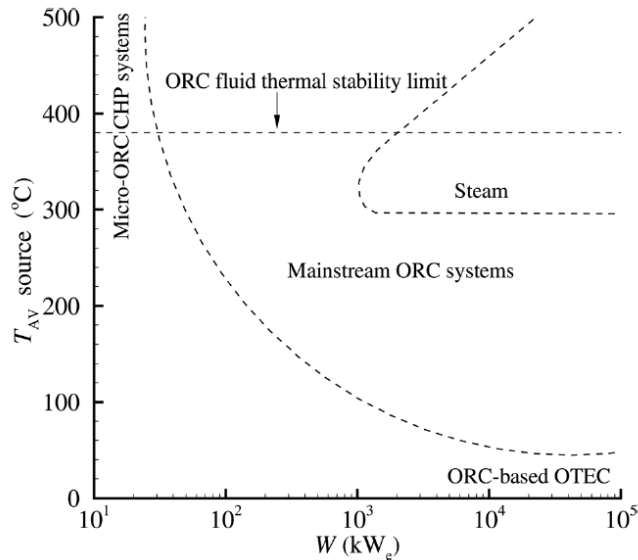
Figure 4: Areas of application of ORC versus steam plants in terms of mean source temperature and power output [7].

HIGH TEMPERATURE ORCS These systems work with a maximum cycle temperature of $300 - 400°C$, and are typically coupled with solar, biomass or waste energy sources;

LOW TEMPERATURE ORCS Here the temperature is below $200\,°C$, with geothermal, industrial and low temperature waste heat sources.

2.3 WORKING FLUIDS

2.3.1 Selection guidelines

Many different fluids could appear suitable for ORC applications. However, there are many thermodynamic, technical, economical and safety constraints that must be satisfied. Among economical, environmental and safety constraints are:

- low cost;

- low toxicity;

- low flammability;

- low or null Global Warming Power (GWP) and Ozone Depletion Potential (ODP), that means a low impact on greenhouse effect and on the thinning of the ozone layer (i. e. low environmental impact).

Analyzing more deeply thermo-fluid dynamic and technical problems, other constraints arise:

- the fluid should have a critical temperature and a liquid saturation curve allowing a good match with the energy source;

- the fluid should have the highest possible heat transfer coefficient (to enhance heat exchangers performances) and lowest possible dynamic viscosity (to reduce pumping costs);

- the fluid must exhibit a low freezing point, below the minimum possible temperature, during either on or off periods;

- caution must be paid to the thermal stability of the fluid: above a certain temperature threshold, the fluid molecules can decompose, leading to a change in composition, thus in fluid properties. This behavior is due to the complexity of these molecules: the heating process leads to a great amount of energy stored in vibrational degrees of freedom. This can cause the break up of the molecule. The decomposition process can be facilitated by water or other impurities able to catalyze the decomposition process.

Generally, low temperature and high power applications use relatively simple fluids. For high temperature and low power applications complex fluids are used. Mixtures are also suitable: the variable temperature of phase transition could be used to better follow the heat source profile. If properly chosen, mixtures can have a major impact on thermal decomposition: the break up of a component could create products that could react with other components of the mixture to give the initial component.

2.3.2 *Fluid panorama*

2.3.2.1 *Low temperature ORCs*

The best fluids for these applications are:

HYDROCARBONS they have null ODP, high GWP and are highly flammable;

HALOCARBONS they are obtained from hydrocarbons by substitution of an hydrogen with halogens. There are different classes:

- *clorofluorocarbons*: derived by substitution by chlorine or fluorine, they are non toxic, non flammable, but exhibit a high GWP and ODP, so their industrial use is forbidden;

- *hydrochlorofluorocarbons*: hydrogen is only partially replaced by halogens. They are weakly toxic and flammable, they have high ODP and GWP;

- *hydrofluorocarbons*: hydrogen is partially replaced by fluorine. They are non toxic an weakly flammable and have

null ODP. GWP lies in a wide range. They are the most interesting for LT applications.

2.3.2.2 *High temperature ORCs*

Fluids for high temperature ORC applications are:

AROMATIC HYDROCARBONS derived from benzene, they are highly flammable, toxic, carcinogenic. They are being abandoned;

FLUOROCARBONS derived from cyclic or polycyclic hydrocarbons, by substitution of hydrogen by fluorine and oxygen and nitrogen, they exhibit a high GWP, are expensive and may release dangerous compounds in case of decomposition. They are scarcely employed.

SILOXANES they are in the family of organosilicones and exhibit high critical temperatures ($240\,°C < T_c < 420\,°C$) and low critical pressures ($7\,bar < p_c < 20\,bar$). They are non toxic, weakly flammable and they have a null ODP and approximately zero GWP. They are relatively inexpensive. A problem is the thermal stability limit that is not far from HT ORCs maximum temperatures. However, these fluids are very commonly used for these applications.

3

LASER DOPPLER VELOCIMETRY

Laser Doppler Velocimetry (LDV), sometimes called *Laser Doppler Anemometry* (LDA), is an optical measurement technique that gained a great popularity between experimental fluid mechanicists, since 1964, when the first LDV instrument was presented by Yeh and Cummins [2]. Its wide acceptance is mainly due to its non-intrusiveness, directional sensitivity, high spacial and temporal resolution and high accuracy.

LDV is a *direct* velocity measurement, since it calculates the velocity v by measuring the time Δt needed for a particle to pass through a known distance Δs:

$$v = \frac{\Delta s}{\Delta t}. \tag{1}$$

LDV is a direct velocity measurement technique that exploits particles tracking properties.

Therefore, the first thing that can be drawn is that some sort of inhomogeneity in the flow is needed, to perform the measurement. It has been previously written that LDV performs a direct velocity measurement, but this claim needs to be further explained and specified: a direct measurement of the velocity of the inhomogeneity is actually being made. This measurement coincides with the velocity of the flow in the considered point *only* if the object of the measurement has a relative velocity (the so called *slip velocity*) with respect to the surrounding fluid that equals zero. These inhomogeneities may be already present in a fluid (e. g. condensation drops in a saturated vapor) or injected for the purpose of carrying out the measurement. The measurement is performed by extrapolating the time Δt from the signal generated by particle scattered light on a receiver.

In the following sections the properties of these inhomogeneities in the flow, the possible options to properly seed the flow, the measurement principle and the signal processing needed to obtain meaningful data are treated.

3.1 SEEDING PARTICLES PROPERTIES

As previously seen, the LDV measures the velocity of some inhomogeneities within the flow. Except for some particular cases, the flow has to be inseminated with small particles. For the measure to be reliable, particles have to follow the flow accurately, so dynamic properties will be analyzed in in Section 3.1.1. Particles should also have good scattering properties, to provide a good signal quality. These properties will be treated in Section 3.1.2.

Generally speaking, beside the dynamic and optical properties, a seeding material should satisfy also other aspects. The material:

- should not be hazardous or toxic;

- should not be corrosive;

- should contaminate in a small amount the facility or its optical interfaces.

3.1.1 *Dynamic properties*

From a qualitative point of view, the smaller the seeding particle is, the better it will follow the flow. This is essentially due to inertia forces that lead the particle to follow a different path relative to the one followed by a fluid element, when subjected to an acceleration of some sort, since particles tend to maintain *constant* the velocity vector (module and direction). Different situations can be shown as an example. In a channel where it is imposed a strong curvature, the flow adjusts himself immediately. A single fluid element, during the turning, experiments an acceleration, since the velocity vector changes direction. The entrained particle will try to follow the fluid flow, but the inertia force associated with its mass tends to maintain the particle on a straight path. In an similar way, a straight passage with an accelerating flow could be taken as an example. Due to the geometry, the direction remains constant, therefore the particle tends to maintain a constant velocity, hence the particle has a lower velocity. The two previous examples can be combined if a simple turbulent flow is analyzed, where a fluid element is constantly accelerated and continuously changes velocity in direction and module over time.

From an analytic point of view, under the assumption of:

1. homogenous velocity profile over the particle;

2. no lift force;

3. spherical particles;

4. negligible particle-particle interaction;

5. $Re_p = \frac{\rho \, d_p \, |\vec{v}_f - \vec{v}_p|}{\mu} = 0$;
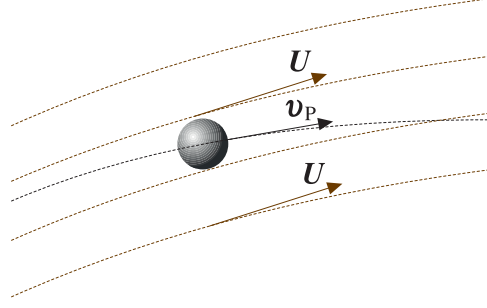
Figure 5: Particle and fluid velocity vectors [29].

the motion of a spherical particle is described by the following equation:

$$\underbrace{\frac{\pi}{6}d_p^3\rho_p\frac{d\vec{v}_p}{dt}}_{\text{acceleration force}} =$$

$$= \underbrace{-3\pi\mu d_p\left(\vec{v}_p - \vec{v}_f - \frac{1}{24}d_p^2\nabla^2\vec{v}_f\right)}_{\text{Stokes drag}} +$$

$$+ \underbrace{\frac{\pi}{6}d_p^3\rho_f\frac{D\vec{v}_f}{Dt}}_{\nabla P \text{ term}} +$$

$$- \underbrace{\frac{\pi}{12}d_p^3\rho_f\frac{d}{dt}\left(\vec{v}_p - \vec{v}_f - \frac{1}{40}d_p^2\nabla^2\vec{v}_f\right)}_{\text{virtual mass term}} +$$

$$- \underbrace{\frac{3}{2}d_p^2\sqrt{\pi\rho_f\mu}\int_{t_0}^{t}\frac{d}{dt'}\left(\vec{v}_p - \vec{v}_f - \frac{1}{24}d_p^2\nabla^2\vec{v}_f\right)\frac{1}{\sqrt{t-t'}}dt'}_{\text{Basset history term}} + \vec{F},$$

$$(2)$$

where

d_p is the particle diameter;

$\vec{v}_f$ is the velocity vector of the fluid (Figure 5);

$\vec{v}_p$ is the particle velocity vector (Figure 5);

ρ_f is the fluid density;

ρ_p is the particle density;

μ is the dynamic viscosity of fluid;

t_0 is the start time;

$\vec{F}$ are the external forces acting on the particle, such as the body force
    (gravity minus buoyancy) $\vec{F}_{G-B} = \frac{\pi}{6}d_p\left(\rho_p - \rho_f\right)\vec{g}$;

$d_p^2 \nabla^2 \vec{v}_f$ are the Faxen terms and are usually negligible, with respect to the other terms [13];

$\frac{d}{dt}$ is the time derivative on the particle trajectory;

$\frac{D}{Dt}$ is the time derivative on the trajectory of fluid elements surrounding the particle.

This equation is the so called Basset–Boussinesq–Oseen (BBO) equation. The third assumption we made, is well verified for small particles. The fourth one, is crucial: if there are significant particle-particle interactions, the tracer will not follow properly the flow. It is commonly assumed that this requirement is satisfied, if the particle separation is about 1000 diameters. This constraint leads to a limit on the concentration of tracer particles in the flow.

There are five terms, on the right hand side:

STOKES DRAG is due to viscous forces; it applies for low particle Reynolds number, calculated with respect to the slip velocity $\vec{v}_p - \vec{v}_f$: $Re_p = \frac{\rho_f (\vec{v}_p - \vec{v}_f) d_p}{\mu} < 1$. So this law applies for small particles and small slip velocity. However, the Stokes drag is conservative and the actual Drag is higher [14];

∇P TERM this term accounts for the pressure gradients generated by the fluid acceleration, in the vicinity of the particle;

VIRTUAL MASS TERM is the force associated with the virtual mass; this mass equals half of the fluid mass displaced by the sphere;

BASSET HISTORY TERM expresses the drag forces due to the unsteadiness of the flow;

BODY FORCES expresses the body forces acting on the particle, such as gravity or centrifugal forces in swirling flows.

There are solution for this equation in different cases. Some examples of these solutions are reviewed in [2] and [14]. Only a particular case can be analyzed here: a particle accelerated from $v_p = 0$ in a flow at constant velocity v_f. By analyzing the step response, it can be assessed whether the particle follows or not the flow properly.

If the assumption of $\rho_p / \rho_f \gg 1$ is made, the last two terms in Equation 2 can be neglected. Further, since steady flow is being considered, $dv_f / dt = 0$, and the equation of motion reduces to

$$\frac{\pi}{6} d_p^3 \left(\rho_p + \frac{1}{2} \rho_f \right) \frac{dv_p}{dt} + 3\pi\mu d_p \left(v_p - v_f \right) = 0, \tag{3}$$

with solution

$$v_p = v_f \left[1 - \exp \left(-\frac{t}{\tau} \right) \right] \tag{4a}$$

$$\tau = \frac{d_p^2 \rho_p}{18 \mu} \left(1 + \frac{1}{2} \frac{\rho_f}{\rho_p} \right) = \tau_0 \left(1 + \frac{1}{2} \frac{\rho_f}{\rho_p} \right) \tag{4b}$$

$$s = \frac{v_f - v_p}{v_f} = \exp \left(-\frac{t}{\tau} \right). \tag{4c}$$

where

τ is the relaxation time;

τ_0 is the time constant for the solution of a sinusoidal fluid velocity oscillation: $\tau_0 = \frac{\rho_p d_p^2}{18 \mu}$.

For high density ratios $\rho_p / \rho_f \gg 1$, Equation 4b reduces to $\tau = \tau_0$. These solutions are very useful, since they offer some values that give us the idea of how much time or space is needed for a particle to approach the fluid velocity: if we inject a particle with a zero velocity, we have to wait 4.6τ if we want $s \leqslant 1\%$. In a similar way, it is required a distance of $4.6\tau u$. The mentioned values are reduced for smaller particles or if the initial particle velocity v_p is higher than zero.

Since in Equation 2, for small particles (like those that are usually in LDV), the Stokes drag dominates the right hand part, authors of [29] show that

$$v_p - v_f = \frac{d_p^2 (\rho_p - \rho f)}{18 \mu} \frac{dv_p}{dt}, \tag{5}$$

under the approximation that $\frac{D v_f}{D t} = \frac{d v_p}{d t}$.

Now, two different equations have been presented: Equation 4 is able to represent the response of a particle to a step in the velocity field, while Equation 5 represents the response of a particle to a generic variation of velocity. It appears very clear, now, the need for particles with a density that matches the fluid one. From Equation 5, if $\frac{(\rho_p - \rho_f)}{\rho_f} = 0$, the slip velocity tends to zero too. This is easily verified in liquid flows, with polystyrol, polystyrene or other polymers [2]. In gas flows, it is more difficult, since typically $\rho_p / \rho_f = O(10^3)$. In such situations, micro-baloons, micro-spheres or microspherical feathers could be used. However it is necessary to reduce the size of the particles, since balloons and spheres have a density of $100 - 700 \, \text{kg/m}^3$. In gases, it is the situation of high density ratios, so Equation 3 and Equation 4 apply. From Equation 4b is clear, that, for a certain fluid, the time constant increases if the particle density rises. This leads to the use of smaller particles in gas and vapor flows, since, as previously seen, it is difficult to have tracers with densities similar to those of the fluid medium.

Neutrally buoyant particles lead to a correct tracking.

Shock waves occurring in a flow with can be seen as a step, and the above equations apply. Therefore, in region downstream the shock wave, the flow tracking is not accurate, since the particle adapts to the new flow regime with an exponential law. In these cases, the relative velocity could assume values beyond the validity of the Stokes drag law. Further discussion about tracking and refinements to the drag term in high velocity flows with shock waves is given in [2] and [14].

3.1.1.1 *Motion equation for finite* Re *number*

In the foregoing discussion, the BBO equation (Equation 2) has been used and useful results, valid under the assumptions that have been made, have been obtained. The $Re = 0$ hypothesis is critical and it needs to be examined.

The particle Reynolds number Re_p and the flow Reynolds number Re can be defined as

$$Re_p = 2\frac{\rho r_p \, |\vec{v}_f - \vec{v}_p|}{\mu} \tag{6a}$$

$$Re = \frac{\rho v_f L}{\mu}. \tag{6b}$$

where r_p is the particle radius. Since a velocity measurement has to be performed, $|\vec{v}_f - \vec{v}_p| \, / \, |\vec{v}_f| \ll 1$ is required. This implies $Re_p \ll (2r_p/L) \, Re$. Usually, r_p/L is small: $r_p/L \sim 10^{-3}$ for liquid flows and $r_p/L \sim 10^{-4}$ for gas flows. So the particle Reynolds number Re_p should satisfy $Re_p \ll 10^{-3} - 10^{-4} Re$. If the flow is laminar, and an ac-

A specific equation for particle Reynolds number greater than one is required, if the flow is turbulent.

curate tracking is required, the particle Reynolds number Re_p results lower than one. On the other side, in a turbulent flow, Re_p results greater than one. This leads to the conclusion that the BBO (Equation 2), as previously seen, is not appropriate for turbulent flows and another equation is required.

Sometimes, a very simple approach is used: neglecting all terms except for the quasi-steady Stokes drag term and modifying it with a ϕ coefficient to account for the deviation when Re_p becomes finite. In literature (e. g. on [6]) there are various correlations for ϕ as a function of Re_p. In cases of moderate acceleration, the unsteady terms could be, however, relevant. The history term should decay asymptotically with time and the added mass term should not be corrected, since it is a purely inertial and non viscous term. Under these guidelines, and after an accurate analysis, Mei proposed a dynamic equation able to describe uni-directional motion of spherical particles at *finite* Reynolds numbers. The interested reader can find more about this equation and a brief discussion on [13].

3.1.1.2 *Particle frequency response*

It is particularly interesting to determine how the particle responds to a variable velocity. In analyzing how well a tracer particle follows
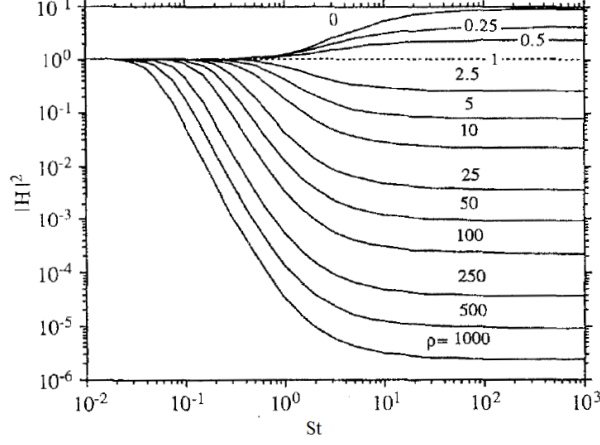
Figure 6: Particle energy transfer function $|H(St)|^2$ as a function of Stokes number St [13].

the flow, it is of particular interest to study its behavior in the high frequency range of velocity fluctuation. Given a fluid flow velocity $v_f(t)$ oscillating at high frequency f (and with a pulsation $\omega = 2\pi f$), we can define a Stokes number

$$St = \sqrt{\frac{\omega r_p^2}{2\nu}} \gg 1. \tag{7}$$

The Stokes number compares the characteristic time of the particle motion with respect to the characteristic time of the flow motion. Indeed, an equivalent definition is

$$St = \frac{\tau}{T}. \tag{8}$$

By doing an asymptotic analysis, for finite values of $Re = \tilde{v}_p d_p/\nu$ ($\tilde{v}_p$ is the amplitude of the velocity fluctuation), in the cited equation of motion valid for finite Re_p reported on [13], an apparently simple formulation for the amplitude of the particle velocity fluctuation is obtained:

$$\tilde{v}_p(\omega) \sim H(\omega)\,\tilde{v}_f(\omega)\,, \tag{9}$$

where $H(\omega)$ is called the *frequency response function* of the particle and is a function of the the Stokes number $St(\omega)$ and the particle to fluid density ratio $\zeta = \rho_p/\rho_f$.

Thus, we can define the *energy transfer function* as

$$|H(\omega)|^2 = |H(St)|^2 \tag{10}$$

where the particle to fluid density ratio ζ is the only parameter. In Figure 6 is reported $|H(St)|^2$ parametrized in ζ. Varying ζ, we can observe different behaviors:
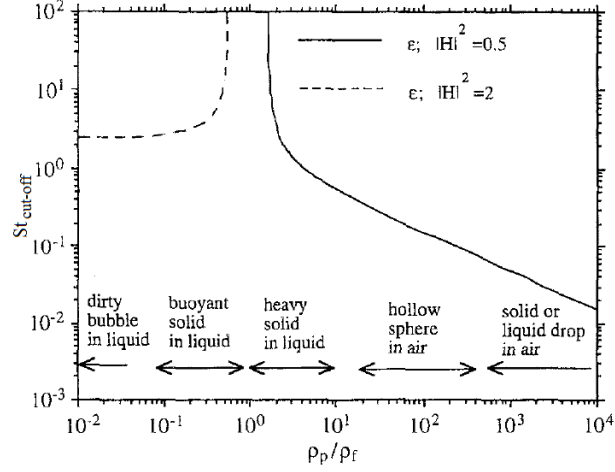
Figure 7: Cut-off Stokes number as a function of particle-to-fluid density ratio, as reported in [13].

$\rho = 1$ the particle has the same density as the flow and $|H(St)|^2 = 1$. The particle has a *perfect response*;

$\rho = 0$ the particle has a negligible density with respect to the fluid and $|H(St)|^2 \rightarrow 9$, for sufficiently high St. This results in a great over-shoot;

$\rho < 1$ this is a similar to the previous one, but less extreme. $|H(St)|^2 > 1$ and particles tend to over-shoot;

$\rho \gg 1$ the particle has a density greater than the fluid and $|H(St)|^2 \rightarrow \frac{81}{16}\rho^{-2}St^{-4}$, for intermediate values of Stokes number. In this region, the particle acts as a low-pass filter. At high St, $|H(St)|^2 \rightarrow \frac{9}{4}\rho^{-2}$ and, since $\rho \gg 1$, the particle energy transfer function is very low and the response of the particle is nearly nonexistent.

From the analytical formulation of $|H(St)|^2$, it is possible to obtain a cut-off Stokes number, once fixed a limit value for $|H(St)|^2$. By taking limit values of 0.5 (for high ρ) and 2 (for low ρ), we obtain the graph of Figure 7, where it is evident that:

- for values of ζ around one the cut off Stokes number is very high, and the good response is confirmed;

- for fixed ζ, if we decrease d_p by a factor of 10, $\omega_{cut-off}$ will increase by a factor of 100, from the definition of St.

In [13] are reported the following interpolations for $St_{cut-off}$:

$$St_{cut-off} \approx \left[2.380^n + \left(\frac{0.659}{0.561 - \zeta} - 1.175\right)^n\right]^{1/n},$$

$$n = 0.93, \text{for } \zeta < 0.561 \quad (11)$$

$$St_{cut-off} = \left[\left(\frac{3}{2\zeta^{1/2}} \right) + \left(\frac{0.932}{\zeta - 1.621} \right)^{\gamma} \right]^{1/\gamma},$$
$$\gamma = 1.05, \text{for } \zeta > 1.621. \quad (12)$$

The cut-off frequency can be determined with

$$f_{cut-off} \approx \frac{\nu}{\pi} \left(\frac{2St_{cut-off}}{d_p} \right)^2, \quad (13)$$

while the particle cut-off diameter, for a specified cut-off frequency, under which the particle follows properly the flow, could be calculated with

$$d_{cut-off} \approx 2St_{cut-off} \sqrt{\frac{\pi f_{cut-off}}{\nu}}. \quad (14)$$

3.1.2 *Optical properties*

In order to have a better signal, it is desirable to have as much light scattered as possible. To understand more about this topic, the scattering process has to be understood more in detail. This is an interaction between radiation and fluid molecules or small particles suspended in it. Unlike reflection, the incoming radiation is deviated in all directions (but not necessarily isotropically) and energy is conserved. Depending on the size of the particle with respect to the wavelength of the incoming radiation, the deviation can be isotropic or anisotropic. When dealing with elastic scattering (λ of the incident beam is conserved in the scattered one) are possible two modes:

RAYLEIGH isotropic, for $\frac{\pi d_p}{\lambda} \ll 1$, thus when the diameter of the particle is much smaller than the wavelength of the incoming radiation;

MIE anisotropic, for $\frac{\pi d_p}{\lambda} \approx 1$.

In LDV applications, typically, particle dimensions are of the order of a micrometer for gas and vapor flows, while tens of micrometers for liquid flows. Therefore, particle diameter is greater than wavelengths of the incoming radiation and the scattering is of the Mie type. This applies to common tracers, but, alternatively, it is possible to use fluorescent particles: they absorb light and emit energy at a higher wavelength. This permits to distinguish them from the light incoming from other objects and are really useful in some applications.

An important parameter, when dealing with scattering, is the so called *scattering cross section* $S_{1,2}$. It is the ratio of the total scattered power P_s to the laser intensity I_0 incident on the particle:

$$S_{1,2} = \frac{P_s}{I_0}. \quad (15)$$

Table 2: Scattering cross section as a function of the particle size [14].

Diameter d_p	Scattering cross section $S_{1,2}$	
Molecule		$\simeq 10^{-33}\,\mathrm{m}^2$
$1\,\mu\mathrm{m}$	$S_{1,2} \simeq (d_p/\lambda)^4$	$\simeq 10^{-12}\,\mathrm{m}^2$
$10\,\mu\mathrm{m}$	$S_{1,2} \simeq (d_p/\lambda)^2$	$\simeq 10^{-9}\,\mathrm{m}^2$
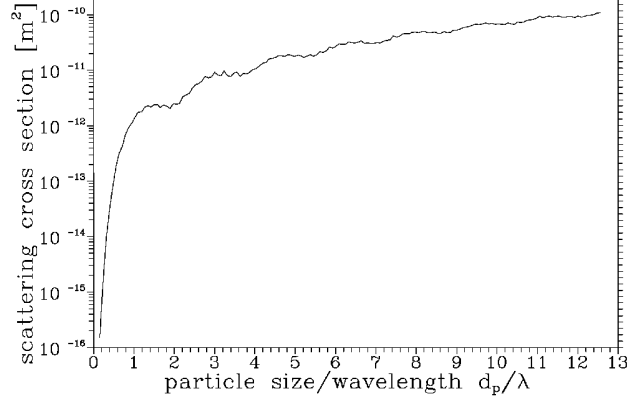
Figure 8: Scattering cross section as a function of particle size on radiation wavelength, for refractive index $n = 1.6$ [14].

As can be seen from Table 2, there are several orders of magnitude, in the value of $S_{1,2}$ between molecules and particles. This behavior is fundamental for LDV: the high value of the light scattered by the particle, with respect to the molecules of the surrounding fluid, permits the identification of the tracer.

The scattering cross section is function of the particle diameter, incident radiation wavelength and particle refractive index (n). In Figure 8 is represented $S_{1,2}$ as a function of d_p/λ. The Mie parameter x_M plays a relevant role, when dealing with Mie scattering:

$$x_M = \frac{\pi d_p}{\lambda}, \tag{16}$$

where

d_p is the particle diameter;

λ is the laser wavelength.

Increasing the particle size improves the signal quality.

When $d_p > \lambda$ (Mie regime), $S_{1,2}$ is proportional to the particle surface area (d_p^2). When $d_p < \lambda$ ($x_M < 3$), $S_{1,2}$ becomes proportional to d_p^4. This different behavior implies a lower limit on the particle diameter, since under a certain dimension (with respect to the laser wavelength) the scattered power becomes too low. Thus, as the diameter of the particle increases, the scattered light also increases, and the signal intensity is enhanced.

Figure 9: Scattering cross section polar diagram, for a refractive index $n = 1.334$ and Mie parameter $x_M = 10$, [29].

The scattering cross section also depends on the relative position to the light emitter from which the tracer is being observed. As can be seen from Figure 9, most of the light is scattered in the front direction. However, a great amount of light is scattered backwards. LDV generally works in a near-forward or near-backward scattering mode, so it takes advantage from this behavior. An important role is played by the particle material refractive index relative to the one of the surrounding medium. In liquids, the relative change in refractive index is lower than in gas flows, therefore a liquid requires larger particles.

The particle size is a compromise between dynamic and signal quality requirements.

This is in contrast with the dynamic requirements. A trade-off is needed, in order to accurately track the flow and obtain a higher signal quality. The foregoing discussion points out that, from an optical point of view, it would be better to increase the particle size as possible, to increase the scattered light and thus increasing the signal to noise ratio.

3.2 SEEDING MECHANISMS

Depending on the specific application, different particles are required, in order to perform a correct measurement and different mechanisms of particle generation are needed. In general, it is desirable to have a monodispersed size distribution and a spherical particles, but these conditions are not always easy to obtain. For both liquid flows and combustion applications, solid particles are required; indeed, in the first case, the liquid seeding would not track properly the flow and, in the latter, the liquid particle would evaporate.

3.2.1 *Liquid particle generation*

There are two different ways to generate a liquid particle: by condensation and by atomization.

3.2.1.1 *Condensation*

Particle generation through condensation is possible spontaneously in a saturated vapor environment. The difficulty lies in controlling the size and concentration of droplets. A precise control on vapor pressure, condensation temperature and seed nuclei concentration is needed. Monodispersed aerosol generator are commercially available [29]. Sometimes, when high particle rates are required, fog generators are used. However, flow rate and size distribution are not well controlled.

3.2.1.2 *Atomization*

Atomization is the most common droplet generation method. There are many types of atomizer available. When the specific application is compatible, the air-assist atomizer (or twin fluid atomizer) is used. It draws liquid from a reservoir into a high speed jet, using the lower pressure created by the high velocity of the jet. This type of atomizer creates a polydisperse spray, so an impactor or separator is needed, to remove large droplets. Droplet size is strongly dependent on the atomizing airflow rate and liquid used. Examples of particle sizes are $0.2\,\mu m$ with di-ethil-hexyl-sebacat and $4-5\mu m$ with water. Nozzle cascades can be used to vary concentration without varying the flow rate, otherwise the flow rate can be varied using by-pass air. A representative example of such type of atomizers is pictured in Figure 10, where a high speed axial jet creates a low static pressure and draws liquid from the lateral nozzle, atomizing it. A popular type atomizer is the Larskin nozzle. The interested reader can find more information in [2] and [29].

Another atomizing system is a single phase one: it is possible to create a stream of droplets by exploiting the instabilities of a laminar liquid jet. Rayleigh analyzed this topic and showed that a round jet tends to disintegrate into droplets due to surface tension forces. This instability is present for wavelengths of $3.5-7D$ and $\lambda = 4.508D$ is the optimal wavelength for unstable behavior (Figure 11). To obtain a monodyspersed jet, it must be externally perturbed at a wavelength in the aforementioned range. The droplet diameter is given by

$$d_p = \left(\frac{6\dot{V}}{\pi f}\right)^{1/3}. \tag{17}$$

This method is particularly suitable in cases where air or other gases cannot be used. More informations about the atomization mechanisms of a liquid jet could be found in [11] and [17].
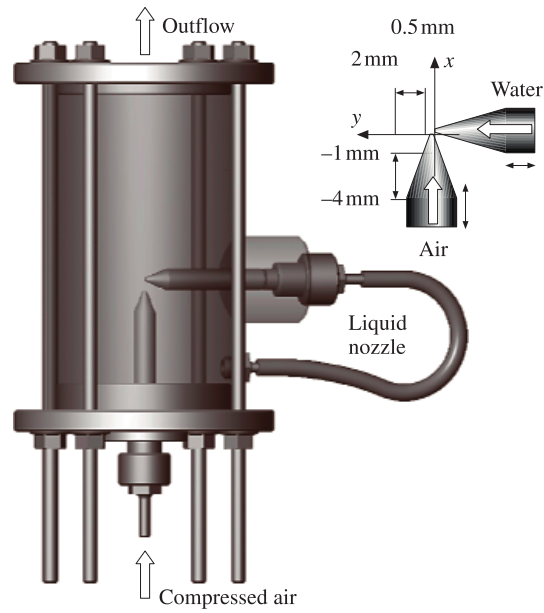
Figure 10: Twin fluid atomizer [2].

(a)   (b)
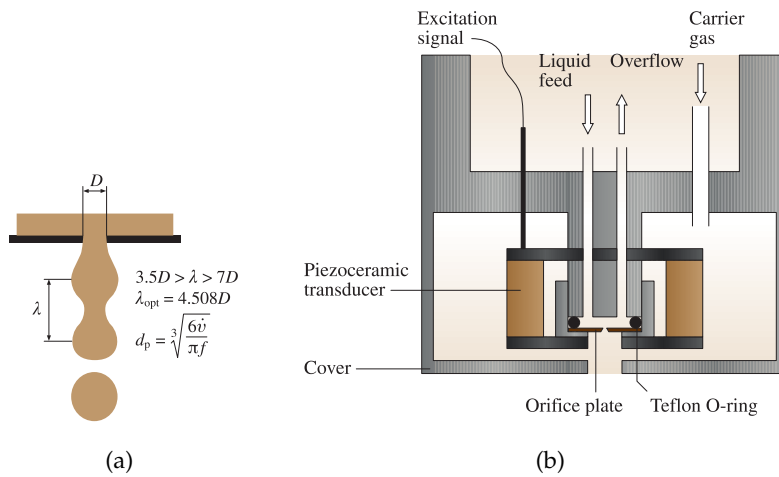
Figure 11: Atomization exploiting Rayleigh instability. (a) Rayleigh instability of a round liquid jet; (b) vibrating orifice generation head; it perturbs the jet at the buckling wavelength [2].
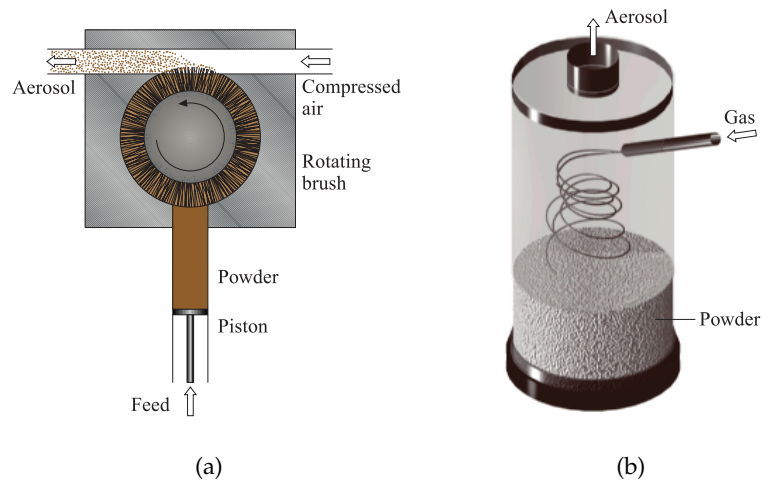
Figure 12: Solid particle generation from powders. (a) Brush seeder. (b) Cyclone aerosol generator [2].

3.2.2 *Solid particle generation*

3.2.2.1 *Atomization*

One method, for seeding the flow with solid particles, is to suspend the tracker in a liquid medium, atomize it in a gas and let the liquid evaporate, until only solid particles remain in the flow. Using suspensions, they must be diluted, to avoid the possibility of having more than one particle per droplet.

3.2.2.2 *Powders*

The second way to use solid particles as a tracker, is to use powders. A common problem, when dealing with powders is that some sort of coagulation is always present. It tends to increase the mean particle diameter and reduce the particle concentration. It is very important to use dry gases and hydrophobic particles.

In Figure 12, are represented two different dispersion devices. In the rotary brush seeder, there is a column of powder that is fed into a rotating brush, which transports a layer of powder in a high speed stream that drags the particles and breaks up the larger coagulated particles. The bulk powder feed rate, the brush rotation rate and the volume flow rate of carrier gas are fundamental parameters in determining the rate of particle delivery. In the cyclone aerosol generator, a gas is injected in a column, where it drags the powder. Another dispersion device is the fluidized bed, where a gas is injected from the lower part in a column and particles with a terminal velocity lower than gas velocity are entrained in the flow.

3.2.3 *Introducing particles in gas flows*

In this section, only topics related to gas flows will be treated. The reader interested in techniques regarding the introduction of particles in liquid and two phase flows can consult [29] and [2].

At this point, various methods to create seeding particles have been treated. The last step in the seeding procedure is the introduction of the tracer in the flow. It is a challenging part of the work and it takes a lot of work and trial and error procedure. The particles must be introduced within the flow without altering the flow properties at the measurement point. Each flow element in the stream tube identified by the measurement volume must be inseminated with the required concentration. Sometimes it is necessary to seed locally, only in the aforementioned stream tube. However, when possible, a global seeding is preferable.

When dealing with liquid droplets, it is important to estimate the time necessary for their complete evaporation, since, if coupled with the information of a guessed velocity of the flow, it gives an information about how far upstream the particles have to be injected.

The last aspect to be considered is the deposition or erosion on walls and optical windows due to seeding particles, that could impact on the quality of measurements.

3.3 MEASUREMENT PRINCIPLES

As it was previously mentioned, in LDV the velocity is measured by analyzing the signal corresponding to the light scattered by the seeding particle illuminated by the laser. There are multiple system configurations, such as the *reference-beam mode*, proposed by Yeh and Cummins in 1964 and the *dual beam mode*, proposed by Lehmann and vom Stein and Pfeifer. In this section we will refer to the dual beam configuration, that is the one of interest for the application on the TROVA and the most common approach. Since LDV is a consolidated measurement technique, only a brief discussion about its functioning is given here. A more complete discussion on this topic can be found on [29] and [2].

In the dual beam configuration, two incident beams are exploited. These beams cross and create a volume at their intersection: this is the *measurement volume*.

The fundamental principle is based on the Doppler effect, that appears twice: the first time, when the laser light of frequency f_b (b for beam) and λ_b impinges on the tracer particle, and the second time, when the light is scattered, with a frequency f_p, from the particle
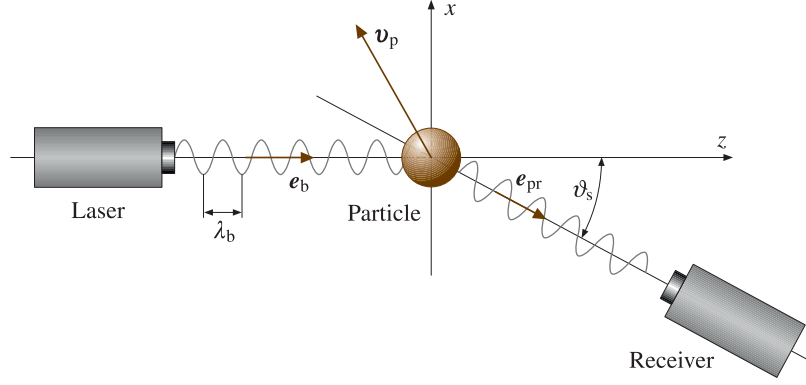
Figure 13: Configuration for applying the basic functioning principle of LDV [29].

and received by the detector with a frequency f_r (r for receiver). The frequency of the light seen by the receiver is

$$f_r = f_b \frac{\left(1 - \frac{\vec{v}_p \vec{e}_b}{c}\right)}{\left(1 - \frac{\vec{v}_p \vec{e}_{pr}}{c}\right)} \approx f_b + \frac{\vec{v}_p \left(\vec{e}_{pr} - \vec{e}_b\right)}{\lambda_b},$$

$$\text{for } |\vec{v}_p| \ll c, \ c = f_b \lambda_b, \quad (18)$$

where

c is the speed of light in the fluid in which the particle is immersed;

$\vec{v}_p$ is the particle velocity.

In Figure 13, this configuration is shown. The Doppler effect is accounted for in the second term of Equation 18 (*Doppler shift*). This term is directly proportional to the velocity of the particle and the difference of normal vectors. Typically, for placements that maximize $\vec{e}_{pr} - \vec{e}_b$, the Doppler shift is of the order $1 - 100\,\text{MHz}$, which is really small if compared to the frequency of the laser light (which is of the order of $\approx 10^{14}\,\text{MHz}$) and is impossible to be resolved directly.

As we mentioned before, the most common configuration is the dual beam. In this case, the interference creates a wave with a frequency (called *beat frequency*) that is in a range that is easier to resolve. Referring to Figure 14a and by applying Equation 18 to the two incident beams, the frequency, coming from the single incident beam, on the detector is

The dual beam configuration results in a more manageable beat frequency than the single beam one.

$$f_1 = f_b + \frac{\vec{v}_p \left(\vec{e}_{pr} - \vec{e}_1\right)}{\lambda_b}, \quad f_2 = f_b + \frac{\vec{v}_p \left(\vec{e}_{pr} - \vec{e}_2\right)}{\lambda_b}. \quad (19)$$

Laser beam λ_1, f_1

$\boldsymbol{e}_2$

$\boldsymbol{v}_\mathrm{p}$

x

$\boldsymbol{e}_\mathrm{pr}$

z

$\boldsymbol{e}_1$

Receiver

Laser beam λ_2 f_2
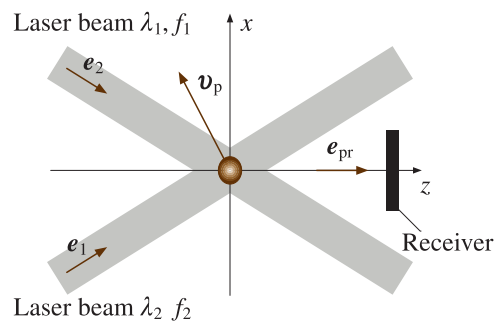
(a) *Scheme of the dual beam configuration.*

,

x

α

$\boldsymbol{v}_\mathrm{p}$

$\boldsymbol{e}_1$

Incident waves

Θ

z

$\boldsymbol{n} = \boldsymbol{e}_1 - \boldsymbol{e}_2$
$= 2\sin\Theta/2\,\boldsymbol{e}_x$

$\boldsymbol{e}_2$

Measurement
volume
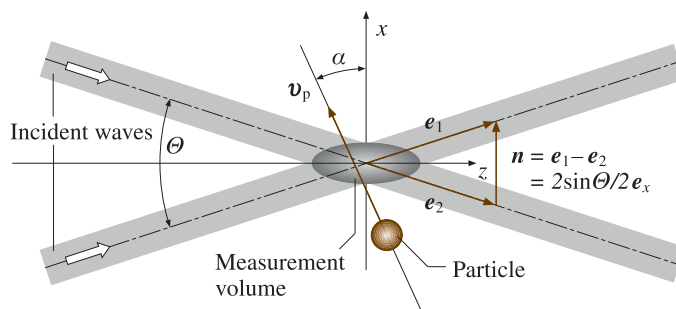
Particle

(b) *Vector relations in dual beam configurations.*

Figure 14: Dual beam configuration [29].

The frequency difference (usually called *Doppler frequency*), using Figure 14b, is

$$f_d = f_1 - f_2 = \frac{\vec{v}_p \, (\vec{e}_1 - \vec{e}_2)}{\lambda_b} =$$

$$= \frac{2 \sin (\Theta/2)}{\lambda_b} |\vec{v}_p| \cos \alpha = \frac{2 \sin (\Theta/2)}{\lambda_b} v_{p\perp}, \quad (20)$$

where $v_{p\perp}$ is the particle velocity perpendicular to the beam bisector. It is important to note that the receiver position does not influences the Doppler frequency. Therefore, the perpendicular velocity has been linked to the difference frequency.

If tracer particles are very small, the fringe model could be used as an alternative explanation. This is a model where the wavefronts of two coherent beams (the lasers used in LDV) interfere in the measurement volume, forming fringes that are spaced of a quantity Δx. These fringes originate from the constructive and destructive interference of the wave fronts. So, a tracer that passes through the measurement volume scatters light with amplitude modulated by the presence of these fringes. This light is detected by the receiver and transformed in an electrical signal with a frequency equal to the Doppler frequency. In Figure 15 is shown the principle underlying the fringe model. In Figure 15a-b, is shown the electric field strength of the two incident waves. These are homogeneous waves, and these images would have been different for lasers, since they have a gaussian distribution of the intensity over the diameter. The interference in the beam crossing region leads to an energy density of the electromagnetic field that can be seen as a wave propagating in the z direction with an amplitude modulated in the x direction (Figure 15c). By time averaging this quantity over one period, the intensity is obtained. It has a sinusoidal form and the spacing of the fringes is given by the period of this function:

$$\Delta x = \frac{\lambda_b}{2 \sin \frac{\Theta}{2}}. \quad (21)$$

Now, the hypothesis of small particle has been made, so it samples locally the intensity, that is constant over its diameter. The tracer scatters a wave with a carrier frequency that is the same of the incident beam one, modulated in amplitude with a frequency f_d, the Doppler frequency. From this information and the fringes spacing, the velocity perpendicular to the fringes can be calculated. If the particle is not small with respect to the wavelength, this model no longer holds. A detailed discussion can be found on [2].

The Bragg cell shifts the frequency of one of the two beams. This results in a moving fringe pattern that permits the recognition of the velocity sign.

The Doppler frequency does not contain the information about the sign of the velocity, because a particle crossing the fringe pattern in either directions will generate the same electrical signal. Directional sensitivity can be achieved by shifting one of the incident beams by

Electric field strengths of incident waves

$E_1 = E_0 \cos\left(\omega_b t - k_b \left(x \sin \frac{\varphi}{2} + z \cos \frac{\varphi}{2}\right)\right)$ $E_2 = E_0 \cos\left(\omega_b t - k_b \left(-x \sin \frac{\varphi}{2} + z \cos \frac{\varphi}{2}\right)\right)$

Electric field strength in the intersection
area of the incident waves

$E = E_1 + E_2$

Intensity proportional to the temporal
mean of the electric field strength

$I = \varepsilon c E_0^2 \cos^2\left(k_b x \sin \frac{\varphi}{2}\right)$

$\Delta x = \dfrac{\lambda_b}{2 \sin \frac{\varphi}{2}}$

Figure 15: (a), (b) Electric field strength of two incident homogeneous waves.
(c) Interference originated from the superposition of the two in-
cident waves. (d) Intensity of the electromagnetic field, with the
characteristic fringe pattern. [2]
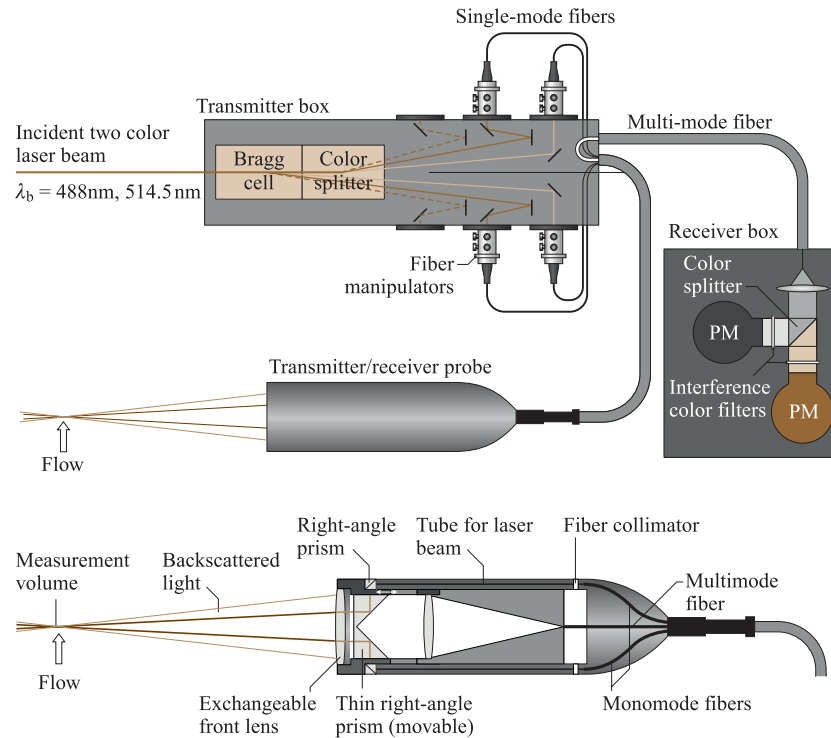
Figure 16: Two colors LDV system [29].

a frequency f_s. This can be achieved by acousto-optic modulators, such as Bragg cells. This shift results in a moving fringes pattern. A particle with zero velocity will result in a received frequency f_s and if the particle is moving accordingly with the fringes the received frequency will be lower than f_s and vice versa.

3.3.1 *Optical configurations*

In practical applications, there is a large number of different configurations to realize LDV. Ideally, the Laser Doppler technique can work with any angle between the detector and the source of the beams, but, as previously mentioned (Section 3.1.2), the majority of the scattered light is on the opposite side of the emitter. However, in many cases, the receiver optics is placed together with the emitting optics, since it is more convenient to position and this configuration needs only one optical access to the test section.

In Figure 16 is represented a common two color LDV system, where the aforementioned Bragg cell is used, followed by a color splitting prism, that divides the laser beam in two colors permitting the measurement of two different velocity components simultaneously. The beams are then transmitted to a transmitter/receiver probe through fiber optic. The scattered light is then collected and focused on a pho-
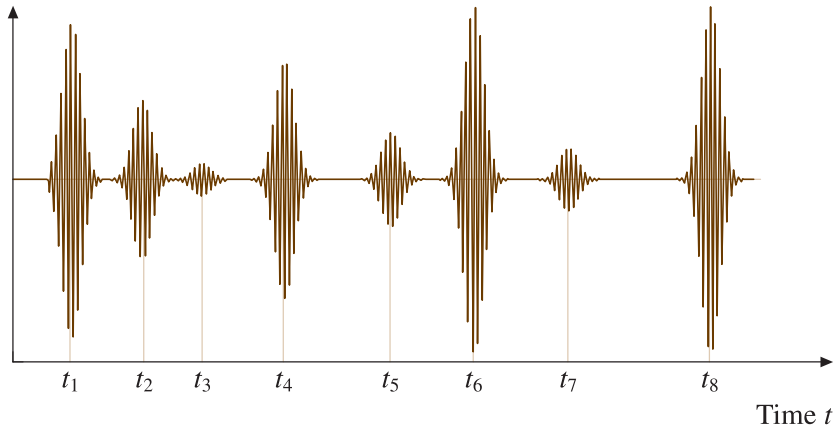
Figure 17: Bursts signal in time [29].

todetector (usually a photomultiplier or photodiode), which converts the light in a voltage modulated signal.

3.3.2 *Spatial resolution*

The spatial resolution in LDV is a complex function of optical system and signal-processing electronics. A parameter that certainly affects the resolution is the dimension of the measurement volume: the measured velocity is an average value of the velocity assumed by the particle in this volume. It depends on optical parameters, see Section 5.4. On the other side, the generated signal depends on the trajectory of the particle and on its dimension. Indeed, if the particle passes through a peripheral part of the measurement volume the contrast of the fringes is lower. Furthermore, if the particle is too large, it scatters the light from more than one fringe and the signal modulation decreases.

The spacial resolution depends on the optics and the signal-processing electronics.

3.4 SIGNAL PROCESSING

When a particle passes through the measurement volume, it generates a signal called *Doppler burst* or *burst signal*. The signal processor receives this signal and estimates the Doppler frequency, the arrival time, the signal length and the signal-to-noise ratio. An example of burst signal, with a high pass filter, to cut the low frequency (pedestral) part due to the mean amplitude variation of the signal is reported in Figure 17.

If an increase of the temporal resolution is required, the number of detected signal per unit time is of interest. An increase in particle concentration, does not improve necessarily the temporal resolution. This is because it increases the mean number of particle present in the

measurement volume. If this value is greater than 0.1, the probability of a single realization is 99.5%. If it is higher, there is a high probability of multiple particle signal, that may lead to a deterioration of the signal due to their superimposition and thus to a lower signal rate [29].

Noise is always present, generated from different sources (electronics, laser, undesired reflections, scattering process). Except for some particular cases, noise is usually assumed of equal intensity over all frequency spectrum (*white noise*). A parameter to assess the strength of the signal with respect to the noise is the signal-to-noise ratio, defined as

$$\frac{\text{SNR}}{\text{dB}} = 10 \log \left(\frac{\sigma_s^2}{\sigma_n^2} \right). \tag{22}$$

This parameter compares the power of signal fluctuations σ_s^2 with the power of noise fluctuations σ_n^2. A noisy signal could lead to a wrong estimation of the Doppler frequency and of the signal duration or to the missing of some bursts. Is evident that noise increases the variance of the signal estimates, leading to more uncertain measurements. In determining the presence of a particle or monitoring SNR, the power spectral density (PSD) and autocorrelation factor (ACF) are suitable. In reducing the noise, a band pass filtering is useful, but care should be paid in determining cut-off frequencies, to maintain unaltered the part of the signal spectrum related to the velocity of the particle.

A noisy signal could lead to a wrong velocity measurement and to a lower data rate.

The arrival time is needed for a reconstruction of a time series of velocities, of the coincidence of different velocity component signals or to correlate velocity measurements to other measurements in the flow, such as those obtained with pressure probes.

Part II

SYSTEM DESIGN

The second part deals with the design of the LDV seeding system. To introduce to the frame in which the seeding system has to be implemented, a brief presentation of the TROVA is given. Right after that, the design of the seeding system is deeply discussed. First, the selection of the seeding material is analyzed, then the preliminary constraints for the design of the system are presented. Many different system configuration are taken into account and finally the actual layout is presented, with a deep discussion on each component selection. Finally the control logic of the system is reported.

TROVA PLANT

As previously mentioned (Chapter 1), non-ideal thermodynamic models are widely present in literature. However, reliable experimental measurements validating those models are lacking. The TROVA facility has been constructed to fill this gap, by measuring thermodynamic properties in expanding flows of fluids for ORC applications. In order to validate the available thermodynamic models, independent pressure, temperature and velocity measurement are needed.

4.1 PROPERTIES TO MEASURE

To fully characterize the thermo-fluid dynamics of a flow, the total pressure p_T, the total temperature T_T, the static pressure p, and flow velocity v_f should be known. In the TROVA, independent measurements of pressure, temperature and velocity are made in a converging-diverging nozzle. The nozzle is designed to exhibit a large isentropic core (except for the near wall regions), therefore total pressure and temperature measurements ahead of the nozzle and static pressure and velocity measurements on the nozzle axis are sufficient to characterize the flow. A direct velocity measurement is needed, since the use of the thermodynamic model to obtain the velocity is not compatible with the purpose of the validation of the model itself.

Due to these characteristics, the TROVA could be used to calibrate real-gas pressure probes. With calibrated pressure probes, it would be possible to measure the flow direction, Mach number, total and static pressure, thus permitting the analysis of non-ideal fluid flows in linear blade cascades or actual machines. Another important technique being applied to the TROVA is the Schlieren technique, that provides useful flow visualizations that permit the location and the analysis of possible shock waves.

The TROVA allows to perform independent measurements of pressure, temperature and velocity, in order to validate non-ideal thermodynamic models.

4.2 WORKING FLUID

The TROVA has been designed to test a vast variety of fluids. The fluids selected for sizing the system and for early tests are syloxane MDM (Octamethyltrisiloxane – $C_8H_{24}O_2Si_3$) and R245fa (1.1.1.3.3-Pentafluoropropane – $C_3H_3F_5$). These fluids are representative of syloxanes and HFC, that are the most interesting fluids for high temperature and low temperature ORCs, respectively.

Table 3: Operating conditions for the early tests at the TROVA.

Test	p_{Tn} [bar]	T_{Tn} [°C]	β	Z_{Tn}
MDM_1	25	310.3	25	0.31
MDM_2	10	276.9	10	0.62
MDM_{1st}	4	253.2	10	0.86
R245fa	37	159.2	18.5	0.47

Between the two fluids, the one selected for initial tests is MDM. MDM is the short name, originating from the following nomenclature:

M $(CH_3)_3SiO_{1/2}$;

D $(CH_3)_2SiO$.

Among organic fluids, MDM has a high critical temperature ($T_c = 290.94\,°C$) and a low critical pressure ($p_c = 14.15\,bar$).

4.3 OPERATING CONDITIONS

Operating conditions in the TROVA permit to explore non-ideal fluid flow regions characteristic of present and possibly future ORC turbines.

Operating conditions for the TROVA plant have been selected in order to explore regions characteristic of present and possibly future ORC turbines and are reported in Table 3.

For MDM_1, the expansion starts in supercritical conditions (Figure 18a) and ends in a region where the fluid behave almost as an ideal gas ($Z = 0.965$). The test MDM_2 is representative of actual ORC turbines and takes place in the close proximity of the vapor saturation curve (Figure 18a). For both these tests, the fluid behavior is highly non-ideal. MDM_{1st} is a test designed as the first test to be performed on the plant and, due to the low reduced pressure, non-ideal effects are attenuated. R245fa is starting in supercritical conditions (the critical pressure is $p_c = 36.51\,bar$). As can be seen in Figure 18b, the R245fa is a less complex compound than MDM, so the vapor saturation line exhibit a higher slope in the $T - s$ diagram (see Section A.5).

A key parameter in the design of the test section is the throat area, which determines the discharged flow rate, as long as the flow is chocked, for determined total inlet conditions. The cross section of the nozzle is rectangular and it has an equivalent diameter $D_{t,eq} = 20\,mm$.

4.4 THERMODYNAMIC CYCLE

Since the plant is a batch system, the fluid undergoes the following processes [25] (Figure 20): the required amount of fluid is stored in

(a) *MDM tests*.

(b) *R245fa test*.

Figure 18: Expansion for the MDM and R245fa tests on the $T - s$ plane.
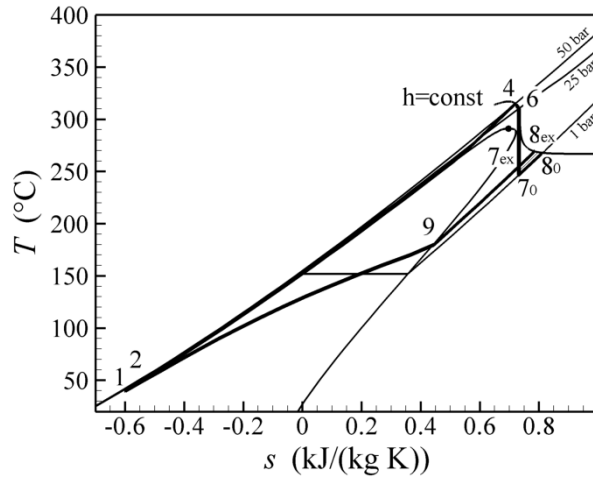
Figure 19: The thermodynamic cycle implemented on the TROVA.

a closed volume, the High Pressure Vessel (HPV), and heated up to superheated or supercritical conditions ($2 \to 4$). The tank pressure is higher than the nozzle stagnation one. The heating power is provided by electrical band heaters and heating wires. The total installed power is $50\,kW$.

The plant is a blow-down Organic Rankine Cycle with no mechanical power extracted.

The pressure is then regulated through the main control valve (MCV) to an almost constant stagnation pressure into the plenum ($4 \to 6$), where total pressure $p_{Tn} = p_{T6}$ and temperature $T_{Tn} = T_{T6}$ of the nozzle are measured. Into the plenum, the flow velocity is low, of the order of $1\,m/s$, therefore the total pressure can be measured with a wall pressure tap and transducer, since the dynamic contribution is completely negligible. Similarly, the total temperature is measured by a statically calibrated thermocouple, since the expected recovery factor reasonably equals one.

The fluid then expands through a planar nozzle (test section), where static pressure along the axis are measured ($6 \to 7$). The test section has an optical access to perform LDV measurements and Schlieren visualizations of the flow field. The diverging planar nozzle portion of the profile has been designed through a standard method of characteristics modified for dense gases (see [10]), while a polinomial function of order five has been used for the converging portion. It should be noted that the flow is not rigorously stationary. Even though the total nozzle pressure $p_{Tn} = p_{T6}$ is maintained constant by the MCV, the total enthalpy reduces in time, due to the emptying of the HPV. However, during the characteristic time of nozzle crossing, the total enthalpy variation is negligible, thus the flow can be treated as a sequence of steady states with transient boundary conditions which are measured during the test. This also holds for the low frequency (of the order of $1\,Hz$) oscillation related to the MCV operation.

The flow is not stationary: the total enthalpy reduces due to the emptying of the HPV.

The fluid is then discharged into the Low Pressure Vessel (LPV), where the fluid is condensed ($7_0 \rightarrow 1$). Since the expansion process takes place in a nozzle, no work is extracted, so all the thermal energy supplied in the HPV should be removed in the LPV. The circuit is then completed by a metering pump that compresses the fluid to the initial high pressure tank ($1 \rightarrow 2$). The plant is completed by a vacuum pump, to remove the non-condensables gases both during the plant filling and operation.

During a test, the HPV emptying causes a decrease in the HPV pressure p_4 and the LPV filling causes an increase in p_8. The characteristic heating time is of the order of a few hours, while the cooling time is of the order of one hour. The characteristic test time ranges between $10\,s$ and a few minutes, depending on the fluid and operating conditions.

4.5 TEST SECTION

The test section is a modular flanged body, designed to accommodate different nozzle profiles. The nozzle has a rectangular cross section and the two vertical sides are a quartz window and a steel plate (see Figure 21). The quartz window is actually an optical access, designed to permit LDV measurements and Schlieren visualizations. The rear steel plate has a series of taps for static pressure measurement along the nozzle axis. The plate is mirror polished, in order to provide a high reflective surface for the application of the Schlieren technique.

The nozzle is made by a couple of profiles and it has a small recessed step in the throat, in order to maintain fixed the throat position even in case of flow fluctuation. These fluctuations, in fact, can change the boundary layer thickness, leading to a different cross section available for the bulk of the flow, thus causing unsteady displacement of the throat location.
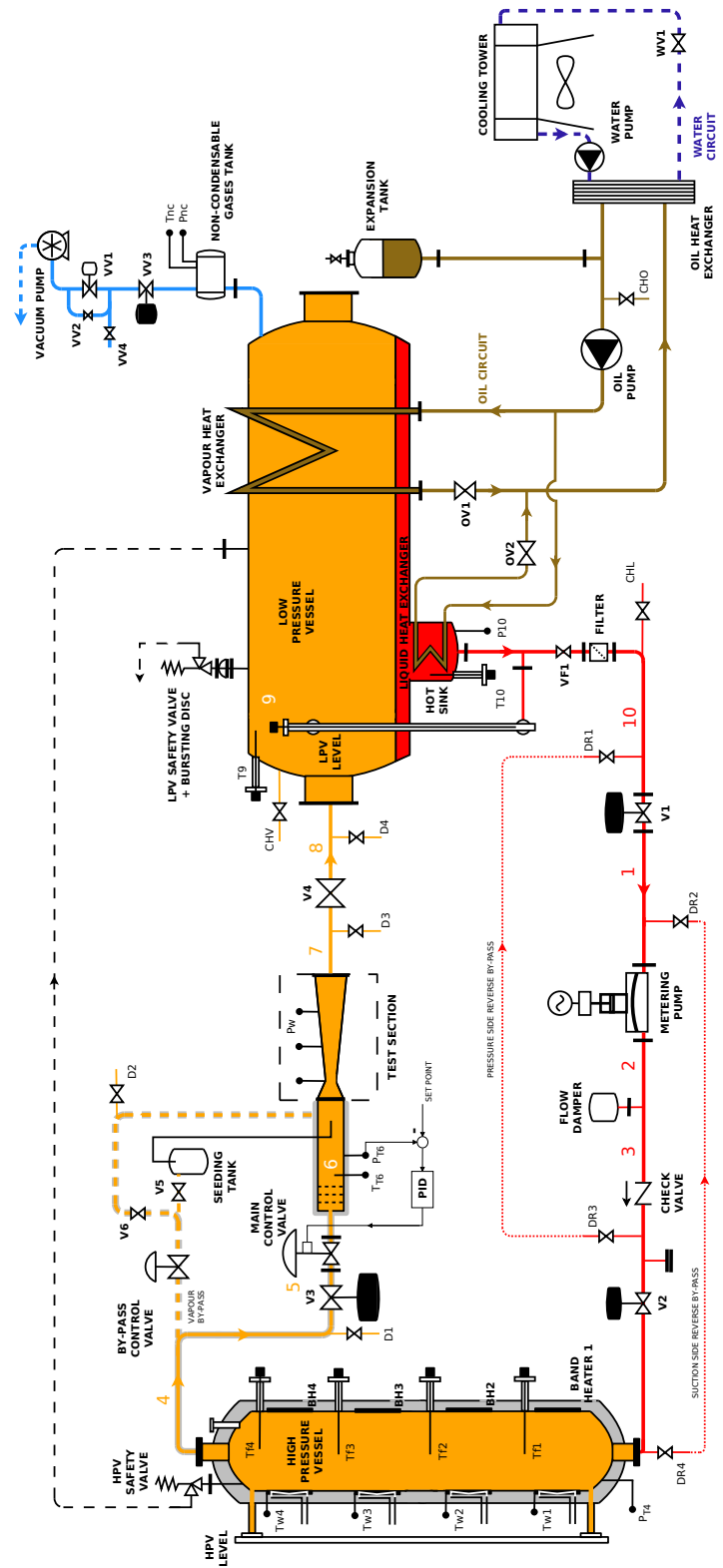
Figure 20: Schematic of the TROVA plant.
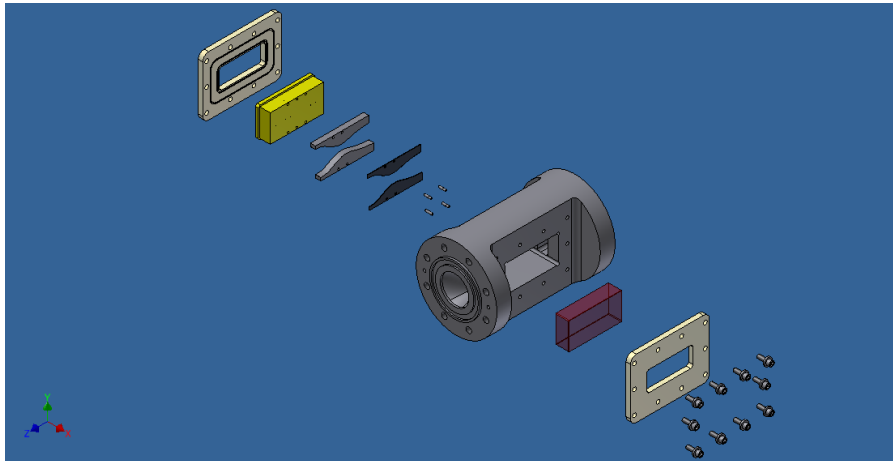
(a) *Test section components.*
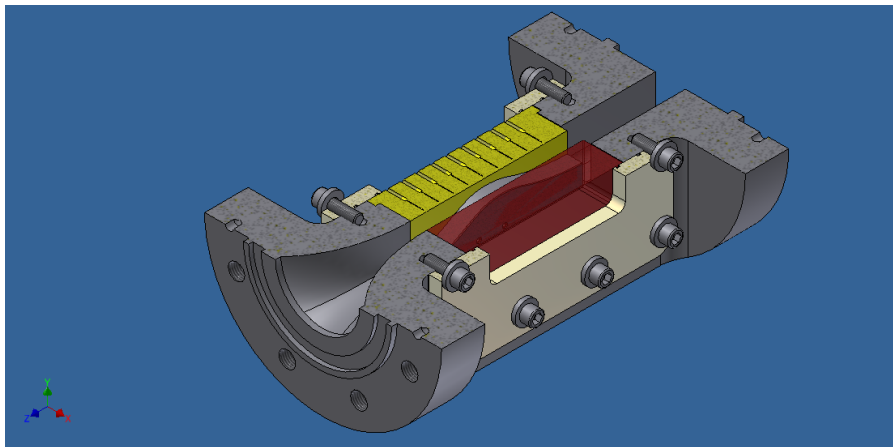
(b) *A section of the test section.*

Figure 21: The test section.

SEEDING SYSTEM DESIGN

This chapter, deals with the design of the seeding system. Initially, the available LDV system (Section 5.1) and the choice of the tracer are discussed (Section 5.2). In Section 5.3 are discussed the critical issues related to seeding the flow in the TROVA. The following section (Section 5.4) treats the design constraints that fix the value of some key parameters, such as the flow rates and volumes involved. Then, some different system configurations that have been considered are presented (Section 5.5) and the chosen is be discussed in depth (Section 5.6). About this configuration, all the processes that leaded to the design and selection of each part and component of the system (Section 5.7) are treated. Each normal system operation is then presented in Section 5.8.

In designing this system, the aim is to optimize it, given the available equipment, economic and time constraints.

5.1 THE AVAILABLE LDV SYSTEM

5.1.1 *Laser emitter*

The laser emitter used is a Argon Ion laser. This laser has several bands of emission either in the visible and ultraviolet range. The principal are $454.6\,nm$, $488.0\,nm$ and $514.5\,nm$, while the secondary are $351\,nm$, $457.9\,nm$, $465.8\,nm$, $476.5\,nm$, $472.7\,nm$ and $528.7\,nm$. The exploited wavelength are $488\,nm$ (blue) and $514.5\,nm$ (green). Obviously, the beam exiting the laser emitter is not monochromatic and it is treated later by the LDV optics. The principal features of the laser emitter are summarized in Table 4.

Table 4: Features of the laser emitter.

Producer	Spectra Physics
Model	2017
Power supply	$208\,V$ ac $\pm 10\%$
Input current	$42\,A$
	$5\,W$
Nominal power	$1.5\,W$ at $488\,nm$
	$2.0\,W$ at $514.5\,nm$
Beam diameter	$1.4\,mm$

Table 5: Features of the LDV system.

Producer		Dantec
Transmission efficiency	$\lambda = 514.5\,\mathrm{nm}$	0.7
	$\lambda = 488\,\mathrm{nm}$	0.6
Transmission optic fiber		Single mode
Receiving optic fiber		Multimode
Bragg frequency shift		40 MHz
Beam expansion ϵ		1.868
Beam distance		38 mm

5.1.2 *LDV optics*

After the laser beam has been emitted, it enters into the LDV optics (Figure 16), where it first encounters the Bragg cell. The Bragg cell divides the beam in two different beams and shifts one of the two by 40 MHz. This cell is an acousto-optic modulator that shifts the frequency of the beam by exploiting the refractive index modulation of a crystal by means of acoustic pressure waves. As previously mentioned (Section 3.3), this shift permits the recognition of the directionality of the flow.

After the Bragg cell, the two beams pass through a color splitter and split in different monochromatic laser beams. At this point, since the LDV system is a two component system, there are four monochromatic beams, two per color. Each of these beams is conveyed into a different micro-manipulator. Micro-manipulators are devices that convey and align the laser beam into the optic fiber that transmits the light to the LDV probe. The setting of the micro-manipulators is crucial, since having the central part of the beam transmitted into the optic fiber reduces loss of light power and results in a good measurement volume (for example with parallel rectilinear fringes).

The optic fibers then transmit the light to the head that emits and focuses the beams through a system of lenses. An optic device that may be mounted on the head is the beam expander, that increases the beam diameter and their distance, with an expansion ratio ϵ. This results in a smaller measurement volume, thus in a higher spacial resolution. On the other side, this results in smaller distances between fringes, that, for a given velocity increases the frequency of the burst signal.

Lenses with different focal length can be mounted on the laser head, impacting on the measurement volume size. The main features of the LDV system optics are summarized in Table 5.

The light scattered from a particle is captured by the receiving optics and conveyed by an optic fiber to the photomultiplier that con-

Table 6: Properties of selected seeding materials [2].

Material	Density [g/cm^3]	Refracting index	Melting temp. [°C]
PSL	1.05	1.59	240
NaCl	2.16	1.54	801
Al_2O_3	3.96	1.79	2015
TiO_2	$3.9 - 4.2$	$2.6 - 2.9$	1750
SiC	3.2	2.6	2700
ZrO_2	5.6	2.2	2980
SiO_2	2.2	1.54	1600

verts the light intensity in an electric signal that is transmitted to the processing unit, the *Burst Spectrum Analyzer* (BSA). The BSA converts the electric signal in the corresponding velocity value.

5.2 SEEDING PARTICLES

5.2.1 *Required particle properties*

The flow, in the TROVA application, is at high pressure and high temperature, hence liquid tracer could not be used, considering also the need of maintaining unaltered the flow properties. Furthermore, the pressure decrease during the expansion could lead to a change in surface tension, thus to an increase in their dimension. This leads to the use of solid particles. Usually metallic compounds are suitable, due their high melting temperature. In Table 6 some materials are reported with the corresponding density, refractive index and melting temperature. Titanium dioxide appears to be a good choice, thanks to his high melting temperature, non reactivity with MDM and his high refractive index. Furthermore it is not dangerous for human beings. Another good material is the Silicon dioxide, that has similar properties, with a lower refractive index and density. In the following, these two materials are considered as main option. Other materials have been discarded due to particle dimension, hardness, chemical compatibility, availability and cost issues. As an example, SiC has a high hardness that can damage the optical window, while Al_2O_3 may catalyze dissociation reactions of the fluid to be tracked. Obviously, PSL is not suitable for seeding in the TROVA, due to the low melting temperature.

When dealing with the design of a LDV system, the first step is an analysis of the flow field to investigate. The Reynolds number of the flow is given by

$$Re = \frac{\rho_f \bar{v}_f L}{\mu}, \tag{23}$$

where

$\bar{v}_f$ is the mean velocity scale;

L is the macro length scale;

μ is the dynamic viscosity of the fluid;

ρ_f is the density of the working fluid.

The channel is a rectangular section convergent-divergent nozzle, so the hydraulic diameter D_H is an appropriate value for the length scale L. The considered flow is turbulent and the turbulence microscales are given by the Kolmogorov length scale η_K:

$$\eta_K = L Re^{-3/4}. \tag{24}$$

This is the characteristic length scale of the smallest dissipative eddies in the flow. The frequency of velocity fluctuation associated with these eddies is

$$f_{max} = \frac{v_f}{2\pi L} Re^{3/4}. \tag{25}$$

Only the mean flow on the nozzle axis has to be tracked. However, it is not in our scope to fully resolve the turbulence: our aim is only to capture mean velocity (this mean has to be intended as a temporal mean over a sufficiently small Δt, to capture the unsteady nature of the flow at low frequency, but sufficiently high to filter out turbulent fluctuations). Indeed, the test section pressure probes are connected to the nozzle through a line-cavity system that acts as a low pass filter, with a cut-off frequency of about $200\,Hz$.

The ability of a tracer particle to properly follow the mean flow can be assessed by integrating Equation 2 (the BBO equation). As previously seen in Section 3.1.1.1, in turbulent gas flows, particle Reynolds number Re_p is not zero. Considering a slip factor $s = |v_f - v_p|/v_f = 0.01$ and the data from a CFD calculation for the tests MDM_2 and MDM_{1st} (CFD simulations for the MDM_1 test are not available), particle Reynolds number lie in the range $0.4 \div 4.5$. This leads to the conclusion that the formulation of the equation of motion for finite particle Reynolds numbers Re_p has to be used. As mentioned in Section 3.1.1.1, a common approach is to simplify Equation 2 that, for a horizontal trajectory, becomes

$$\frac{\pi}{6} d_p^3 \rho_p \frac{dv_p}{dt} = -3\pi \mu d_p \left(v_p - v_f \right) \phi, \tag{26}$$

where the term on the right hand side of Equation 26 is the quasi-steady Stokes term modified with the ϕ coefficient to account for the deviation in the Stokes drag when the particle Reynolds number is not zero. A simple relation for the ϕ coefficient is $\phi = 1 + 0.15 Re^{0.687}$ [6].

Table 7: Maximum slip factors s for different particle diameters and material.

Test	TiO$_2$		SiO$_2$	
	$d_p = 1\,\mu m$	$d_p = 0.5\,\mu m$	$d_p = 1\,\mu m$	$d_p = 0.5\,\mu m$
MDM$_2$	5.57%	2.35%	4.06	1.61%
MDM$_{1st}$	3.86%	1.36%	2.70	0.90%

A numerical integration of Equation 26, for a trajectory coincident with the nozzle axis, was performed, with a slip factor $s = 0.01$ at the nozzle inlet, for different particle diameters. The numerical integration of Equation 26 is quite straightforward, if the time derivative of particle velocity is written as

$$\frac{dv_p}{dt} = \frac{\partial v_p}{\partial x}\frac{dx}{dt}. \tag{27}$$

By rearranging Equation 26 as

$$\frac{dv_p}{dt} = \underbrace{\frac{18\mu}{d_p^2 \rho_p}}_{1/\tau_p} (v_f - v_p)\, \phi \tag{28}$$

and substituting Equation 27 into Equation 28

$$v_p \frac{dv_p}{dx} = \frac{\phi}{\tau_p} (v_f - v_p) \tag{29}$$

is obtained. By setting a the value of particle velocity v_p and fluid velocity v_f at the nozzle inlet, the calculation can be performed proceeding along the nozzle axis and using data from a CFD simulation. The velocity boundary condition can be fixed through the slip factor s. Indeed, it has been verified that the solution of the equation has a small sensitivity to the inlet slip factor s, for small changes in s. The results are reported in Table 7 for an inlet slip factor $s = 1\%$. A CFD simulation for the test MDM$_1$ is not available, therefore, only tests MDM$_2$ and MDM$_{1st}$ are reported. It is evident that particle diameter d_p less than $0.5\,\mu m$ should be chosen. It is also confirmed the decrease in slip velocity (Section 3.1.1), for a given point on the axis, with a decrease in the material density.

Particle diameters less than $0.5\,\mu m$ should be chosen. The motion of the particle is little influenced by the slip factor at the nozzle inlet.

5.2.2 Adopted seeding particles

After a research between the available seeding powders on the market, particles of two types have been selected: titanium dioxide and Aerosil 200 (which is composed by SiO$_2$ for 99.8%). They are designed for PIV application in combustion environments and need to be dehydrated before the use, for 30 minutes at 150 °C. Table 8 reports the

Table 8: Properties of TiO$_2$ and Aerosil 200.

	TiO$_2$	Aerosil 200
Bulk density [kg/m^3]	150	50
Specific weight [kg/m^3]	$3900 - 4200$	2200
Melting point [°C]	1830	1700
Primer particle [nm]	20	12
Cluster particle [nm]	$150 - 250$	$100 - 150$

properties of the selected materials.

In order to determine the compatibility, the degree of agglomeration and the visibility of the particles in MDM, a simple experiment has been performed. In two different bottles filled with 200 ml of MDM a quantity corresponding to 0.08% and 0.05% in weight of TiO$_2$ and Aerosil 200 respectively has been dissolved. The recipients have been heavily shaken then left apart. After a few seconds, both were partly sedimented and partly suspended. Aerosil exhibited a flaky consistence, while TiO$_2$ appeared more like micro-spheres. The latter seamed to form greater agglomerates, but this could be only an optical effect due to the different type of agglomeration. After months of dissolution they did not presented appreciable sign of some sort of incompatibility with MDM. The choice between the two material has to be made experimentally since a priori it is difficult to predict which one could be the better solution, given that Aerosil 200 has a lower density, thus it can follow better the flow, for fixed particle diameter.

The choice between the two tracers is challenging, so it has to be made based on experimental observations.

At this point, it is interesting to determine the cut off frequency of the particle. The procedure followed is the one showed in Section 3.1.1.2. Independent of the particle material (TiO$_2$ or SiO$_2$) the particle to fluid density ratio is greater than 1.621, so Equation 12 applies. Given the solution of a CFD calculation, the density ratio ζ is known at each point and the Stokes number can be calculated. Subsequently, using Equation 13, the cut-off frequency can be obtained. In Figure 22 it is reported the cut-off Stokes number $St_{cut-off}$ as a function of the particle-to-fluid density ratio ζ. In Figure 23 it is reported the cut-off frequency $f_{cut-off}$ as a function of the axial coordinate x. Data relative to the test MDM_1 are not reported, since a CFD simulation is not available for this test.

The particle cut-off frequency is very high compared to the frequency to be resolved for the mean flow tracking.

The obtained cut-off frequencies are very high for the considered application. However, in the TROVA, there is not the need to fully resolve the turbulence: only the mean flow on the axis has to be tracked.
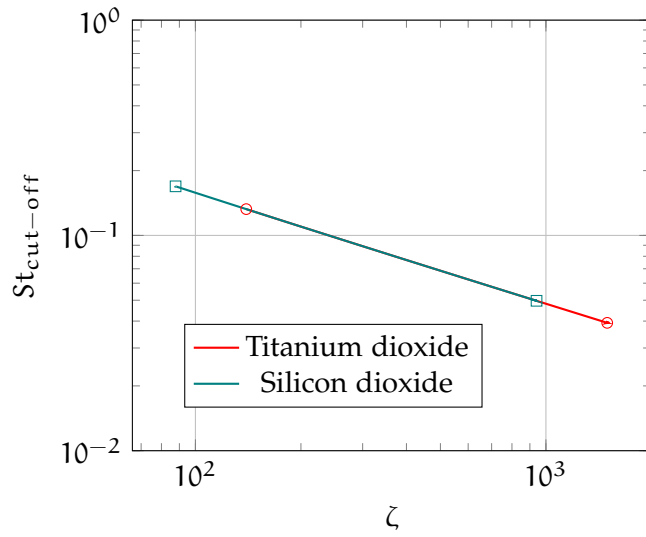
(a) MDM_{1st}
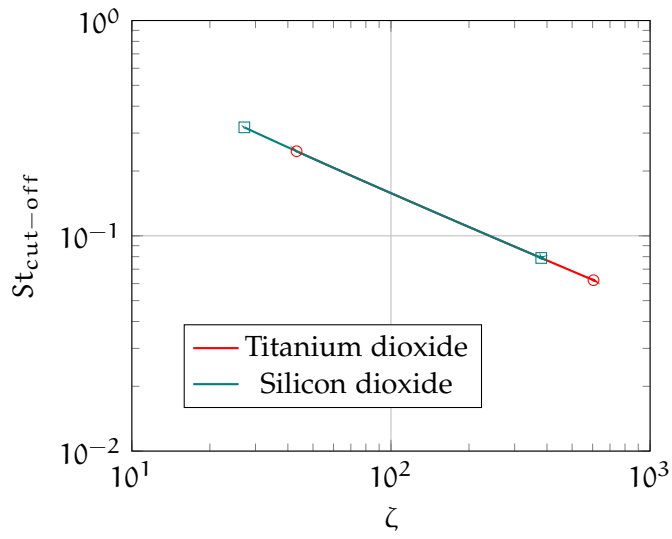
(b) MDM_2

Figure 22: Cut-off Stokes number $St_{cut-off}$ as a function of the density ratio $\zeta = \frac{\rho_p}{\rho_f}$ for titanium dioxide and silicon dioxide.
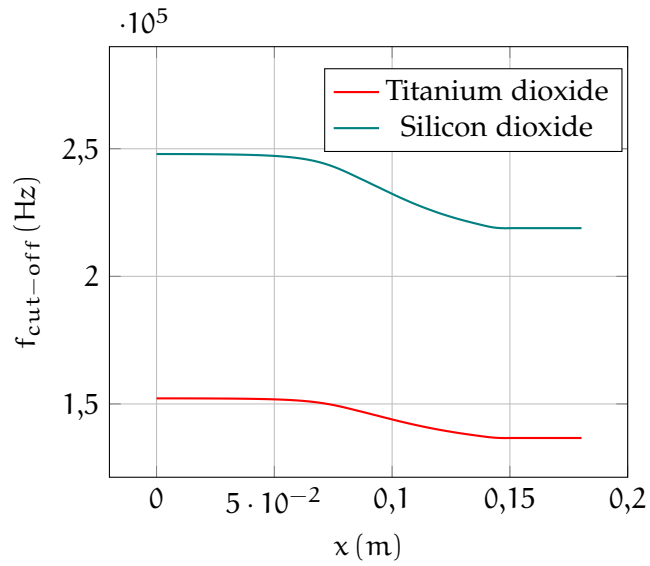
(a) MDM_{1st}
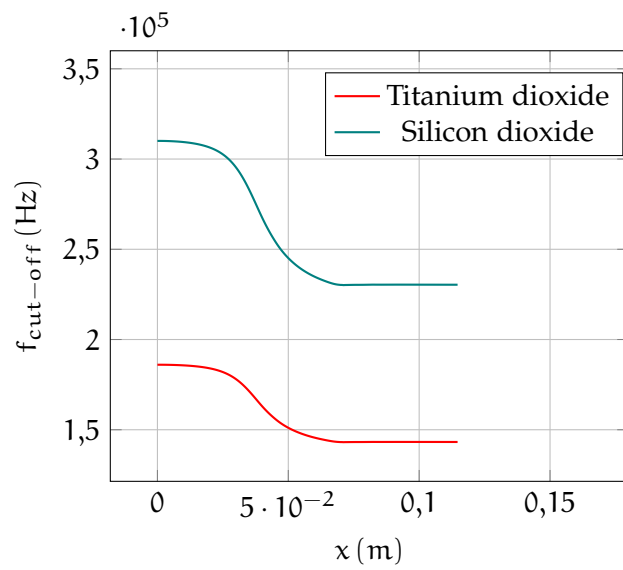
(b) MDM_2

Figure 23: Cut-off frequency $f_{cut-off}$ as a function of the position of the measurement point over the axis of the nozzle, for titanium dioxide and Silicon dioxide.
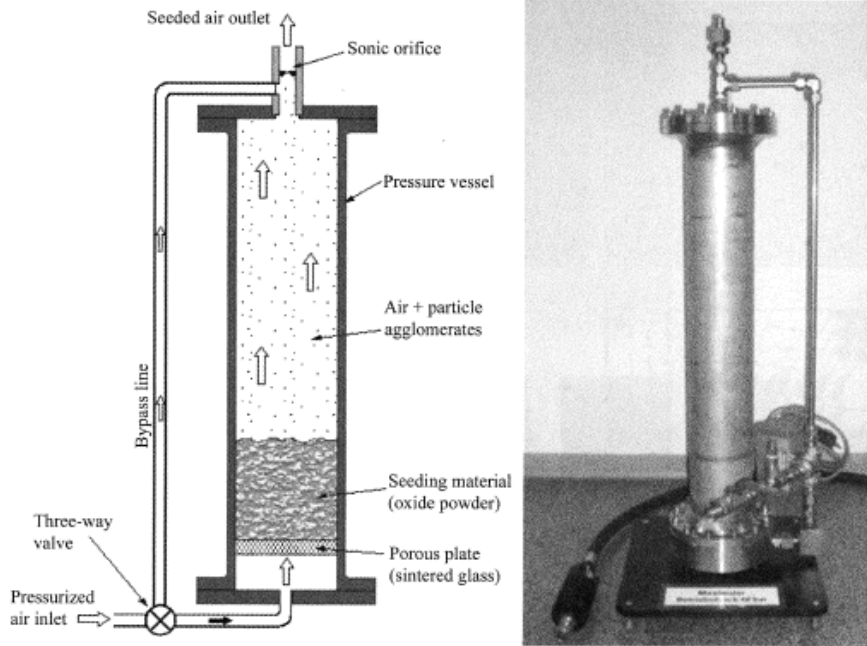
Figure 24: Fluidized bed seeding device for high pressure seeding applications [18].

5.3 SEEDING IN THE TROVA

Seeding in the TROVA facility is critical: the flow is at a high temperature and pressure and the thermo-fluid dynamic properties of the flow need to be kept unaltered. The use of atomized liquids is not possible, since the droplets may evaporate and contaminate the fluid. Solid particle are to be used. As previously mentioned (Section 3.2.2), we can either exploit the atomization of a liquid suspension or powders. The rotary brush seeder does not satisfy our constraints, since it needs a gas flowing through the brush that drags the particles. Within the TROVA, this gas *has to be* MDM vapor, to avoid the contamination of the working fluid. The vapor would be drawn from the HPV at high p and T, so it would complicate the design of the piston and the choice of the brush material. In particular, care would have been payed to the design of the moving seal on the piston, subjected to a maximum pressure difference greater than $\Delta p = 25\,\text{bar}$. Another possible system is the fluidized bed, analyzed in [18] for PIV measurements in high temperature reacting gas flows (Figure 24). Through a 3/2 valve, a gas is fed into the vessel at a velocity sufficient to fluidize the bed and suspend smaller particles (thus performing a first separation step). The gas with suspended particles flows through a sonic nozzle, that performs a second stage of size control, by braking up larger agglomerates. A commercial solution as been found [30], but due to its low maximum operating pressure and temperature (16 bar and 30 °C) it has been discarded. Initially, a cyclone system was con-

sidered. It consisted of a tank containing an amount of powder where a vapor flow (drawn from the HPV through the by-bass) is injected tangentially and creates a swirling flow that drags smaller particles and exits from the upper side. A selection on the size of the particles being entrained is made, since the bigger ones tend to be centrifuged by the flow. This method was also discarded, due to the big amount of powder needed and to vapor condensation problems on the vessel wall (at least in the initial part of the test). However, initially, this idea was adopted and the mentioned vessel was constructed, but never used.

The atomization of a suspension of MDM and the tracer is exploited to seed the flow.

To overcome the presented issues, another system is necessary. One solution is to exploit the atomization of a MDM-tracer particle suspension. It does not involve high quantity of powder, since the suspension has to be in the right concentration to deliver the needed particle rate. The system is at ambient temperature, since there is not the need of vapor flows. The pressure, however, has to be higher than the plenum one, in order to inject the liquid. This system, obviously, presents its own issues. Some of these are immediately clear, for instance the liquid has to evaporate before the particle enters the test section, while others depend on the specific layout of the seeding system.

5.4 DESIGN CONSTRAINTS

The system has to comply with some constraints that fix the values of the flow rates and volumes involved. The mentioned parameters are strongly correlated with optical parameters of the LDV system and the desired data rate.

A key parameter, when dealing with LDV measurements, is the mean particle concentration in the flow $\bar{n}_p$, because the higher is the particle concentration, the higher is the data rate. This is due to the fact that if the mean particle concentration $\bar{n}_p$ increases, more particle are likely to cross the measurement volume, thus increasing the data rate. On the other side, if the mean particle concentration increases, the probability of having more than one particle at the same time in the measurement volume is higher. Multiple particle in the measurement volume should be avoided, since the system would receive the contemporary scattering of more than one particle, resulting in an incorrect measurement. A statistical analysis results in three different mean particle number in the measurement volume $\bar{N}_p = V\bar{n}_p$ ranges [2]:

$\bar{N}_p < 0.1$ in this range, the probability of a single realization is 99.5%, thus the probability of multiple realization is 0.5%;

$\bar{N}_p \geqslant 0.1$ for these number of particle values, there is a significant probability of multiple particle signal, that deteriorate the signal quality and the data rate;

$\bar{N}_p > 10$ in this range, the probability of multiple signals is so high that the signal obtained is quasi continuous.

Given the previous particle number $\bar{N}_p$ ranges, a practical bound for the maximum mean particle concentration is obtained:

$$\bar{n}_p \leqslant \frac{0.1}{V_d}, \tag{30}$$

where the V_d is the measurement volume. The measurement volume V_d, by assuming it is an ellipsoid, can be obtained as a function of the focal length of the LDV optics F, the expansion ratio ϵ, the beam diameter before expansion d_w, the laser wavelength λ and the angle between laser beams θ:

$$a_0 = \frac{2F\lambda}{\pi\epsilon d_w \cos\theta/2}, \tag{31a}$$

$$b_0 = \frac{2F\lambda}{\pi\epsilon d_w}, \tag{31b}$$

$$c_0 = \frac{2F\lambda}{\pi\epsilon d_w \sin\theta/2}, \tag{31c}$$

$$V_m = \frac{4}{3}\pi a_0 b_0 c_0, \tag{31d}$$

where a_0, b_0 and c_0 are the semi axis of the ellipsoidal measurement volume. The dimension of the measurement volume impacts directly on the spacial resolution. Another important parameter related to the measurement volume are the fringe spacing Δx_f and the the number of fringes in the measurement volume n_f:

$$\Delta x_f = \frac{\lambda}{2\sin(\theta/2)}, \tag{32a}$$

$$n_f = \frac{a_0}{\Delta x_f} = \frac{8F\tan(\theta/2)}{\pi\epsilon d_w}. \tag{32b}$$

Once determined optics and laser parameters, the measurement volume and the mean particle concentration needed can be easily obtained from Equation 31d and Equation 30. To achieve a higher data rate it is necessary to take the particle concentration $\bar{n}_p$ equal to $\bar{n}_p = \frac{0.1}{V_m}$.

At this point, if data from a CFD simulation are available, the mean particle flow rate needed can be obtained. Indeed, given the fluid velocity v_f, and the nozzle area profile, the volumetric flow rate $\dot{V}$ flowing through each section of the nozzle can be determined. Finally, the mean particle flow rate $\dot{n}_p$ can be obtained as

$$\dot{n}_p(x) = A(x)v_f(x)\bar{n}_p. \tag{33}$$

The x dependance has been made explicit, since the mean volumetric particle flow rate should be chosen as a function of the axis coordinate of the point where the measurement has to be done. The particle volumetric flow rate to be injected can be obtained by assuming spherical particles with

$$\dot{V}_p = \frac{\pi d^3}{6} \dot{n}_p. \tag{34}$$

The particle loading M is a degree of freedom and the particle rate $\dot{n}_p$ depends on the position on the nozzle axis. Once these parameters are known, the flow rates to be injected can be obtained.

The needed amount of particles is injected atomizing a MDM–particle suspension. The particle to liquid mass ratio $M = m_p/m_{MDM}$ is a degree of freedom in the design of the system. It can be chosen to better fit the characteristics of the system components. The mass flow rate of the seeding powder to be inseminated can be easily calculated with $\dot{m}_p = \rho_p \dot{V}_p$ and the particle loading M can be expressed alternatively as $M = \dot{m}_p/\dot{m}_{MDM}$, so the MDM mass flow rate can be obtained as

$$\dot{m}_{MDM} = \frac{\rho_p \dot{V}_p}{M} \tag{35}$$

and the volumetric one is

$$\dot{V}_{MDM} = \frac{\rho_p \dot{V}_p}{\rho_{MDM} M}. \tag{36}$$

The suspension mass flow rate is $\dot{m}_{susp} = \dot{m}_{MDM} + \dot{m}_p$, so the suspension mass and volumetric flow rate can be expressed as

$$\dot{m}_{susp} = \rho_p \dot{V}_p \left(1 + \frac{1}{M} \right) \tag{37a}$$

$$\dot{V}_{susp} = \frac{\rho_p}{\rho_{MDM}} \dot{V}_p \left(1 + \frac{1}{M} \right). \tag{37b}$$

However, in the considered application, M is much smaller than one, so $\dot{m}_{susp} \approx \dot{m}_{MDM}$.

The total volume to be injected during a test V_{inj} can be determined by knowing the duration of a test:

$$V_{inj} = \dot{V}_{susp} t_{test}. \tag{38}$$

5.5 POSSIBLE LAYOUTS

The considered system needs to be pessurized, to deliver a desired flow rate and to atomize the suspension in droplets of an appropriate dimension. Thus, a suitable layout must have a MDM–tracer reservoir, a pressurization system, some sort of system to control the flow rate and an atomizing device. Depending on the different existing methods and devices, some different configuration are proposed and summarized in Table 9.

Table 9: Seeding system layouts.

Reservoir	Pressurizing system	Flow measurement and control	Atomizer
Syringe pump	Syringe pump	Syringe pump	Ultrasonic atomizer
Stirred tank	High pressure nitrogen	Flow meter and metering valve	Ultrasonic atomizer
Stirred tank	High pressure nitrogen	Flow meter and metering valve	Hydraulic atomizer

The two pressurizing systems proposed are a syringe pump and high pressure nitrogen (a deeper explanation will be given successfully). The fundamental parameters of the syringe pump to be considered are:

SYRINGE VOLUME it fixes the maximum liquid volume available for the injection;

MAXIMUM FORCE AND SYRINGE SECTION the maximum pressure that the pump can reach depends on the force applicable on the piston and on the syringe cross section, since $p = F/A$;

SYRINGE MATERIAL it sets the maximum pressure achievable, due to mechanical stress constraints;

MAXIMUM AND MINIMUM FLOW RATES they need to be coupled with the process.

In our application, a high pressure is required, so stainless steel, high forces and small cross sections syringes are needed. The reduction of the syringe cross section corresponds to a reduction in its volume, that has to match the one required to perform a full test on the TROVA. In the first configuration, the syringe pump is also the flow measurement and control system. By displacing the piston of an amount Δx, an amount of liquid given by $\Delta x A$ is pumped, where A is the area corresponding to a section of the cylinder. Considering that this displacement takes place over time, by imposing a displacement a flow rate is imposed: $\dot{V} = vA = \frac{\Delta x}{\Delta t} A$. Two different atomizing methods are considered: the ultrasonic atomizer and the hydraulic atomizer (that exploits the Rayleigh instability). The ultrasonic atomizer is a nozzle fed by a pump and made vibrate longitudinally. This movement creates a wave pattern on the free liquid surface of the nozzle. By increasing the power supply, the vibration and thus the wave amplitude increases to a point where droplets start to detach. Different flow metering devices have been considered:
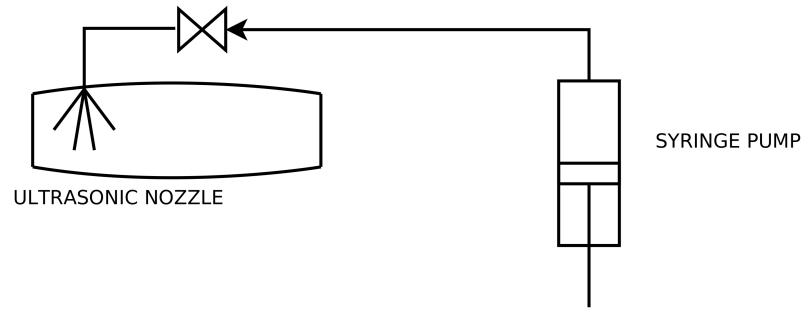
Figure 25: System A scheme.

GEAR FLOW METER it withstands high pressures (e. g. $350\,bar$) and works with a wide range of flow rates and low viscosity fluids;

TURBINE FLOW METER it is based on a small Pelton wheel and it has a lower flow rate bound that is higher than the previous meter. Works with high pressures;

Δp MEASUREMENT it is the simplest method. By measuring the pressure drop over a constant section straight pipe in laminar regime it is possible to use the Hagen-Poiseuille equation to extract the volumetric flow rate

$$\Delta p = \frac{128 \mu L \dot{V}}{\pi d^4}, \tag{39}$$

where $\dot{V}$ is the flow rate, L and d are the length and pipe diameter, respectively.

All pressurizing system/atomizer have been considered, except for one: the syringe pump/hydraulic atomizer one. The reason is that the syringe pump imposes a constraint on the flow rate. To reach the required pressure, it is necessary to use small syringes rather than the big ones. This implies a reduction in the maximum volume and, for a given duration of the test, in the flow rate. This low flow rate request is met by the ultrasonic nozzle, that can work with maximum $50\,ml/min$. Indeed, the hydraulic atomizer requires a much higher flow rate (e. g. $70 - 300\,ml/min$), so the coupling with the syringe pump is impossible.

In the following part of the section some aspects of the considered layouts are shown in detail.

5.5.1 *System A*

This system is represented in Figure 25. It consists of a syringe pump that pumps the required flow rate through the ultrasonic nozzle that atomizes the liquid. As previously mentioned, there is a maximum limit on the flow rate and the syringe volume. To deliver the needed
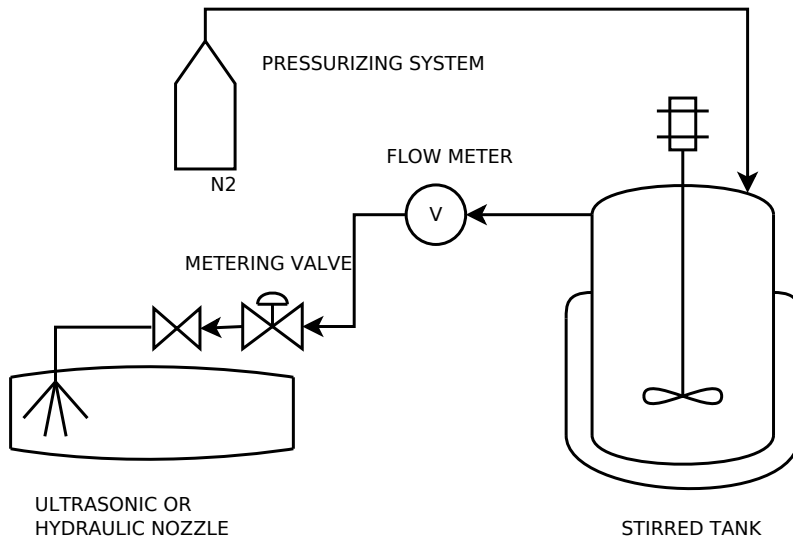
Figure 26: System B and C scheme.

quantity of particles to achieve the required concentration in the flow, a higher particle loading is necessary. Note that there is not a system to maintain an homogeneous suspension concentration and avoid the solid particles sedimentation, so before each test the operator should shake manually the syringe.

5.5.2 *System B*

This system (Figure 26) is composed by a tank filled by the MDM–tracer particles suspension, pressurized with nitrogen. To prevent the sedimentation of the solid, a stirrer may be present. The liquid is drawn from the tank and the flow rate depends on the pressure difference between the tank and the plenum where the suspension has to be injected. To finely regulate the flow, a valve could be added. The atomization is provided by the ultrasonic nozzle.

5.5.3 *System C*

The last system is schematically shown in Figure 26. As you can see, it is fundamentally identical to the previous system, except for the atomizer, that is the hydraulic nozzle. This atomizer requires higher flow rates, thus a lower particle loading could be used.
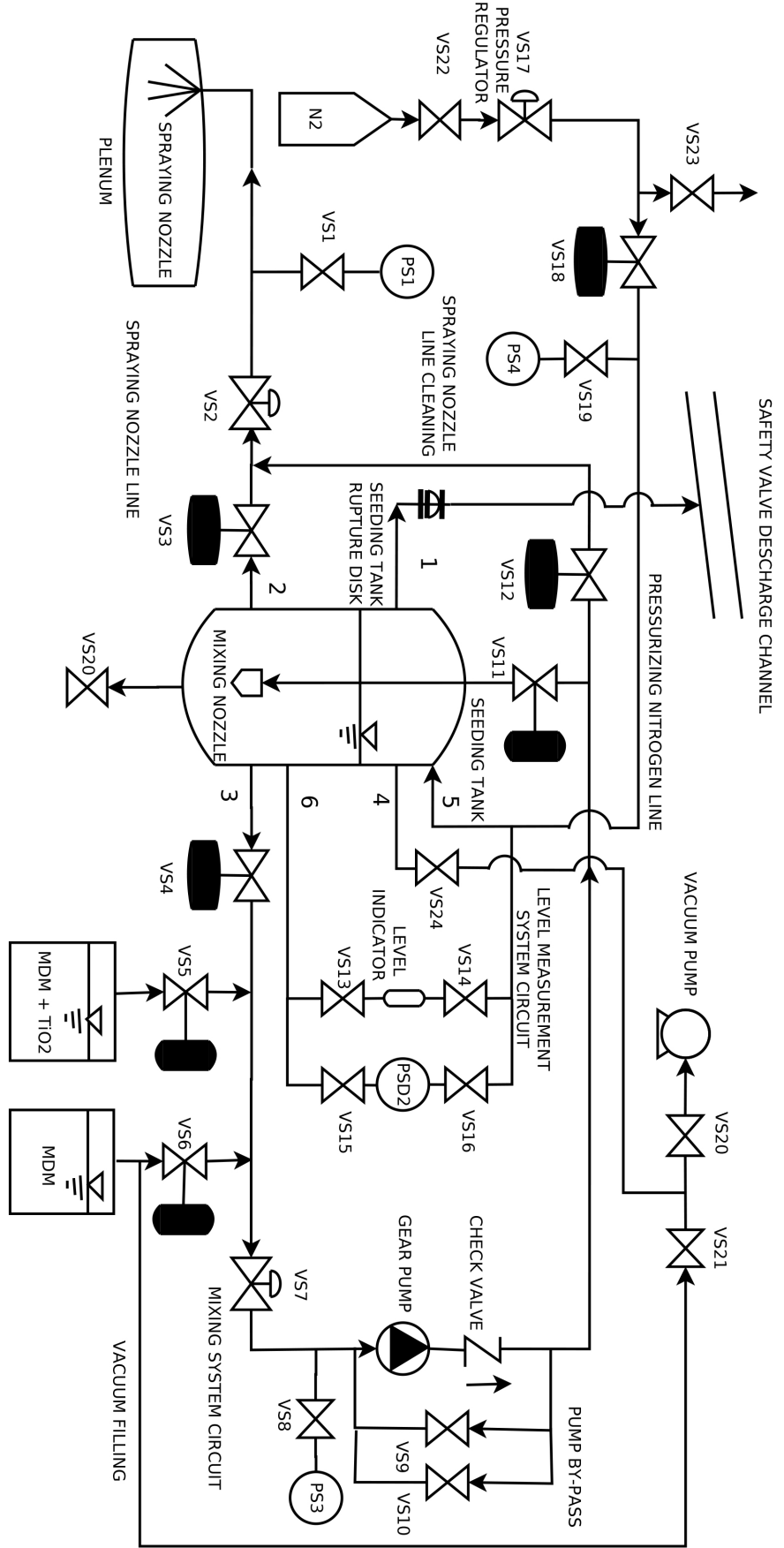
Figure 27: The designed system.

5.6 FINAL LAYOUT

By fixing a representative particle diameter $d_p = 250$ nm, the suspension particle loading can be selected to obtain the volumetric flow rate $\dot{V}_{susp}$ and the volume V_{inj} (see Section 5.4). With a particle concentration M in the range from $5 \cdot 10^{-5}$ to 10^{-7}, volumetric flow rates $\dot{V}_{susp}$ between 50 and 300 ml/min and injected volume V from 50 to 300 ml are obtained.

Figure 27 shows the complete layout of the system that has been finally chosen, namely the System C, described in Section 5.5. It is composed of a tank, surrounded by five subsystems. This tank is partly filled by a MDM–particle suspension, that has to be be injected into the flow, and it is pressurized with nitrogen.

The five subsystems are:

MIXING SYSTEM CIRCUIT The main purpose of this circuit is to maintain the suspension stirred, to avoid sedimentation. Furthermore, this circuit is designed also to draw the MDM–particles suspension from a reservoir, filling the seeding tank and to draw pure MDM to clean the other subsystems that could experience particle sedimentation. When functioning as a mixing circuit, it draws the suspension from the seeding tank and, through a pump, it recirculates it in the tank. The liquid is re-injected through a nozzle that creates a liquid jet that energizes and enhances the turbulence of the content. This leads in a homogeneous concentration and to the break-up of bigger particles;

LEVEL MEASUREMENT CIRCUIT It is useful, during the regular operations of the system, to know the level of the liquid suspension: this circuit serves this purpose, with a visual level indicator and a differential pressure meter (between the gas and liquid side);

PRESSURIZING NITROGEN LINE The seeding tank needs to be pressurized at a higher pressure than the plenum one. This is done by a circuit that maintains the pressure in the tank to a set value, by using high pressure nitrogen and a pressure regulator;

SPRAYING NOZZLE LINE This circuit draws the suspension from the seeding tank and atomizes it into the flow, regulating the rate at which the suspension is injected, with a metering valve;

VACUUM SECTION This section is useful to eliminate air in the system.

5.7 COMPONENTS CHOICE AND SIZING

In this section, each subsystem is analyzed in detail, giving information about their functioning and design issues.

Table 10: Connections of the seeding tank. Refer to Figure 28 and Figure 29 for the legend.

Connection	Line or subsystem connected
1	Rupture disk discharge pipe. The burst disk is positioned between the flanges in the drawing.
2	Spraying nozzle line.
3	Mixing system circuit, pump suction side.
4	Vacuum pump and filling.
5	Pressurizing nitrogen line and level measurement circuit, top connection.
6	Level measurement circuit, bottom connection.
7	None. It serves as drainage.
8	Mixing system circuit, pump pressure side.

5.7.1 *Seeding tank*

A pressure vessel is required, to contain the suspension, before the injection. Such a vessel should be designed for a pressure given by the maximum pressure achievable in the defined test (25 bar) plus the Δp required for the atomization of the proper flow rate. As mentioned in Section 5.3, in an early time, a cyclone tank was constructed. This vessel had a design pressure of 96 bar at ambient temperature and 50 bar at 400 °C, so it meets the pressure requirements, and has a volume suitable for our application (≈ 3.5 l). It is a vessel with a dished lower head and a flanged higher head. It needs some modifications to be adapted for the use as seeding tank. Some flanged connections have been added and other have been modified, to permit the vessel interfacing with the other subsystems. Figure 28 reports the drawing of the vessel with the modifications made to convert it from the cyclone configuration to the seeding tank of the new system and in Figure 29 it is reported an isometric representation. The new connections are sloping to permit the drainage of the liquid and are flanged LT/LG ANSI 6000, with a sleeve welded on a flange, to permit an easy connection with double ferrule compression fittings. Pipes are of Schedule 80. These classes and schedule ratings are required to match the needs of high pressure and temperature resistance.

In Table 10 is reported the list of connections and the subsystem to which they are connected, referring to the names reported in Figure 28 and Figure 29.

The bottom of the tank has to be flat, in order to permit the a proper functioning of the jet mixing system (see Section 5.7.2). The vessel has been designed with a draining line in axial position on the bottom, since this is the lowest point of the tank (see Figure 28, detail
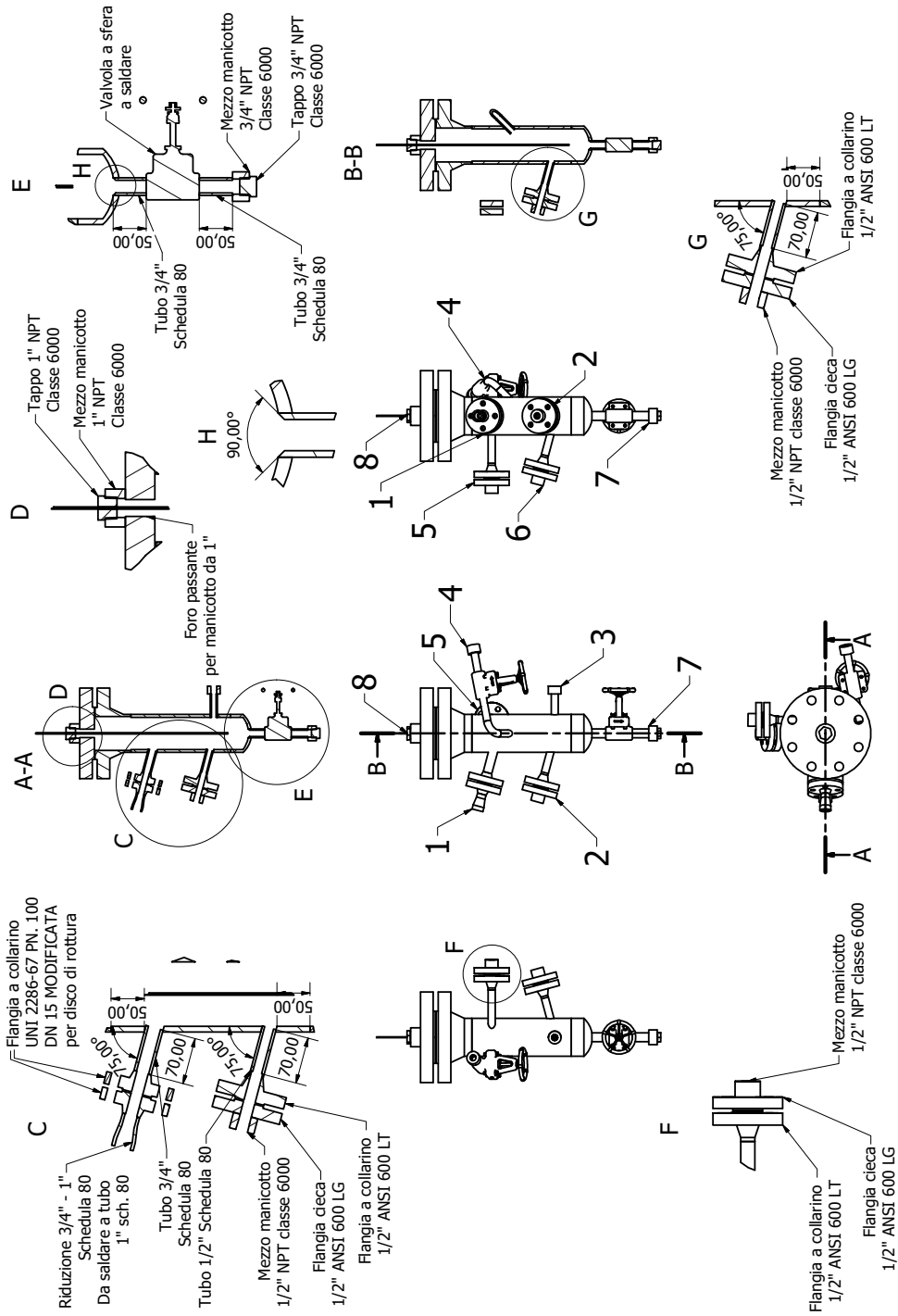
Figure 28: The drawing of the changes made on the seeding pressure vessel.
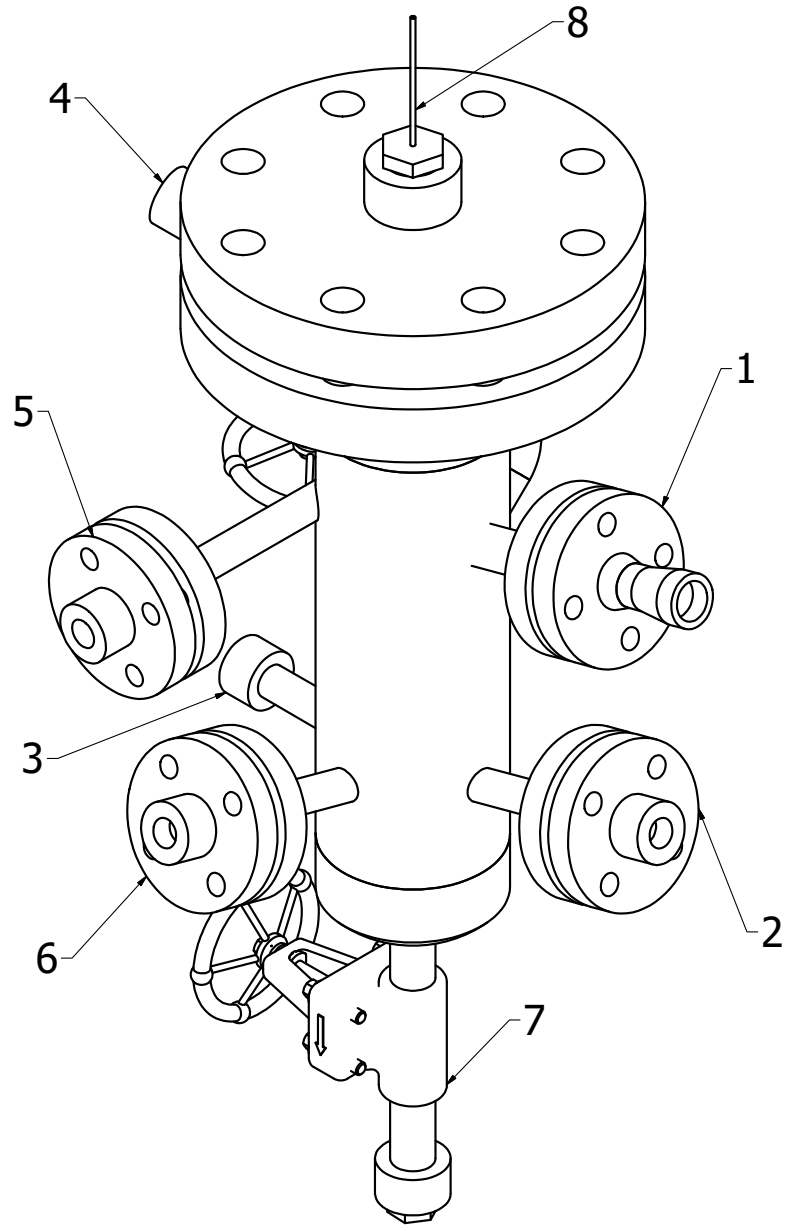
Figure 29: Isometric representation of the tank.
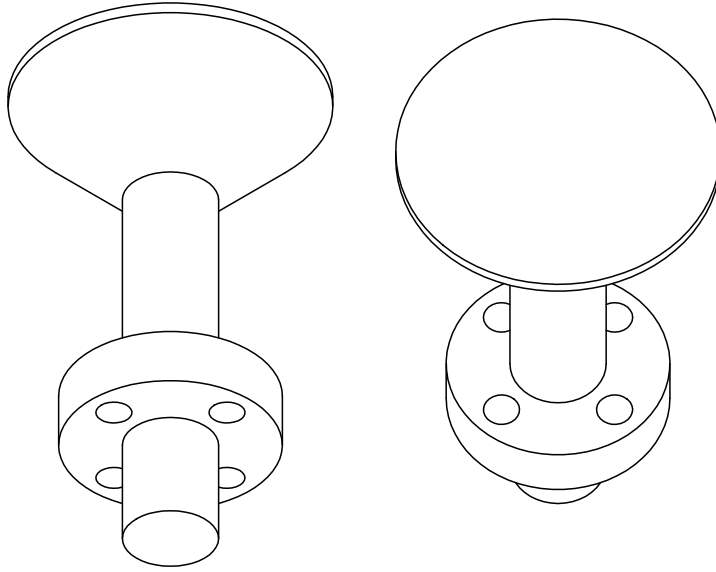
Figure 30: The drainage plug.

E). To obtain a flat surface, a plug analog to an automotive valve (and functioning in a similar manner of a sink stopper) has been designed (Figure 30). During normal operation of the tank, the plug is inserted into the 90° flared part (detail H in Figure 28, the conical part of the plug has a 90° angle) providing a flat bottom for the mixing. When it is necessary a drainage of the tank, the drain valve VS20 is opened and the plug is relieved from the lower side by the operator, with a proper stem. The disk, with four circumferential holes, provides the centering of the plug into the pipe and the mentioned holes permit the drainage of the liquid.

5.7.2 *Mixing system*

5.7.2.1 *Particle settling*

A common problem, when dealing with solid suspension is the particle settling. In the considered application, the sedimentation should be avoided, since this would result in a non-uniform particle concentration, thus in a variable particle flow rate injected. An index of the entity of the settling is the so called *free* (or *still-fluid*) *settling velocity*, the velocity for which the drag force, the buoyancy force and the gravitational force are balanced. The settling velocity could be obtained by a simple force balance on the particle in the vertical direction, yielding

$$m_p a_p = - \underbrace{\rho_p V_p g}_{\text{Gravity force}} + \underbrace{\rho_l V_p g}_{\text{Buoyancy force}} + \underbrace{C_D \frac{1}{2} \rho_l \left(v_l - v_p\right)^2 S}_{\text{Drag force}}, \quad (40)$$

where $V_p = \pi d_p^3/6$ is the spherical particle volume and $S = \pi d_p^2/4$ is the reference area. The free settling velocity is obtained letting $v_l = 0$ and $a_p = 0$, obtaining

$$v_s = \sqrt{\frac{4}{3}\frac{g d_p\,(\rho_p - \rho_l)}{C_D \rho_l}}, \tag{41}$$

where v_s is the settling velocity. The drag coefficient assumes a different formulation depending on the fluid dynamic regime. Assuming laminar regime, the drag coefficient C_D is function of the particle Reynolds number $Re_p = \rho_l\,|v_p - v_l|\,d_p/\mu = \rho_l v_s d_p/\mu$. Following the Stokes law $C_D = 24/Re_p$, yielding

$$v_s = \frac{g d_p^2\,(\rho_p - \rho_l)}{18\mu} \qquad Re_p < 0.3. \tag{42}$$

The solid concentration has an effect on the settling velocity of a single particle, Equation 42. This is due to the interaction between particles, to the upward fluid motion generated by the downward moving particles and to the increase of the apparent suspension density and viscosity. However, in the considered application, the free settling velocity is a sufficiently accurate estimate, since it is always greater than the hindered settling velocity, thus it is a conservative index for particle sedimentation. Furthermore, the volumetric particle concentration is low, so the solid concentration contribution is negligible. In the considered application, for particle diameter d_p from 100 nm to 200 nm, the settling velocity v_s ranges between 10^{-7} m/s and 10^{-8} m/s. However, the selected seeding powders tend to agglomerate and form bigger clusters. Given the quadratic dependency of the settling velocity on the particle diameter d_p, the settling velocity becomes higher, resulting in settling time of the order of hours for particle diameters of the order of a few μm.

The free settling velocity is low, but a mixing system is required, due to the coagulation.

This leads to the need of a mixing system to maintain the suspension stirred.

5.7.2.2 *Design of the mixing system*

The most common mixing device consists of an impeller rotating at a fixed velocity. This solution has been discarded, due to the high resulting cost. One less common method is the jet mixing: the turbulence created by a high speed jet is exploited, to mix the suspension. The reader interested in jet mixing configurations can find more information in [32]. The best configuration is a down pointing mixing nozzle, creating an axial jet that impacts on the lower cap of the tank. This jet creates two counter rotating vortices (if the tank is seen in section) and enhances the turbulence, thus the mixing. For this reason, on the lower cap, has been mounted the plug of Figure 30. The nozzle needs to be immersed and should be below half of the suspension height.

Commonly, the smaller practical distance between the nozzle and the bottom of the tank is assumed. However, it should not be lower than eight nozzle diameters, to avoid the tank erosion. This distance does not play a significant role in the minimum velocity to suspend the solid. The so called *just suspended* velocity can be estimated with [16]

$$v_{js} = 2 \left(\frac{\rho_p - \rho_l}{\rho_l} \right)^{2.08} \frac{v^{0.16} g^{0.42} d_t^{1.16} d_p^{0.1} C_w^{0.24}}{d_j}, \tag{43}$$

where

v is the kinematic viscosity;

d_t is the tank diameter;

C_w is the percentage weight fraction of solids;

d_j is the jet diameter.

With a jet diameter $d_j = 2\,mm$, a just suspended velocity between $10^{-4}\,m/s$ and $10^{-3}\,m/s$ is found, for particle dimension d_p and particle density ρ_p of the selected seeding powders (Table 8) and particle loading M in the aforementioned range (Section 5.4).

A good practice is to assume a jet velocity of at least $10\,m/s$ [16]. The designed system draws a liquid flow rate from the lower part of the seeding tank and recirculates it through a pump and a mixing nozzle. The selected pump represents a critical component. The working fluid is the fluid tested on the TROVA (siloxane MDM), therefore the pump should not have lubricated parts that could contaminate the fluid. The flow rates required are small, of the order of a few liters per minute and it has to provide the fluid only the energy to overcome the pressure drop on the circuit. Pump geometry is well discriminated by a couple of non-dimensional parameters called *specific diameter* and *specific velocity*, defined as

The mixing nozzle creates an axial jet impinging on the lower cap at $10\,m/s$, that enhances the turbulence of the suspension.

$$D_s = D \frac{\Delta h_{is}^{1/4}}{\sqrt{\dot{V}}} \tag{44a}$$

$$\omega_s = \omega \frac{\sqrt{\dot{V}}}{\Delta h_{is}^{3/4}}. \tag{44b}$$

For low volumetric flow rates (low ω_s), volumetric pumps give better performances than turbo-pumps. Due to the need of a oil free machine, a gear pump has been selected. In gear pumps, the working fluid has also to lubricate the rotating gears that displace the fluid from the low pressure reservoir to the high pressure one. For this reason, gear pumps are usually used with high viscosity fluids. Unfortunately, MDM is a low viscosity silicon oil ($\mu = 874.86\,Pa\,s$), therefore the pump will tend to have a shorter life than in case of using a common oil.

The pump is a gear pump. The low viscosity of MDM is a critical aspect, since this leads to a poor lubrication of the gears.

A problem strictly connected with the specific selected pump is the maximum suction side pressure. It must not exceed $25\,\mathrm{bar}$. To avoid overpressure on the suction side, the needle valve VS7, imposing a proper pressure drop, and the pressure meter PS3 are present. The suitable valve, in general, should avoid cavitation and should permit the right coupling between the pressure drop Δp and the volumetric flow rate $\dot{V}$. This relation is represented by the flow factor K_v and the flow coefficient C_v, defined as

$$K_v = \dot{V}_{si}\sqrt{\frac{1}{\Delta p_{si}}\frac{\rho_f}{\rho_w}} \tag{45a}$$

$$C_v = \dot{V}_i\sqrt{\frac{1}{\Delta p_i}\frac{\rho_f}{\rho_w}} \tag{45b}$$

$$K_v = 0.865 C_v, \tag{45c}$$

where

$\dot{V}_{si}$ is the volumetric flow rate through the valve in $\mathrm{m^3/h}$ or $\mathrm{ml/min}$;

$\dot{V}_i$ is the volumetric flow rate through the valve in US units, gpm;

Δp_{si} is the pressure drop across the valve, fixed at $100\,\mathrm{kPa}$;

Δp_i is the pressure drop across the valve, fixed at $1\,\mathrm{psi}$;

ρ_f is the fluid density;

ρ_w is the water density.

The flow factor K_v and the flow coefficient C_v represent the flow rate of water at the fixed pressure drop across the valve. The pump is supplied with an electric engine, rotating at a constant speed of $1450\,\mathrm{rpm}$. The gear pump, at the mentioned speed, supplies $2320\,\mathrm{ml/min}$. Given that the system will probably work at a maximum pressure of $35\,\mathrm{bar}$, by taking a safety margin of $2\,\mathrm{bar}$, the maximum pressure drop on the needle valve is $12\,\mathrm{bar}$. The lowest pressure drop is $1\,\mathrm{bar}$, when the system is operating at $24\,\mathrm{bar}$ and a further $1\,\mathrm{bar}$ decrease is required to work safely. The C_v resulting from these Δp ranges are reported in Table 11. In Figure 31 is reported the C_v curve for the VS7. The needle valve VS7 has a maximum C_v of 0.16, so, when the valve is fully open, the pressure drop is $0.83\,\mathrm{bar}$. Thus, if the pump is activated with a tank pressure $p_t = p_{atm}$, there is no cavitation, since the saturation pressure at $T = 20°C$ of MDM is $3.5\,\mathrm{mbar}$. Two by-pass connected in parallel to the pump are also present, to regulate the delivered flow rate.

On the suction side of the pump, there are two reservoir, one containing pure MDM and one filled with MDM–particle suspension at the desired concentration. The first is used to clean the lines from

Table 11: C_v values for VS7.

$\dot{V}$ [ml/min]	2320	2320
Δp [bar]	1	12
ρ/ρ_w	0.826	
K_v [l/min]	2.109	0.609
K_v [m^3/h]	0.127	0.037
C_v [gpm]	0.147	0.042
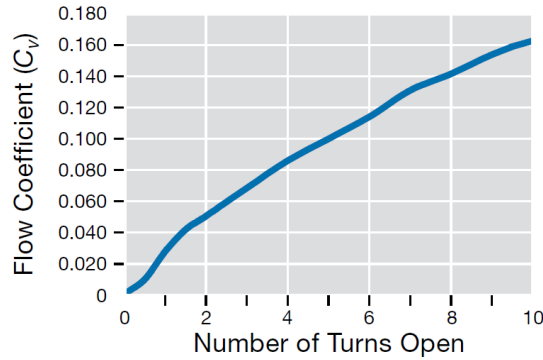
Figure 31: C_v for the needle valve VS7.

seeding powder residues and the second is used to fill the seeding tank with the required suspension amount for a test.

Concerning shut-off valves, they are direct solenoid valves with a maximum line pressure of 105 bar. The valves on the suction and pressure side of the pump (VS4 and VS11) are normally open valves, since, in case of failure of the actuator, the flow rate imposed by the pump has to be garanteed, otherwise the pump motor fails. The valves on the reservoirs (VS5 and VS6) ere normally closed. As for the needle valve, the C_v (or K_v) of the valve is a very important parameter. In this case, it is not the pressure-flow rate coupling the critical thing, since these are not metering valve and the pump is volumetric (thus it imposes a flow rate, regardless of the head). The most important issue to be considered is the cavitation. Given the flow factors reported in Table 12, Δp of 0.95 bar are obtained for VS5 and VS6 and 0.54 bar are obtained for VS4 and VS11. In case of the valves VS5 and VS6, since the reservoirs are at ambient pressure, the pressure directly downstream the valves would be 50 mbar, well above the saturation pressure of MDM at ambient temperature. However, since non-condensable gases can increase the incipient cavitation pressure or cavitation nuclei can be present, it is better to reduce the flow rate acting on the by-pass.

Table 12 reports the principal characteristics of the mixing system components.

The mixing system is designed also to fill the tank and clean the lines.

Table 12: Principal specifications of the components of the mixing system.

Component	Name	Specifications	
Shut-off valve	VS5 and VS6	Model	Evian 121V5463
		Rest position	Normally closed
		Actuator	Solenoid (direct)
		K_v	1.5 l/min
		Rating	105 bar
		Differential P	$0 - 60$ bar
	VS4 and VS11	Model	Evian 122V8306
		Rest position	Normally open
		Actuator	Solenoid (direct)
		K_v	3.5 l/min
		Rating	105 bar
		Differential P	$0 - 12$ bar
Pressure transducer	PS3	Model	SMERI T72
		Type	Absolute
		Full scale	50 bar
		Accuracy	0.1% FS
		Signal	$4 - 20$ mA
		Power supply	$12.5 - 30$ Vdc
	VS1	Actuator	Manual
		Type	Ball
		Rating	300 bar
Metering valve	VS7	Model	Swagelok SS-4L2
		Type	Needle
		Material	346 SS
		P_{max}	68.9 bar
		T range	$-23\,°C$ to $204\,°C$
		Seals	FKM
		$C_{v,\,max}$	0.16 gpm

5.7.3 *Vacuum system*

This system is composed by the TROVA vacuum pump connected to the system through the valve VS20. This system is necessary for the first filling of fluid or for the removal of air (oxygen has to be removed from the system) before the pressurization.

5.7.4 *Pressurizing system*

The pressurizing system is composed by a high pressure nitrogen tank, connected to a pressure regulator (VS17) and a two way actuated valve (VS18). A valve (VS23) connects the system to the environment. The functioning principle is simple: N_2 is stored in a high pressure reservoir and, when the on/off valve is opened, the gas flows to the seeding tank (the low pressure reservoir) and pressure tends to stabilize to a value that is intermediate between the initial two. After the transient has terminated and since nitrogen can be treated as an ideal gas, the resulting pressure is given by

$$pV = mRT \qquad (46)$$

where V is the volume occupied by the gas, p is its pressure, m is its mass in the system considered, T is its temperature and R is the ideal gas constant. If the gas is free to expand, the pressure in the seeding tank can become too high, so a pressure regulator is required. It maintains a set pressure in the low pressure side by regulating dynamically the mass flow rate from the N_2 tank to the seeding tank. From Equation 46, can be seen that a change in the set pressure, the fluid temperature or volume implies a change in the mass of gas. Thus a flow rate is required:

The system pressure is regulated by dynamically injecting nitrogen into the seeding tank.

$$\dot{m} = \frac{1}{R} \frac{d\,(pV/T)}{dt}. \qquad (47)$$

An absolute pressure transducer (PS4) is placed downstream the pressure regulator and the on/off valve to monitor the pressure value in the seeding tank. In Table 13 some specifications of the components of this subsystem are reported. Since high purity gas is not needed, a 5.0 nitrogen (corresponding to a purity of 99.999%) has been chosen. In the seeding tank, nitrogen and MDM are not separated by a membrane, so the diffusion of the gas into the liquid has to be considered. The concentration of nitrogen in MDM is proportional to its partial pressure, following the Henry law

$$p_{N_2} = H\,(T)\,x_{N_2}, \qquad (48)$$

where

$H\,(T)$ is the Henry constant;

Table 13: Principal specifications of the components of the pressurizing line.

Component	Name	Specifications	
Nitrogen tank	N₂	Manufacturer	Sapio
		Pressure	$200\,bar$
		Purity	5.0
		Volume	$40\,l$
Pressure regulator	VS17	Model	Insert Deal R133HDQ
		$P_{in,\,max}$	$220\,bar$
		P_{out}	$5 - 50\,bar$
		$\dot{m}_{max}$	$544\,kg/h$ ($P_{in} = 200\,bar$, $P_{out} = 50\,bar$, $T = 20\,°C$)
Shut-off valve	VS18	Model	Evian 121V5463
		Rest position	Normally closed
		Actuator	Solenoid (direct)
		K_v	$1.5\,l/min$
		Rating	$105\,bar$
		Differential P	$0 - 60\,bar$
Pressure transducer	PS4	Model	ABB 2600T 364HS
		Type	Relative
		Full scale	$80\,bar$
		Lower limit	$0.7\,mbar$
		Minimum span	$0.8\,bar$
		Accuracy	$\pm 0.075\%\,FS$
		T_{max}	Sylicon oil: $121\,°C$
	VS19	Actuator	Manual
		Type	Ball
		Rating	$300\,bar$

x_{N_2} is the molar fraction of nitrogen in the liquid phase.

The temperature dependance of the Henry constant is described by the Van't Hoff equation

$$\frac{d\,(\ln H)}{d\,(1/T)} = -\frac{\Delta H_s}{R}, \tag{49}$$

where ΔH_s is the solubilization enthalpy, thus an increase in temperature T reduces the concentration of the gas in the liquid. N_2 is a very stable compound, so it is very unlikely the possibility of chemical reactions between nitrogen and MDM, although temperature higher than $300\,°C$ may be reached. The gas initially solubilized, however, tends to be released in the LPV, that is under vacuum conditions (due to the low saturation pressure of MDM at ambient temperature, which is the large majority of the fluid in LPV). The released N_2 is then removed with other non condensable gases with a vacuum pump.

The non condensables are evacuated with the TROVA vacuum pump.

5.7.5 *Atomizing system*

The atomizing system is the last subsystem, before the injection of the particles. The liquid suspension is drawn from the seeding tank and sprayed through a nozzle. The flow rate depends on the Δp across the atomizer. The nozzle has a $\dot{V} - \Delta p$ characteristic curve that is influenced by the geometry and by the working fluid. The seeding tank is pressurized in order to have the pressure difference that roughly gives the required flow rate. A fine regulation is done with the metering valve VS2. A pressure transducer is needed right before the nozzle, to monitor the pressure difference across the atomizer.

In Table 14 are reported the specifications of the atomizing line components. The chosen atomizer is an hollow cone hydraulic nozzle. Its behavior depends on the fluid to be sprayed, and on the operative conditions. Generally speaking, an increase of the Δp on the nozzle implies a reduction of the droplet size and an increase in the flow rate. Data about droplet sizes, as function of the inlet pressure were not available for the selected model. However, according to the manufacturer indications, similar nozzles led to particle dimensions of $\approx 200\,\mu m$ at $30\,bar$ and $\approx 85\,\mu m$ at $10\,bar$ of pressure drop. These are only guidelines, since the nozzle was not the considered one and the tested fluid was water. These motivations lead to the conclusion that a sizing test with the chosen nozzle and fluid should be done in the future. Concerning the $\dot{V} - \Delta p$ curve, in Table 15 are reported the flow rate values for certain relative pressure values, for water in an atmosphere at ambient pressure. These table can be used as a guideline in the selection of the degree of pressurization of the seeding tank, but for a fine regulation, a needle valve is required, as previously mentioned. An experimental measurement of the curve with

The flow rate through the nozzle is regulated following the experimental $\dot{V} - \Delta p$ curve.

Table 14: Principal specifications of the components of the atomizing line.

Component	Name	Specifications	
Nozzle		Model	PNR RZQ 0080 B3
		Material	AISI 316
		Spray angle	60 °C
Metering valve	VS2	Model	Swagelok SS-6MG-MM
		Type	Needle
		Material	346 SS
		P_{max}	68.9 bar
		T range	−23 °C to 204 °C
		Seals	FKM
		$C_{v, max}$	0.03 gpm
Shut-off valve	VS3	Model	Evian 121V5463
		Rest position	Normally closed
		Actuator	Solenoid (direct)
		K_v	1.5 l/min
		Rating	105 bar
		Differential P	0 − 60 bar
Pressure transducer	PS3	Model	SMERI T72
		Type	Absolute
		Full scale	50 bar
		Accuracy	0.1% FS
		Signal	4 − 20 mA
		Power supply	12.5 − 30 Vdc
	VS1	Actuator	Manual
		Type	Ball
		Rating	300 bar

Table 15: $\dot{V} - \Delta p$ curve for water.

p [bar]	2.0	3.0	4.0	5.0	6.0	10	15	20	50
$\dot{V}$ [l/min]	0.07	0.08	0.09	0.10	0.11	0.15	0.18	0.21	0.33
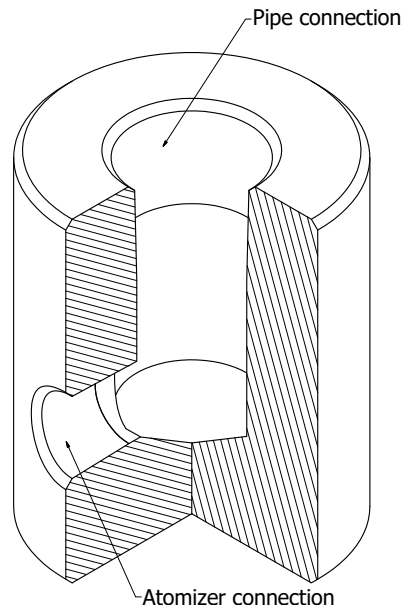
Figure 32: Spray nozzle mount.

MDM has been performed (see Chapter 6). There is a system that permits a rotation of the nozzle in counterflow or equiflow with the main MDM flow, without opening the plenum.

The atomizer is mounted having the jet coaxial with the plenum, on a custom made seat mount that provides a tough mounting without disturbing the flow (Figure 32). The pipe enters into the plenum vertically and the mount provides a 90° curve to align the nozzle with the horizontal direction.

As previously seen, Equation 4b gives the response time of a particle subjected to a step in fluid velocity. The response time τ relative to a particle of the selected powders accelerating from 0 m/s to fluid velocity ranges from 10^{-6} s to 10^{-7} s. Since the fluid velocity u in the plenum where particles are injected is of the order of 1 m/s, the distance to have a slip factor $s = 1\%$ is $4.6\tau u = 4.6 \cdot 10^{-6} \div 4.6 \cdot 10^{-7}$ m, far below the distance between the injection point and the test section. Furthermore, the particle is injected with a velocity $v_0 \neq 0$, so the needed distance is even lower.

Since the nozzle mount is a bluff body immersed in a flow, a wake will originate downstream. The flow outside the wake has a velocity of about 1 m/s. Reaching the test section, the flow accelerates to a mean value of about $15 - 20$ m/s, thus, even if the flow in the wake is completely separated (thus with a velocity of ≈ 0 m/s), the flow acceleration is so high, compared to the velocity defect in the wake, that the velocity profile at the test section inlet is expected to be uniform. Thus the wake influence on the nozzle flow can be neglected.

Table 16: C_v values for VS2.

$\dot{V} \, [\mathrm{ml/min}]$	300	70
$\Delta p \, [\mathrm{bar}]$	1	5
ρ/ρ_w	0.826	
$K_v \, [\mathrm{l/min}]$	0.273	0.028
$K_v \, [\mathrm{m^3/h}]$	0.016	0.002
$C_v \, [\mathrm{gpm}]$	0.019	0.002
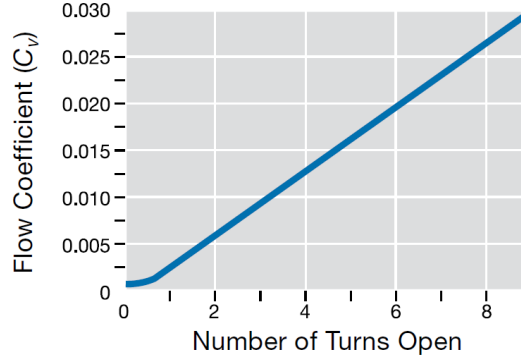
Figure 33: C_v [gpm] as function of the number of turns on VS2.

The metering valve, VS2, has to work with a flow rate between 70 ml/min and 330 ml/min, as imposed by the nozzle. The accepted overpressure of the tank with respect to the atomizer inlet is in the range 1 bar to 5 bar, thus the maximum and minimum values for C_v are 0.019 gpm and 0.002 gpm (Table 16). As can be seen from Figure 33, the selected valve perfectly lies in this range.

The pressure transducer PS1 and the shut-off valve VS3 have the same characteristics as PS3, VS5, VS6 and VS12, see Section 5.7.2.

5.7.5.1 *Droplet evaporation*

A parameter to be controlled, once the atomizer is chosen, is whether a droplet evaporates before it reaches the test section. First of all, it must be verified if the flow has a sufficient energy to heat up and evaporate the fluid. The energy balance on the plenum, if seen as an adiabatic system, is (Figure 34)

$$\dot{m}_1 h_1 \, (T, p) + \dot{m}_2 h_2 \, (T, p) = \dot{m}_3 h_3 \, (T, p) . \tag{50}$$

Temperature T_3 obtained for the different tests are reported in Table 17 and correspond to superheated vapor conditions. The energy available for complete evaporation of the liquid is quite high, as can be seen with the $\dot{Q}_{des}/\dot{Q}_{sat}$ ratio, the ratio of the power necessary to desuperheat the vapor up to saturated vapor to the power required to
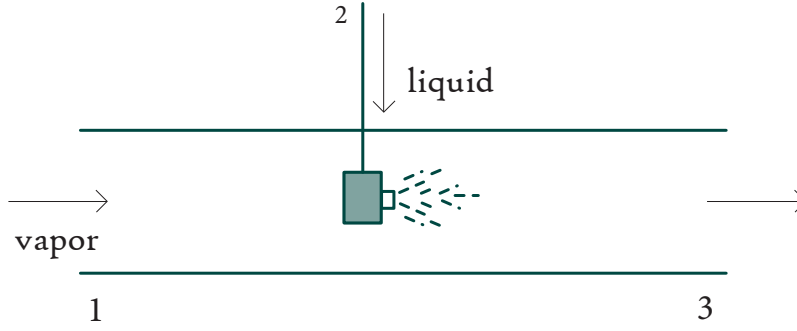
Figure 34: Scheme for the energy balance.

Table 17: Plenum energy balance data for a liquid flow rate $\dot{m}_l =$ 250 ml/min and liquid injected at $T_l = 20\,°C$.

Test	T_1	T_3	T_{sat}	$\dot{Q}_{des}/\dot{Q}_{sat}$
MDM_2	276.9	276.3	268	15.9
MDM_{1st}	253.2	251.6	214.3	26.7

reach saturated vapor conditions from the spray liquid state. Results are reported only for the MDM_2 and MDM_{1st}, since simulations for the test MDM_1 are not available, thus the mass flow rate cannot be estimated. The flow experiences a minor temperature reduction as a result of the mixing and evaporation of the liquid spray.

A simplified method to estimate the droplet lifetime could be used (based on [31]). The following assumption were introduced: droplet evaporation in a quiescent infinite medium, quasi-steady evaporation, uniform droplet temperature T_d equal to the saturation point $T_d = T_{sat}(p)$ and constant properties. By applying the mass and the energy transfer to the gas phase, an energy balance at the droplet-gas phase interface and noting that $dm_d/dt = -\dot{m}_{ev}$ (where m_d is the droplet mass and $\dot{m}_{ev}$ is the evaporated mass) after some manipulation a linear expression for the squared droplet diameter d_d^2 can be obtained:

$$d_d^2(t) = d_{d,0}^2 - \underbrace{\frac{8k_v}{\rho_l c_{pv}} \ln\left(\frac{c_{pv}(T_v - T_{sat})}{h_{fg}} + 1\right)}_{K} t, \tag{51}$$

where $d_{d,0}$ is the initial droplet diameter, k_v the vapor phase thermal conductivity, c_{pv} the vapor constant pressure specific heat, T_v the surrounding vapor temperature and h_{fg} the vaporization enthalpy. The droplet lifetime t_d can be calculated from

$$t_d = \frac{d_{d,0}^2}{K}, \tag{52}$$

letting $d_d^2(t_d) = 0$. By taking constant properties at a mean temperature between the boiling temperature T_{sat} and the surrounding vapor temperature T_v, droplet lifetimes of the same order of the time required to cross the distance between the atomizer and the test section are found.

The adopted model considers a droplet in a stationary medium other than the droplet material vapor (so the diffusion of the vapor is considered). Furthermore, in the TROVA, the droplet is injected at a much lower temperature than the surrounding superheated vapor and this can result in an initial partial condensation of the vapor on the droplet surface, thus increasing the droplet lifetime. There is also a slip velocity between the droplet and the surrounding medium (not considered in the model) that enhances the surface heat transfer, therefore initially the condensation can be further increased and subsequently, when the droplet has a sufficiently high temperature, the evaporation is increased, influencing the droplet lifetime t_d.

The droplet lifetime is comparable with the time required to cross the distance between the atomizer and the test section. A test should be performed to assess the evaporation rate.

5.7.6 *Safety devices*

The designed seeding system has to be protected against overpressure. An overpressure protection system has to permit the venting of the mass necessary to maintain the system pressure below a set value $p < p_{set}$. The underlying concept is that, once the opening pressure value is reached, the safety device should evacuate all the incoming energy, in order to maintain the system pressure unaltered. It is fundamental that the only energy required to perform this task is the fluid one.

A safety device should be designed, in order to protect the system from overpressures.

Although the TROVA is already protected with a relief valve on the HPV and a relief valve in series with a burst disk on the LPV, the seeding system is connected to the rest of the plant only through the atomizer, which has an orifice of $0.16\,\mathrm{mm}^2$. This orifice is inadequate in discharging the needed mass flow rate in case of emergency.

There are several handbooks providing synthetic and practical resumes on how to size a pressure safety device, such as [33] and [8], all referring to the API standards, [3] and [4]. The design procedure needs a series of parameters to be known. Fluid properties are a fundamental input for the proper sizing, in particular the following properties have to be known:

- fluid and state;

- molecular weight;

- viscosity;

- specific gravity, which for a liquid is referred to water, while for a gas it is referred to air;

- specific heat ratio;

- compressibility factor.

Operating conditions should also be known:

- operating pressure;

- operating temperature;

- maximum allowable working pressure.

To complete the set of sizing data, the relieving conditions are needed:

- required relieving capacity;

- set pressure;

- allowable overpressure;

- superimposed back pressure;

- built-up back pressure;

- relieving temperature.

The operating pressure and temperature are the values at which the system is normally operating. However, the equipment must be designed for a higher value, to allow for peaks and oscillations. The maximum allowable working pressure (MAWP) is the maximum allowable pressure in normal working, accounting for fluctuations and peaks. The set pressure for which a relief valve is designed is normally coincident with or slightly lower than the MAWP. The allowable overpressure is the referred to the MAWP and it is usually 10%.

There are essentially two types of pressure safety devices: pressure relief valves and rupture disks. A relief valve is basically made by an orifice closed by a disk, pre-loaded against the discharge section by a spring. The spring is designed to exert a force able to maintain the valve closed until the force exerted by the pressure on the disk balances the spring one. When the valve is open, it discharges the flow rate determined by the conditions in the tank and the orifice (the flow is usually chocked). When the pressure falls below the balancing value, the valve automatically closes. It is clear that only the fluid energy is needed to the operation of a relief valve. The pressure value downstream impacts on the opening, since it adds a positive contribution to the spring force and the valve tends to open for higher pressure. The back pressure may be a constant value, always present, or may build up during the discharge process, due to the filling of the downstream environment. A problem connected with this type of safety devices is the seat leakage. These devices should work for several hours with varying temperature and pressure conditions, that may lead to an improper seat tightness. The leakage could be a problem for the valve (that could be damaged by the leaked fluid), for the

cost of the lost fluid, and possibly for safety. Rupture disks are made by a diaphragm with a cross incision on the center, designed to open at a fixed pressure value. Once opened, the burst disk discharges fluid until the upstream and downstream pressure balance. Burst diaphragm, since it is a disc mounted between two flanges, does not suffer of leakages.

The most important task, in sizing a safety device, is the determination of the controlling cause of overpressure. There are many factors that can cause an over pressure and they have to be analyzed in magnitude and in the probability of their occurrence. In the TROVA seeding system there are two main cause of overpressure:

- the failure of the pressure regulator (VS17);

- an accidental fire.

The two causes of overpressure are the failure of the pressure regulator (VS17) and fire and can be considered separately.

The pressure regulator would discharge continuously a mass flow rate, until the upstream and downstream reservoir are at the same pressure, and this may result in a pressure greater than the MAWP. In case of fire, since the tank is a closed system, the incoming heat power increases the temperature, thus, at fixed volume, increases the pressure. The contemporary occurrence of these two events is very unlikely, so their magnitude can be evaluated separately. In the design procedure the mass flow rate to be discharged has to be defined. Once m_r is known, and given the opening conditions, it permits the determination of the orifice necessary to discharge the required flow rate. Indeed, the flow is usually chocked and the tank conditions and the orifice area are usually sufficient to determine the flow rate.

In the seeding tank, operating conditions can be very different: indeed, while the temperature is equal to ambient temperature, the pressure may be subcritical or supercritical, since the pressure in the plenum can range from 4 bar to 25 bar. This leads to an extremely wide range of opening condition, thus to considerable uncertainties in the sizing of the device. Furthermore, for the relief of supercritical fluids, the standards procedure for gas relief provides an oversizing (since standards are based on the ideal gas assumption), leading to more expensive valves and the destructive phenomenon called *chatter* (the continuous opening and closing of the valve, due to an excessive discharged flow rate). Rigorous design procedures to properly size a relief valve for supercritical fluids are available in literature ([9] and [15]). However, they treat the case of a tank filled with liquid that becomes super-critical due to a fire event. The seeding system case is different: great amount of nitrogen may be present into the tank (depending on the liquid MDM level and the degree of pressurization), leading to a further uncertainty in the sizing. Indeed, in case of fire, it is very uncertain the estimation of the power absorbed by the nitrogen gas phase and the MDM liquid phase. Depending on the contained nitrogen mass, on the absorbed power and on the working

pressure, the system can reach a pressure greater than the MDM critical pressure before the liquid reaches a saturated liquid state. These factors lead to the great uncertainty in sizing of a relief valve, therefore a rupture disk has been chosen.

A rupture disk has been chosen.

In case of failure of the pressure regulator, it is necessary to know the flow rate for the maximum N_2 reservoir pressure. This flow rate is given by the producer. The maximum flow rate in case of failure is 544 kg/h as shown in Table 13. According to [3], the orifice area can be obtained by

$$A = \frac{131160 m_r \sqrt{TZ}}{K C_d p_1 K_b \sqrt{M_m}}, \tag{53}$$

where

$A \; [mm^2]$ is the minimum effective area needed to discharge the required flow rate;

K is a coefficient which is a function of the ratio of specific heats at standard conditions;

C_d is the discharge coefficient;

K_b is the capacity correction for back pressure;

M_m is the molecular weight of the gas;

$p_1 \; [kPa]$ is the absolute relieving pressure;

$T \; [K]$ is the temperature at valve inlet;

$m_r \; [kg/h]$ is the required relieving capacity;

Z is the compressibility factor.

The relieving pressure is the sum of the maximum allowable pressure, the allowed over-pressure and the atmospheric pressure. With a maximum allowable pressure of 50 bar and a discharge coefficient $C_d = 0.6$ (it is a reasonable value for burst disks), a 19.2 mm² orifice is obtained. In Table 18 are reported the data used for the calculation.

In case of fire, as previously mentioned, the determination of the absorbed heat and of the relief conditions is very uncertain. Considering the seeding tank containing only a gas phase (e. g. in supercritical conditions), the orifice area may be calculated by

$$A = \frac{F A_v}{\sqrt{p_1}}, \tag{54}$$

where

$A \; [inches^2]$ is the minimum required effective area required to discharge the required flow rate;

Table 18: Orifice calculation data for pressure regulator failure.

MAWP [bar]	50
Over-pressure	10%
m_d	544 kg/h
K	356 for N_2
C_d	0.6
K_b	1
A	19.19 mm^2

A_v [inches^2] is the exposed surface area of the vessel;

p_1 [kPa] is the absolute relieving pressure;

F is a coefficient taking into account the discharge coefficient C_d, the fluid temperature and the ratio of specific heats.

The F coefficient is given by

$$F = \frac{0.1406}{C_d K} \frac{(T_w - T_1)^{1.25}}{T_1^{0.6506}}, \tag{55}$$

where

T_w is the vessel wall temperature in degree Rankine;

T_1 gas temperature in the tank in degree Rankine;

K is a coefficient function of the ratio of specific heats at standard conditions, the same as in Equation 53;

C_d is the discharge coefficient.

An expression for the K coefficient is

$$K = 520 \sqrt{k \left(\frac{2}{k+1} \right)^{\frac{k+1}{k-1}}}. \tag{56}$$

From Equation 54, a decrease in temperature leads to an increase in the orifice area. The lowest temperature compatible with Equation 54 is the critical temperature, since, below that value, MDM is liquid and Equation 54 is no more valid. With an absolute relieving pressure $p_1 = 50$ bar and a temperature , $T_1 = T_c$, the resulting nozzle orifice area is $A \approx 34$ mm^2. The determination of the thermodynamic status of the fluid to be relieved is strongly uncertain, mainly due to the uncertainty on the thermal power absorbed by the liquid and the gas phase. Due to this uncertainty, the selected burst disk has been strongly oversized and a 2 cm^2 orifice has been selected.

Table 19: Principal features of the selected burst disk.

Producer	Donadon SDD
Type	C-SCD
DN	1/2"
Material	ASTM A 240 316L
Bursting pressure	$50\,\mathrm{barg}$ at $22\,°\mathrm{C}$
Maximum operating pressure	$40.3\,\mathrm{barg}$ at $22\,°\mathrm{C}$
Tolerance on bursting point	$\pm5\%$
Discharge area A	$2\,\mathrm{cm}^2$

The principal features of the selected burst disk are reported in Table 19. It has been selected in ASTM A 240 316L, since the tank should work at ambient temperature and no de-rating with the increase in temperature has to be considered. The discharge line is connected with the TROVA relief valve discharge pipe.

5.8 SYSTEM CONTROL

The system is designed to be controlled either manually, through a series of switches on a control panel, or automatically, through the control program of the TROVA plant. Each solenoid valve and the pump can be controlled remotely from the control room. Currently, the software has not been implemented yet, therefore the operator should follow a precise procedure, to operate the system safely and avoid components damage. The software will be written in the forthcoming future. In the following are shown the procedure to follow for some common operation on the system.

Each actuated part should be controlled manually or by the software.

5.8.1 *First filling with MDM*

After the building of the system, or after a maintenance stop, the system should be re-filled with MDM. This operation can be easily done by connecting the system to the TROVA vacuum pump, through the connection 4 (see Figure 29). All valves, except for those connecting the system to the atmosphere, must be open. Once the system is under vacuum conditions, the system is connected to the pure MDM reservoir. When the valve VS21 is opened and VS20 is closed, MDM is sucked into the tank, and fills it. The level can be monitored through the visual level indicator and PSD2.

5.8.2 *Pressurization and de-pressurization*

During the pressurization of the system, VS13, VS14, VS3, VS12, VS5, VS6 and VS24 must be closed. Although, depending on the pressurization level, closing VS4 and VS11 may not be required, it is a good practice to close these valves, in order to preserve the pump from pressure values exceeding 25 bar. First, the system should be depressurized to vacuum conditions, to eliminate all the non-condensable gases. To pressurize the system, it is sufficient to open VS18 and VS22 and regulate the pressure to the desired value through VS17. The pressure value should not overstep the maximum operating value imposed by the burst disk: 40.3 bar. To de-pressurize the system, VS17 should be closed and the discharge valve VS23 should be opened.

5.8.3 *Filling*

The filling of the system should be performed at atmospheric pressure. Depending on the fluid required, VS5 or VS6 should be opened. Also VS11 should be opened. VS4 should be closed and the pump should be activated.

5.8.4 *Cleaning*

The cleaning operation is analogous to the filling one, with the difference that the liquid is drawn only from the pure MDM reservoir and the fluid is pumped through VS11 *or* VS12, to clean the nozzle *or* the atomizer respectively. During the cleaning of the spraying nozzle, all by-passes should be open, since the full flow rate provided by the pump would result in a pressure of a few hundreds of bar.

5.8.5 *Mixing*

The first important thing is to control the tank pressure through PS4. If the pressure value is higher than 25 bar, the procedure cannot continue. The system should be de-pressurized. If the pressure value is under 25 bar, VS4 and VS11 can be opened and the pump activated. If the desired tank pressure is higher than 25 bar, the pressurization should be divided in two steps: first it is necessary to pressurize below 25 bar, activate the pump, and regulate VS7 in order to have the desired pressure drop. Finally the system can be pressurized further to the desired value. This is necessary because the pressure on the suction side of the pump is reduced by the metering valve VS7 *only* if liquid is flowing.

5.8.6 *Test*

Before the start of a test, PS4 and PSD2 should monitored to have a tank pressure greater than the plenum one and a sufficient liquid level to start the test. If these requirements are satisfied, VS3 can be opened and the atomization starts. During the discharge of the tank, PS1 should be monitored to control the atomized flow rate. To conclude the test, VS3 should be closed. The end of the test can occur in advance if the tank pressure drops below the plenum value or the liquid level is not sufficient.

5.8.7 *Software*

The software should monitor the pressure value measured by PS1, PSD2, PS3 and PS4. Concerning PSD2, the pressure difference should be converted in the liquid level measurement. Obviously, each valve and the pump should be controlled by the software. The software should permit the actuation of each valve and the pump, through a button. Furthermore, a loop to perform automatically each of the presented operations should be implemented. The software permits to introduce an important automatic safety control on the tank pressure to avoid the exceeding of the maximum operative pressure.

The software should permit the implementation of automated safety procedures.

Part III

SYSTEM COMMISSIONING

The third part deals with the commissioning of the designed seeding system. The determination of the experimental $\Delta p - \dot{V}$ curve for the atomizer, the positioning of the LDV probe, an overview of the Burst Spectrum Analyzer and the tests that have been carried out on the seeding system during several TROVA tests are presented in Chapter 6. Conclusions of the present work and future developments are reported in Chapter 7.

6

SYSTEM IMPLEMENTATION AND RESULTS

6.1 THE CONSTRUCTED SEEDING SYSTEM

After the design process, the system has been finally constructed. In Figure 35 is reported a picture of the system. The tank at the center is the seeding tank, while the small diameter pipe entering the large diameter horizontal pipe (the plenum) is the atomizing line.

6.2 THE ATOMIZER CHARACTERISTIC CURVE

As previously seen in Section 5.7.5, an experimental investigation of the pressure–volumetric flow rate $\Delta p - \dot{V}$ curve of the atomizer is required, in order to control the injected flow rate. This curve correlates the pressure difference across the atomizer in order to inject a certain volumetric flow rate. The $\Delta p - \dot{V}$ curve can be obtained by filling the tank with MDM, pressurizing it at different pressure values and letting discharge the resulting flow rate through the atomizer at ambient pressure. The pressure difference on the nozzle is monitored by PS1, while the tank pressure is monitored by PS4. The flow rate is obtained from the level measurement of the liquid in the tank over time. The chart of Figure 37 reports the pressure difference Δp imposed on the nozzle and the pressure difference between the seeding tank and the ambient Δp_t as a function of the volumetric flow rate $\dot{V}$. The pressure difference on the nozzle Δp can be expressed as

$$\Delta p = \frac{\rho}{2} \left(\frac{\dot{V}}{C_d A} \right)^2 , \qquad (57)$$

where C_d is the discharge coefficient. By fitting the experimental data with a curve $\Delta p = K\dot{V}^\alpha$ and $\Delta p_t = K_t \dot{V}_t^\alpha$ (Δp and Δp_t in bar and $\dot{V}$ in ml/min), $K = 4.7646 \cdot 10^{-4}$, $\alpha = 2.0377$, $K_t = 8.8179 \cdot 10^{-4}$ and $\alpha_t = 1.9448$ are obtained (see Figure 37).

A relation of the type $\Delta p = K\dot{V}^\alpha$ is obtained for the atomizer which permits the control of the flow through the spraying nozzle.

In Figure 36 is reported a picture of the spray, for atomization in ambient air.

6.3 LDV PROBE POSITIONING

An important aspect to be treated is the LDV probe positioning. A good and accurate positioning is fundamental to perform a good measurement. The LDV probe is connected to an automatic traversing system, which is equipped with stepper motors. This system permits an accurate positioning of the probe along three orthogonal axis (three

Figure 35: Picture of the constructed seeding system.

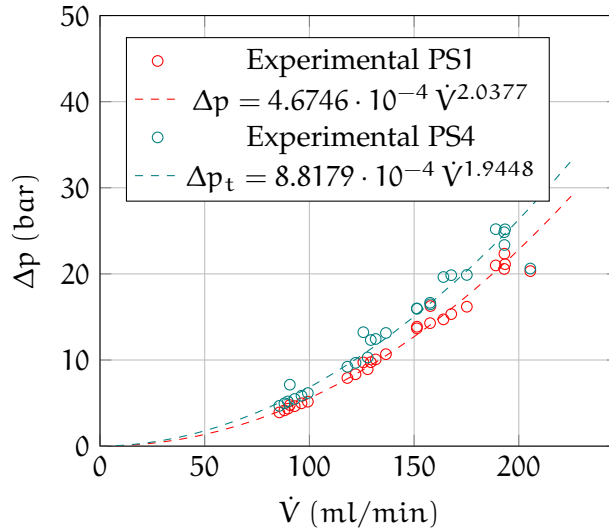Figure 36: Picture of the spray generated by the atomizer.

Figure 37: Pressure difference Δp imposed on the nozzle as a function of the volumetric flow rate $\dot{V}$.

degrees of freedom) and is controlled by the LDV software. In Figure 38 are shown the traversing system axis and their relative position with respect to the test section. The positioning of the traversing system is crucial: the traversing system axis $x - y - z$ must be parallel to the nozzle ones $x_n - y_n - z_n$. One more aspect has to be considered: the plane containing the two laser beams must be parallel to the $x - y$ (hence $x_n - z_n$) plane, to measure a velocity with no components on the y_n axis.

While positioning the LDV probe, the fact that the laser beams cross the quartz window and a region with MDM vapors has to be taken into account. Indeed, crossing materials different from air results in a change of the distance (from the lens) at which the beams are focused. The configuration of the TROVA application is depicted in Figure 39b. The Snell law is

$$\sin \theta_1 n_1 = \sin \theta_2 n_2, \tag{58}$$

where

θ_1 is the incident beam angle with respect to the surface normal;

n_1 is the refractive index of the first material;

θ_2 is the refracted beam angle with respect to the surface normal;

n_2 is the refractive index of the second material.

Equation 58 relates the angle of an incident an refracted beam crossing a surface between two different materials. The Snell law is valid for isotropic materials only. The material density plays a relevant role in determining the refractive index value. In Figure 40 are reported
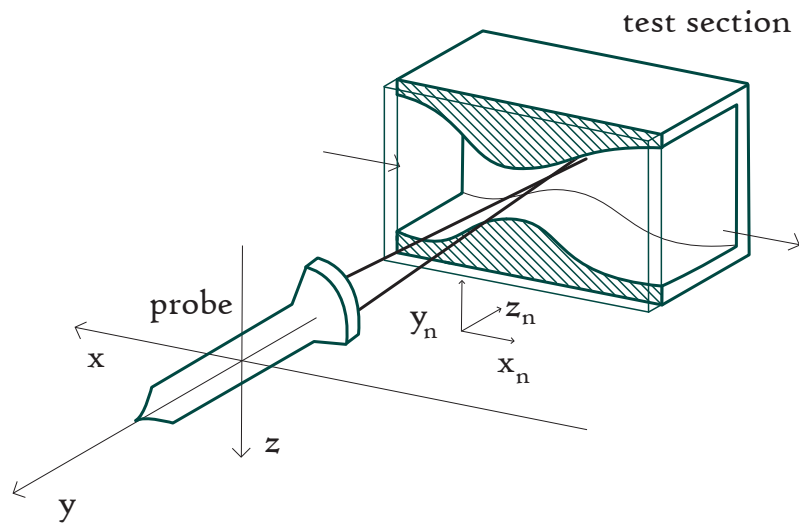
(a)
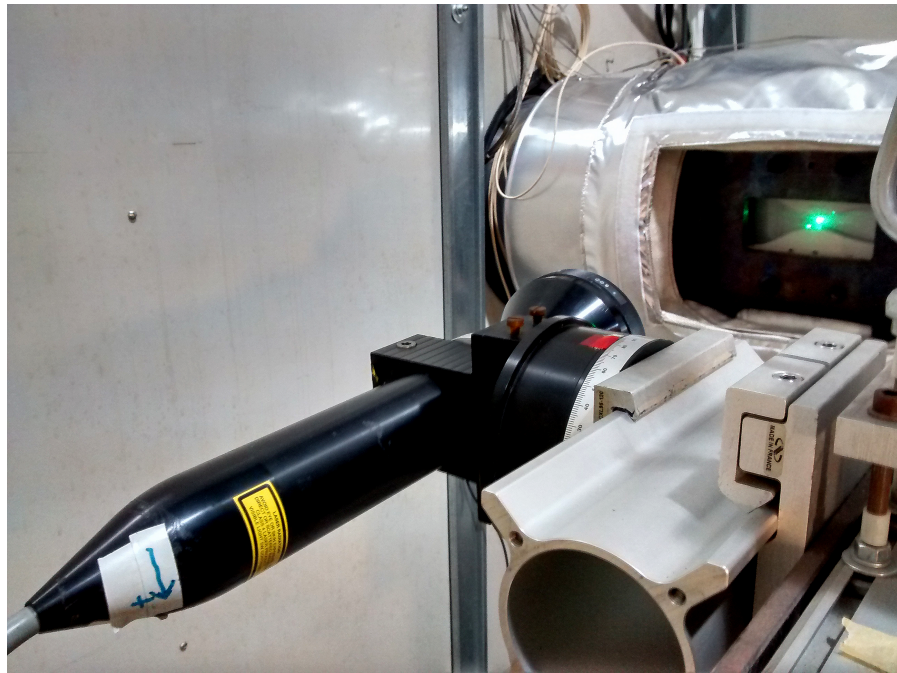
(b)

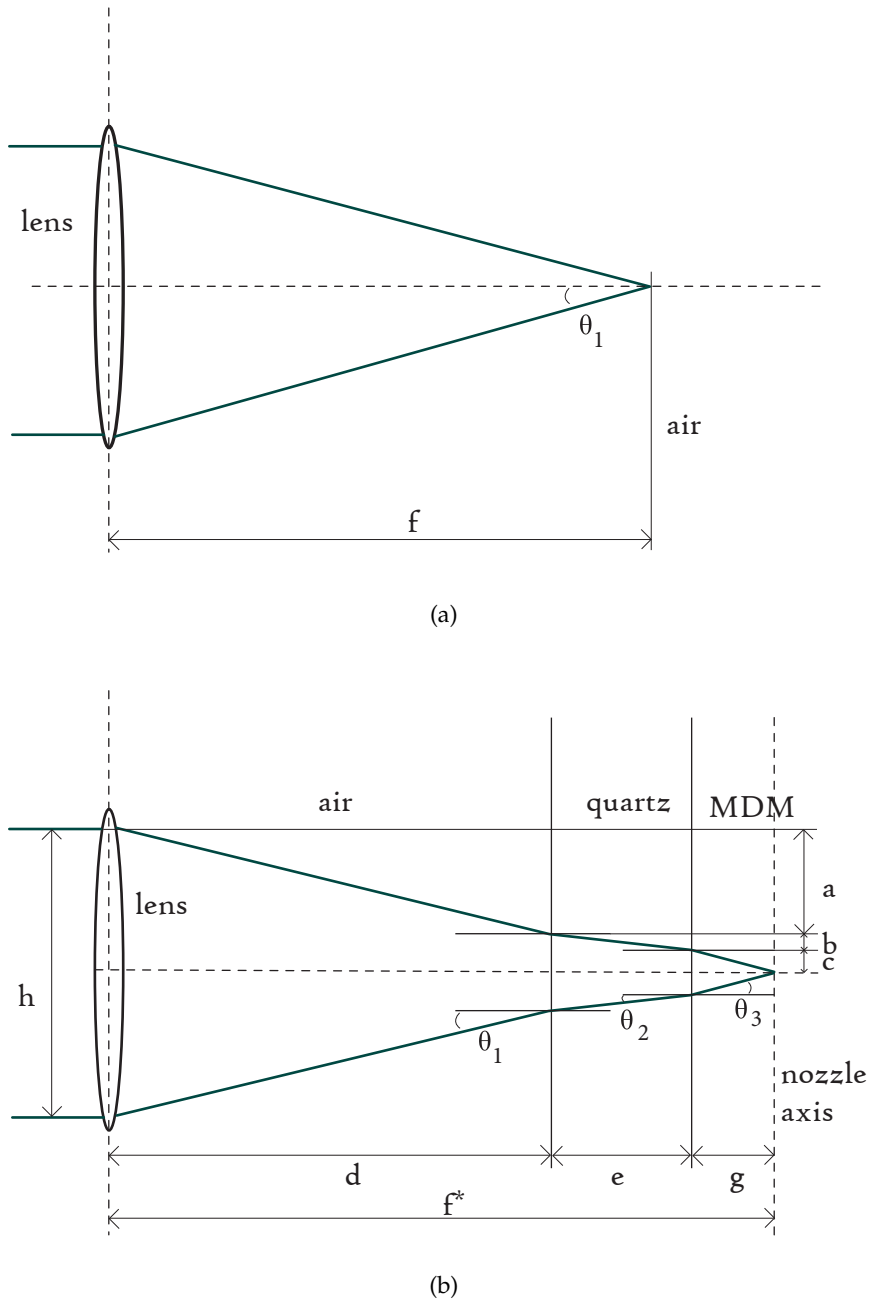Figure 38: Nozzle and traversing system relative position and axis.

(a)

(b)

Figure 39: (a) Beam focusing in air. (b) Beam focusing in the TROVA test section: after a first air part, the beams cross the quartz window and the MDM vapor.
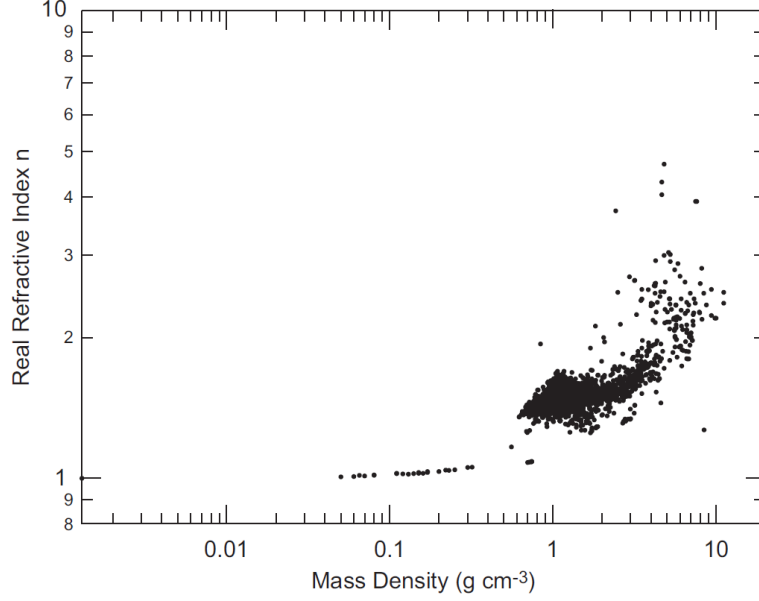
Figure 40: Experimental values of the refractive index n as a function of the material density ρ [12].

experimental values for the refractive index as a function of the material density [12]. The Lorentz-Lorenz relation is

$$\underbrace{\frac{\left(n^2 - 1\right) M_m}{\left(n^2 + 2\right) \rho_m}}_{\text{Molar refraction}} = \underbrace{\frac{N_A \alpha}{3}}_{\text{Molar polarization}}, \tag{59}$$

where

n is the refractive index;

M_m is the molar mass;

ρ_m is the material density;

N_A is the Avogadro number;

α is the mean molecular polarizability.

In [12] it is reported that the molecular polarizability α of a given material does not change much with temperature and pressure, thus the molar polarization and the molar refraction do not change with pressure and temperature. This result can be used to obtain the refractive index of the MDM vapor at the measurement point from available data referring to liquid MDM. In Table 20 is reported the molar refraction and the data used to obtain it. By manipulating Equation 59, the refractive index can be obtained as

$$n = \sqrt{\frac{M_m + 2R_M \rho_m}{M_m - R_M \rho_m}}, \tag{60}$$

Table 20: Molar refraction calculation data for MDM at ambient conditions (T = 20 °C, p = 1 atm).

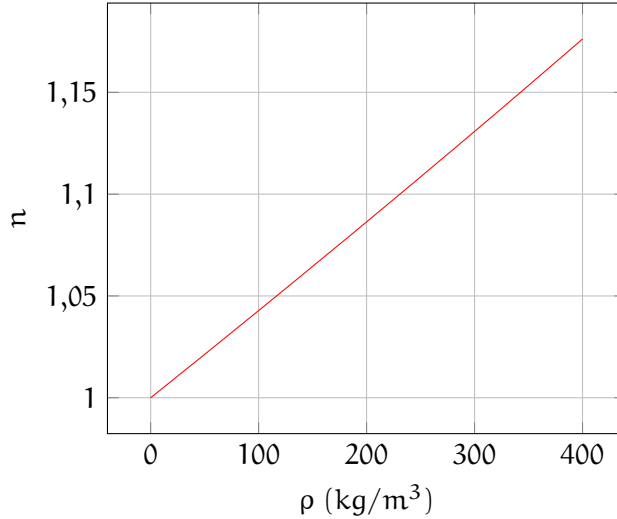|	
n_{liq}	1.3848 [1]
$\rho_m\ (kg/m^3)$	826.44
$M_m\ (kg/kmol)$	236.53
Molar refraction R_M	0.067

Figure 41: Refractive index n of MDM as function of density ρ.

where R_M is the molar refraction. In Figure 41 is reported the refractive index n as a function of the material density ρ. Once the n value is obtained, the distance f^* from the lens where the laser beam are focused is given by the solution of (for the nomenclature refer to Figure 39)

$$
\begin{cases}
a = d \tan \theta_1 \\
b = e \tan \theta_2 \\
c = g \tan \theta_3 \\
a + b + c = \frac{h}{2} \\
n_1 \sin \theta_1 = n_2 \sin \theta_2 = n_3 \sin \theta_3 \\
\frac{h}{2f} = \tan \theta_1 \\
f^* = d + e + g
\end{cases}
. \qquad (61)
$$

The distance from the lens where the laser beams are focused, in the TROVA test section, is higher than in air, due to the higher refractive index of the quartz and MDM with respect to air.

The data and the results for the calculation of f^* are reported in Table 21. The calculation of the distance d of the LDV probe from the quartz surface permits to position the measurement volume at the desired point. Due to the uncertainty correlated to the assumption of constant molar refraction, the correct positioning of the probe should

Table 21: f* calculation data.

f (mm)	600
h (mm)	38
e (mm)	45
g (mm)	9.35
f* (mm)	614.44

be verified. By setting a low photomultiplier voltage (see Section 6.4) and moving the probe along the y axis, the two points where the measurement volume impinges on the rear plate or on the quartz inner surface can be detected. Indeed, when the measurement volume impinges on a surface, the noise in the photomultiplier signal, visualized on an oscilloscope, increases and the probe must be placed in the middle of these two points.

6.4 BURST SPECTRUM ANALYZER

Before dealing with the testing of the system, a short overview on the parameters that influence the data processing in the Burst Spectrum Analyzer (BSA) is needed.

The BSA converts the Doppler signal in a velocity measurement.

The BSA converts the burst Doppler signal in a velocity measurement. The processor is controlled by a computer, which passes to the BSA the settings for the measurement. The BSA analyzes the frequency modulated signal, calculates the velocity associated to the signal and transmits the data to the computer, which saves the data in memory. There are different parameters that can be set by the operator:

PHOTOMULTIPLIER VOLTAGE The voltage value to be used is related to the laser power, the seeding quantity and the transparency of the optical windows. A higher voltage value makes the system more sensitive, but it increases the noise. So an optimum value has to be found as a trade-off between these two aspects, with a trial and error procedure;

GAIN This parameter impacts the signal amplification. It is obvious that increasing the gain also increases the noise;

FILTER CENTER VALUE The filter center value is the central value of the range of expected velocities. To perform a more accurate measurement, the system applies a filter to the signal, in order to focus on the range of Doppler frequencies corresponding to the expected velocity measurement;

FILTER SPAN The filter span is the width of the filter to be applied, thus the width of the velocity interval around the central value in which velocity measurements are expected;

RECORD LENGTH The BSA performs a *discrete Fourier transform* on the sampled signal and analyzes the spectrum to estimate the Doppler frequency. With an interpolation method, the frequency associated to the maximum power in the spectrum is estimated and taken as the Doppler frequency. The record length is the number of samples taken to reconstruct the frequency spectrum.

The photomultiplier voltage, the gain and the sample length must be set following the user's experience. The parameters related to the filters should be set based on the expected values and corrected, once again, with a trial and error procedure by analyzing the results of the performed measurements.

The BSA software requires the laser and optics data, in order to calculate the measurement volume parameters (as seen in Section 5.4) and the calibration factor C, that converts the Doppler frequency in velocity

$$v = C f_d. \tag{62}$$

6.5 EXPERIMENTAL RESULTS IN MDM SUPERSONIC FLOWS

After being constructed, some early tests have been performed, to assess the seeding capability of the system and the accuracy of the measurement. The seeding system has been tested with titanium dioxide and Aerosil 200 (silicon dioxide). The purpose of these early tests is to assess and verify that the designed system operates as expected and to perform a LDV measurement at one point where the velocity can be calculated with good approximation. For these purposes, different tests are necessary:

A velocity measurement trial at a point of the nozzle axis without seeding the flow. This is the reference case to which other cases must be compared;

B velocity measurement trial at a point of the nozzle axis, spraying pure MDM. This test is useful to assess if complete evaporation is achieved;

C velocity measurement trial at a point of the nozzle axis, spraying the MDM–seeding particle suspension. This test permits to understand if the flow is correctly seeded.

The tests have been carried out by measuring the total pressure, the total temperature before the atomizer and downstream of the test

section and the static pressure at the nozzle exit. Furthermore, the velocity at a point of the nozzle axis has been measured.

6.5.1 *Test A*

The Test A is a reference case, carried out without injecting the seeding nor the spray. No measurements were reported.

This test consists in focusing the LDV optic at a point in the nozzle and performing a measurement *without* spraying the suspension in the flow. If the flow is not seeded, the system should not validate any measurement. However, some impurities may be present in the flow. Indeed, some rust particles or dust may be present and could be detected by the system electronics. Furthermore, if a particular amount of noise is present, the system could validate fake burst signals. If some measurements are made in this configuration, tests B and C must be compared to the result of this test, to make any conclusion.

The tests have been conducted with different laser power and LDV parameters (see Table 22). In the early tests that have been performed, the LDV revealed some low velocity measurements, of the order of $50\,\mathrm{m/s}$, see Figure 42. The measurement volume is placed on the nozzle axis at the geometrical throat and the expected velocity in this point, for the total condition of the test, is $124.1\,\mathrm{m/s}$. These measurements are compatible with very large particles crossing the nozzle with a high slip velocity. However, another possible cause can be the presence of unwanted reflections. In fact, the measurement volume is placed near the rear plate and laser beams can be reflected in the receiving optics. Indeed, this was the reason for these low velocity measurements: the x axis of the traverse system was slightly off the parallel position and the reflected laser beams impinged on the probe lens. After this misalignment has been corrected, the performed tests no longer reported velocity measurements.

6.5.2 *Test B*

The test B is carried out by spraying pure MDM. Except for the initial and final transient periods, the evaporation is complete.

The Test B consists of a velocity measurement with a spray of pure MDM. If the vaporization of the spray is complete, no measurement point should be validated by the LDV system. Several tests have been performed with temperature and pressure conditions in the plenum in the range $p_{T4} = 1 - 2.2\,\mathrm{bar}$ and $T_{T4} = 225 - 250\,^{\circ}\mathrm{C}$ and atomized flow rate of $200\,\mathrm{ml/min}$. The pressure is quite below the one of the MDM_2 and MDM_{1st} tests. This choice was made to have a longer test time, since the TROVA is a blow down facility and the time of a recharge and heating of the HPV is of the order of several hours. In the condition of test B, the ratio of the desuperheating power to the saturation power $\dot{Q}_{des}/\dot{Q}_{sat}$ is ≈ 9, that is low, compared to the one of the MDM_1, MDM_2 and MDM_{1st} tests (see Section 5.7.5.1). This is a purely energetic consideration. On the other side, for a lower pres-

Table 22: LDV parameters for the reported tests. Lens focal length is 600 mm and the laser color is green.

| Test	Filter		Photomultiplier		Record length (–)
	Center value (m/s)	Span (m/s)	Voltage (V)	Gain (dB)	
A	97.5	130	952	35	64
B	97.5	130	952	35	64
C1a	97.5	130	928	25	64
C1b	130	260	928	30	64
C2	130	260	928	30	64
C3a	163	260	984	20	64
C3b	163	260	984	20	64
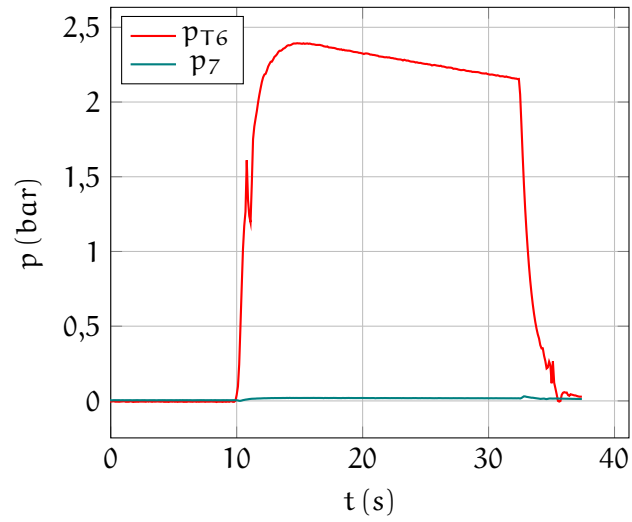
(a) *Nozzle total pressure p_{T6} and nozzle static outlet pressure p_7.*
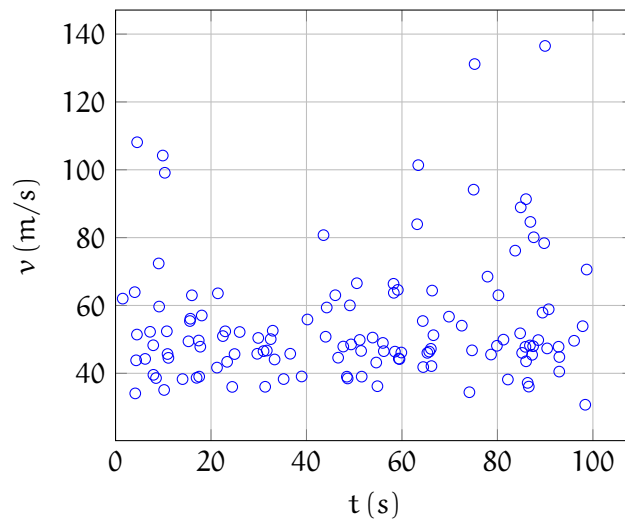
(b) *Velocity measurements.*

Figure 42: Pressure and velocity measurements for the Test A.
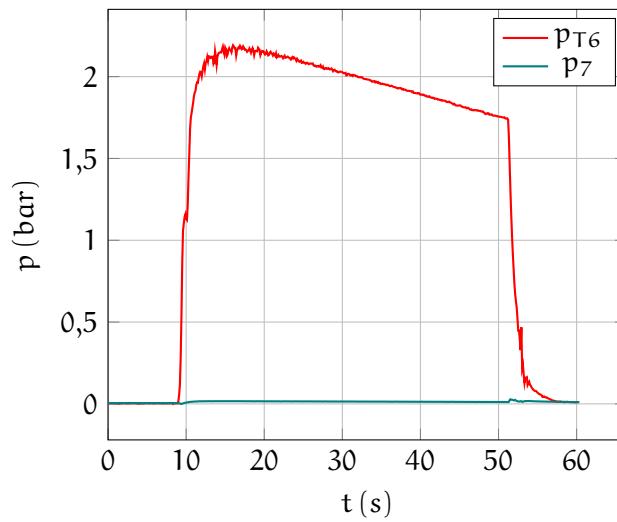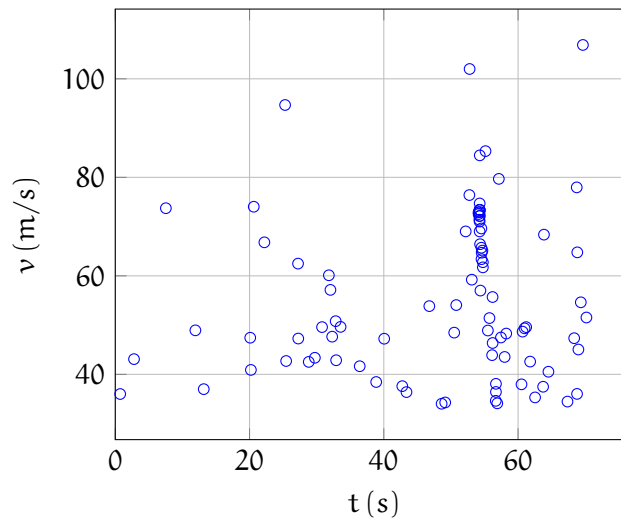
(a) *Nozzle total pressure* p_{T6} *and nozzle static outlet pressure* p_7.

(b) *Velocity measurements.*

Figure 43: Pressure and velocity measurements for the Test B.

sure, the atomized droplets tend to have a larger size, thus requiring a greater time for complete evaporation.

In Figure 43 are reported the velocity and the pressure measurements over time for the Test B. As it can be seen, the system validated some measurements of the same type of those attributed to noise in the test A. At the end of the test, at about $t = 54$ s, there is a large number of counts. An explanation of this phenomenon is given in Section 6.5.3.1. These tests lead to the conclusion that except for the transient period at the test conclusion, the evaporation is complete.

6.5.3   *Test C*

The test C consists in the atomization of the MDM-seeding particle suspension in the plenum. The Test C is divided in three different subcases:

C1 the seeding powder is Aerosil 200;

C2 the seeding powder is TiO$_2$;

C3 the seeding powder is made of impurities resulting from a pump failure.

The results and details of these tests will be presented in the following subsections.

6.5.3.1   *Test C1*

In Test C1, Aerosil is used as a tracker. The system detected particles only during initial and final transients.

The Test C1 has been carried out by spraying a MDM–Aerosil 200 suspension. The concentration of the seeding powder in the suspension is higher than the calculated one (see Section 5.4). This is because the seeding can remain attached to the tank walls or can be partially sprayed on the plenum walls, thus reducing the suspension concentration. Different concentrations have been tested, from $M_{Aerosil} = 0.1\%$ to $M_{Aerosil} = 0.5\%$.

In Figure 44 (Test C1a) are reported the measurements relative to a test with $M_{Aerosil} = 0.5\%$. The measurement volume has been positioned $15\,mm$ downstream the nozzle geometrical throat. This displacement of the measurement volume from the initial geometrical throat point is due to the fact that, during the early tests with Aerosil 200, an amount of seeding powder deposited on the optical window, in the convergent and throat part of the nozzle.

As for tests B, there is a set of measurements at the beginning and at the end of the test. These data are reasonably due to two reasons: at the start of the test, the valve V3 opens first, followed by the opening of MCV at a fixed position. During the opening of the MCV, a pressure wave propagates in the plenum and the fluid starts to move, until the regime condition is reached. Even though the transient is relatively fast, a short period of time where a low flow rate, thus a low energy carried by the flow, is present. This can lead to an incomplete evaporation of the spray, if VS3 is opened at the start of the test. The second aspect to be considered is that the spraying system itself has its own transient. In fact, initially, the pipeline downstream the valve VS3 is filled with MDM vapor at the plenum pressure (in the range $4 - 10\,mbar$). When the valve VS3 is opened, the pipes are gradually filled with liquid MDM and the flow rate gradually goes from $0\,ml/min$ to the desired value. During this transient, the atomizing process is not stationary:
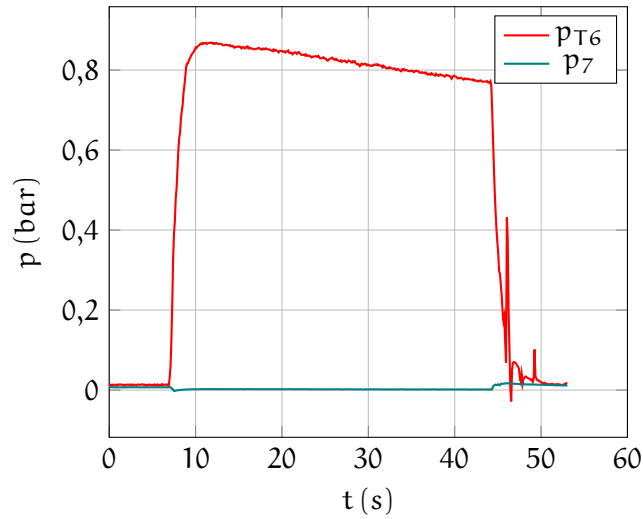
(a) *Nozzle total pressure p_{T6} and nozzle static outlet pressure p_7.*
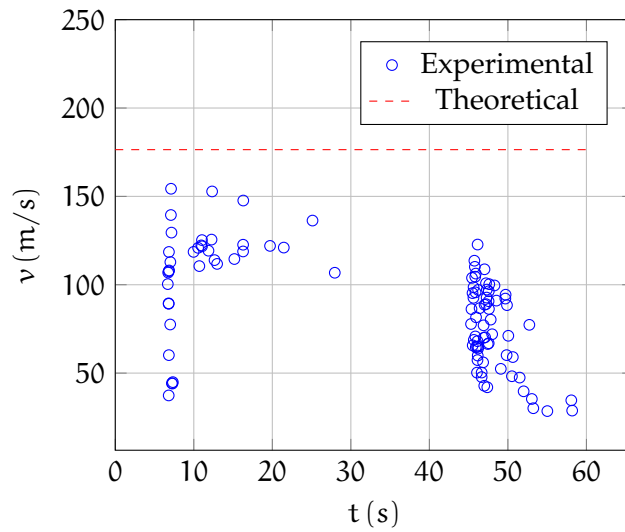
(b) *Velocity measurements.*

Figure 44: Pressure and velocity measurements for the Test C1a.

- initially, the flow rate is not atomized and the liquid is injected like a liquid jet, with a low aperture angle (see Figure 45a);

- in a second part of the transient, the liquid starts to be atomized, but the droplet size is large and the cone angle is small, thus some coalescence is possible (see Figure 45b, Figure 45c, Figure 45d and Figure 45e);

- in the last part of the transient, the liquid starts to atomize in small droplets and the cone becomes large (see Figure 45f).

The first two part of the transient result in a set of liquid (only partially evaporated) particles that are entrained in the flow and carried through the nozzle and at the measurement volume. Regarding the end of the test, the explanation is the same, with the V3 and MCV closing, but the transient has a longer duration.

In the first part of the test, measurements between $110\,\mathrm{m/s}$ and $160\,\mathrm{m/s}$ are obtained and the expected velocity, for these conditions, is about $180\,\mathrm{m/s}$, so these measurements are compatible with some seeding particles of big diameter remained in the atomizer piping after the previous test. Indeed, this test was carried out right after having cleaned the tank (the atomizing line has not been cleaned) from the powder resulted from the cited pump failure (for details see Section 6.5.3.3). This hypothesis is confirmed by the following tests (see Figure 46, Test C1b), that did not reported the aforementioned measurements.

In Figure 46 is present an amount of measurements around $0\,\mathrm{m/s}$. This is probably due to the fact that filters were very wide (from $0\,\mathrm{m/s}$ to $260\,\mathrm{m/s}$), combined with a possible small misplacement of the measurement volume. Indeed, if the measurement volume is partially on the rear plate surface or the inner glass surface, it can scatter light with an amplitude modulated with the Bragg cell frequency, thus resulting in a $0\,\mathrm{m/s}$ measurement. In the other tests, where narrower filters have been set or the measurement volume position has been changed, these $0\,\mathrm{m/s}$ measurements are no longer present.

6.5.3.2 Test C2

In Test C2, the tracker is TiO_2. The system detected particles only during transients.

The test C2 is analogous to the Test C1, but made with TiO_2, instead of Aerosil 200. These tests have been performed $22\,\mathrm{mm}$ downstream of the geometric throat, due to a further fouling of the optical window. The measurements made during a test with $M_{TiO2} = 0.8\%$ are reported in Figure 47. As in the previous tests, there is a great amount of measurements at the end of the test. The measurements at the start of the transient are not present. Currently, the actuation of the valve VS3 is manual, and in this test the opening has been delayed slightly, so it occurred when a great amount of vapor was already flowing, thus resulting in a complete evaporation of the droplets.
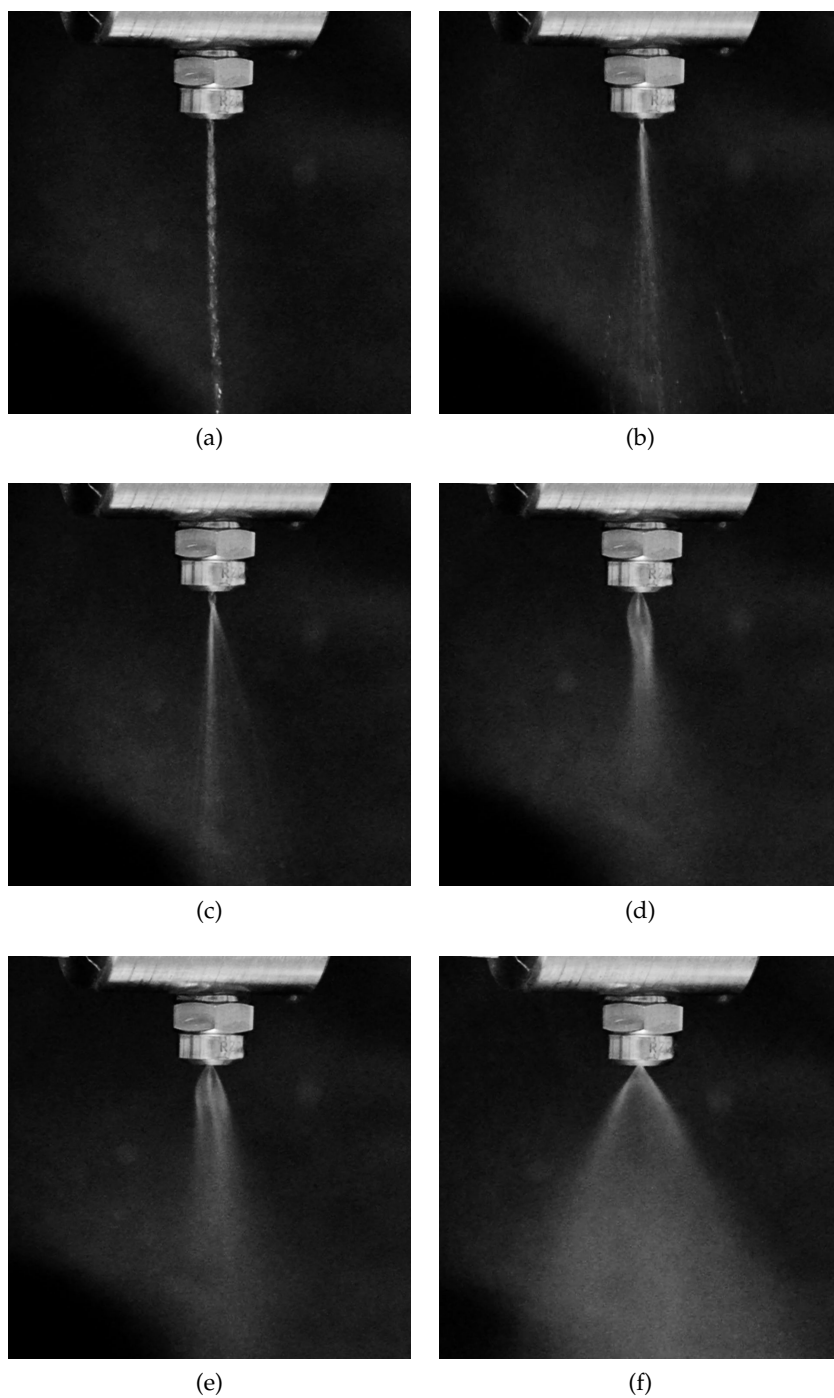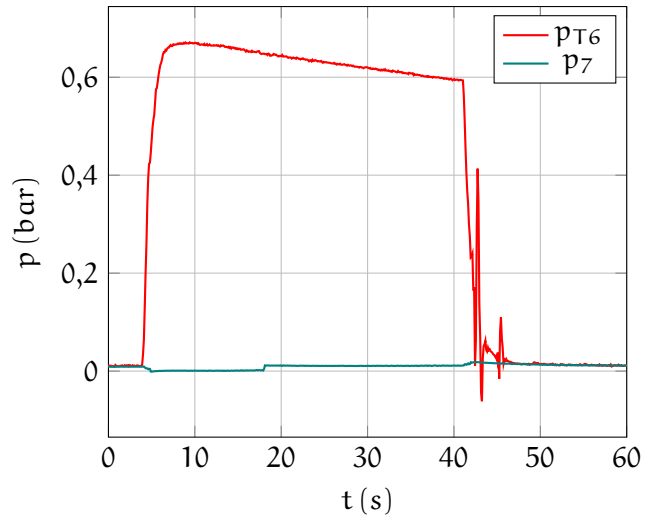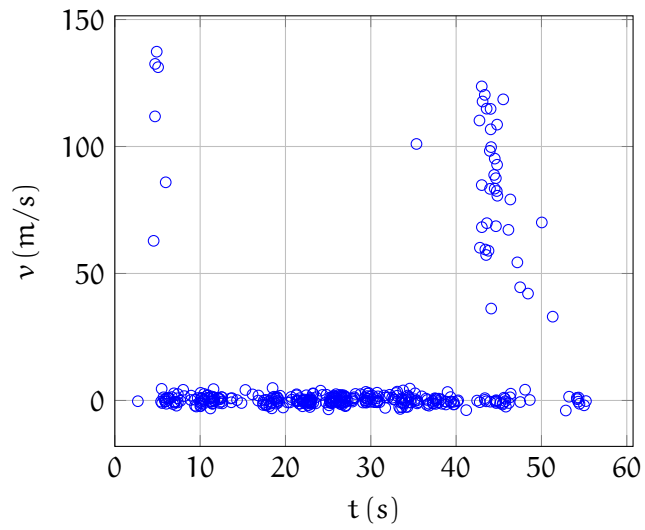
Figure 45: Sequence of pictures of the initial transient of the atomizer used in the seeding system.

(a) *Nozzle total pressure* p_{T6} *and nozzle static outlet pressure* p_7.

(b) *Velocity measurements.*

Figure 46: Pressure and velocity measurements for the Test C1b.
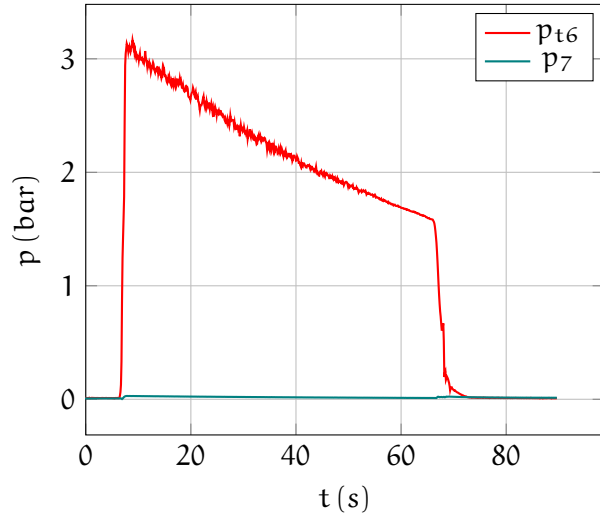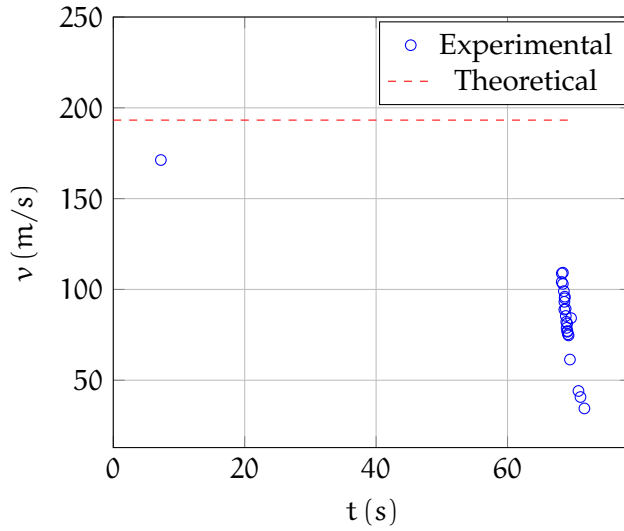
(a) *Nozzle total pressure* p_{t6} *and nozzle static outlet pressure* p_7.

(b) *Velocity measurements.*

Figure 47: Pressure and velocity measurements for the Test C2.

In Figure 47 there is only one measurement around 170 m/s. Since the expected velocity at the beginning of the test is 193.2 m/s, this measurement is compatible with a big particle with a high slip velocity.

6.5.3.3 *Test C3*

During the tests C1, a mixing pump failure occurred. The MDM contained in the seeding tank has been contaminated with an apparently metallic powder. In Figure 52 is reported a picture of the filtered powder and a comparison between pure MDM and the suspension resulting from the pump failure.

Two tests have been carried out by spraying the MDM containing the mentioned powder. The measurements made during these tests are reported in Figure 49 (Test C3a) and Figure 50 (Test C3b). The measurement volume was placed 15 mm downstream the nozzle throat. The expected velocity for these condition in this point are between 173.3 m/s and 176.5 m/s for the test C3a and between 174.6 m/s and 178.9 m/s for the test C3b. The Mach number in the measurement point has been obtained by an inviscid CFD simulation in condition similar to those of the tests. In general, MDM vapor is not an ideal gas, but in the considered conditions it has almost an ideal behavior (the reduced pressure is low) and it has been verified, comparing data from CFD simulations, that the Mach number, for a given position on the axis, depends only slightly from total conditions. At these conditions, therefore, the Mach number depends only on the area to critical area ratio and the specific heats ratio. Once the Mach number is obtained, it is possible to calculate the velocity corresponding to that Mach number for the desired total condition, for an isentropic expansion. The two velocity limits have been obtained from the lowest pressure–maximum temperature condition of the test and for highest pressure–minimum temperature of the test (the latter condition is less ideal than the previous, since it is closer to the saturation curve).

The obtained values are lower than the expected ones; this difference can reasonably be ascribed to the density and the particle dimension of the injected powder which are such that the slip factor is high, between $s = 0.17 - 0.18$ for Test C3a and between $s = 0.21 - 0.23$ for Test C3b. In Figure 51 is reported the velocity distribution for the measurements.

6.6 COMMENTS ON THE TEST RESULTS

Despite a few issues that have to be further investigated and solved, the results of the tests are encouraging: the seeding system works and performs all operations as expected. There are a few aspects that may be improved: the system is able to measure velocities, as seen

(a) *Pure MDM.*
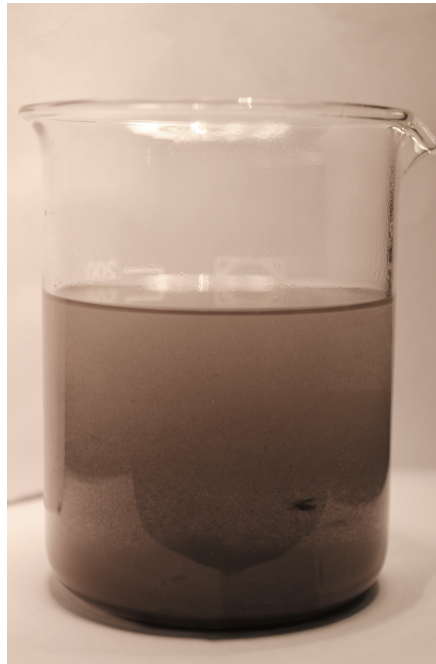
(b) *MDM–pump powder suspension.*

(c) *The powder obtained after filtering.*

Figure 48: Picture of pure MDM, of the suspension of MDM and the powder resulting from the pump failure and of the powder after filtering.
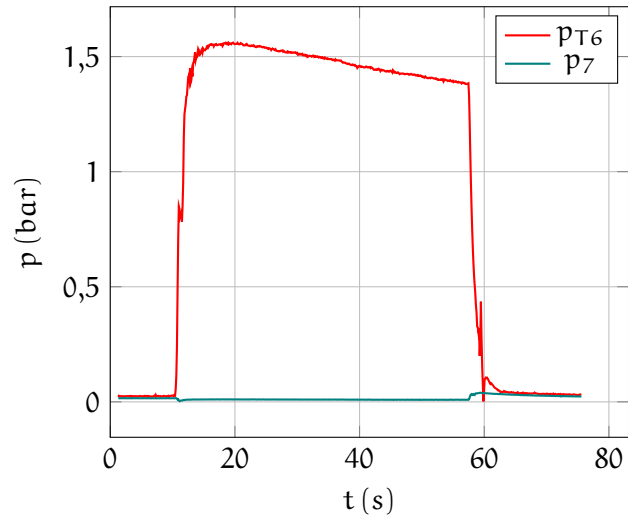
(a) *Nozzle total pressure p_{T6} and nozzle static outlet pressure p_7.*
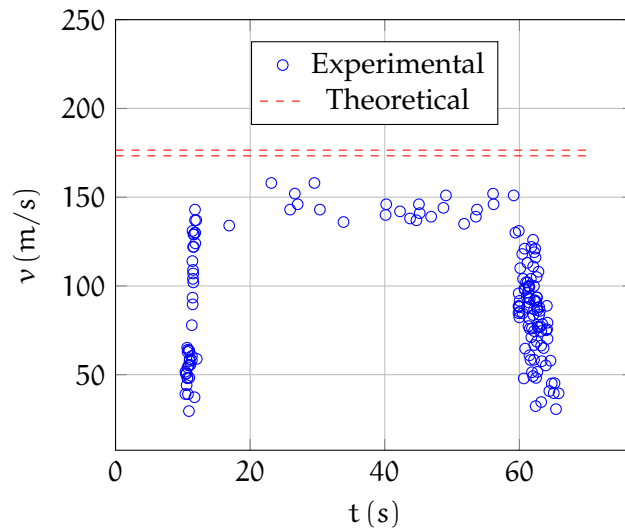
(b) *Velocity measurements.*

Figure 49: Pressure and velocity measurements for the Test C3a.
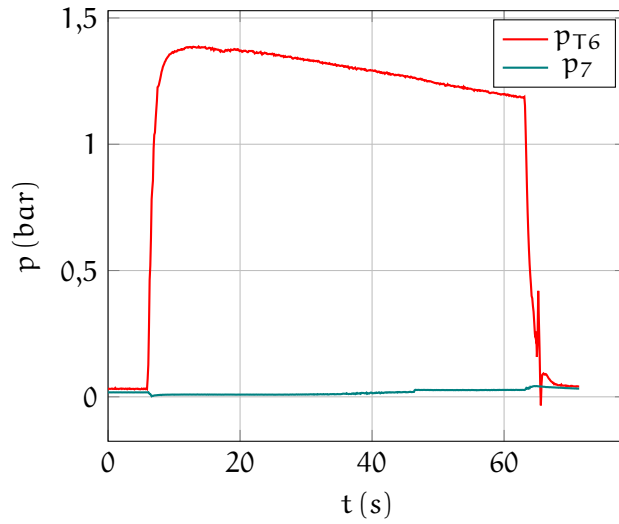
(a) *Nozzle total pressure p_{T6} and nozzle static outlet pressure p_7.*
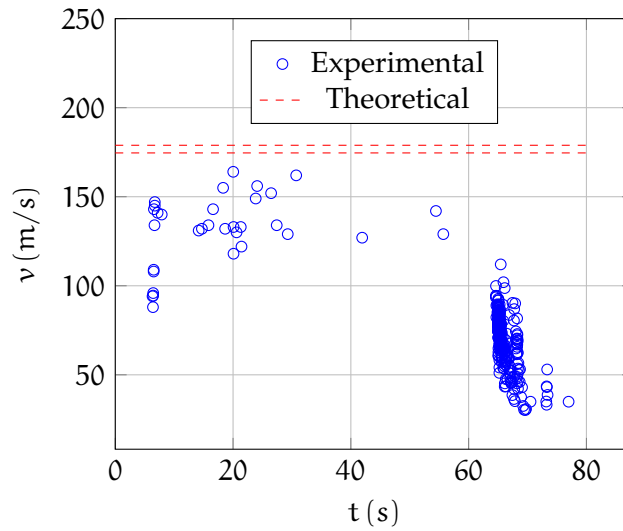
(b) *Velocity measurements.*

Figure 50: Pressure and velocity measurements for the Test C3b.
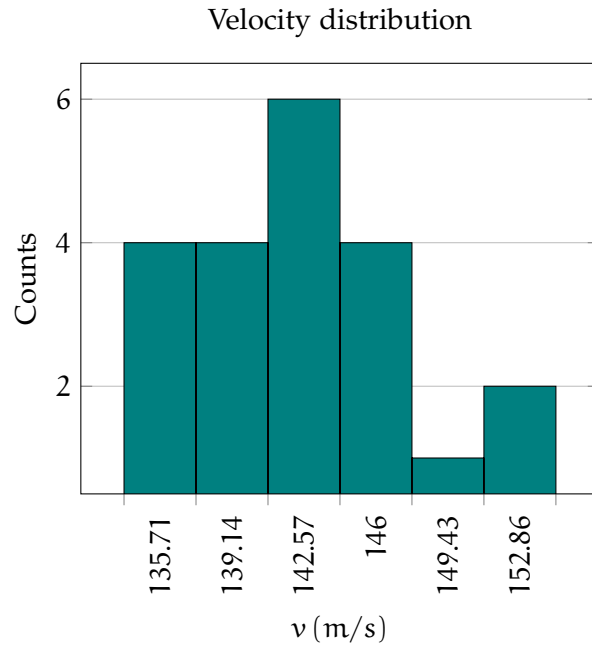
(a) *Velocity distribution for the test C3a.*

(b) *Velocity distribution for the test C3b.*

Figure 51: Velocity distributions for tests Test C3, without considering the measurements relative to the initial and final transient.

in Test C3, but this occurred only with a seeding that was not the one selected, thus with unknown characteristics. This (together with the fouling of the nozzle and optical window by the tracer particles) leads to the conclusion that a certain amount of seeding reaches correctly the test section. However, as seen in tests C1 and C2, the LDV sy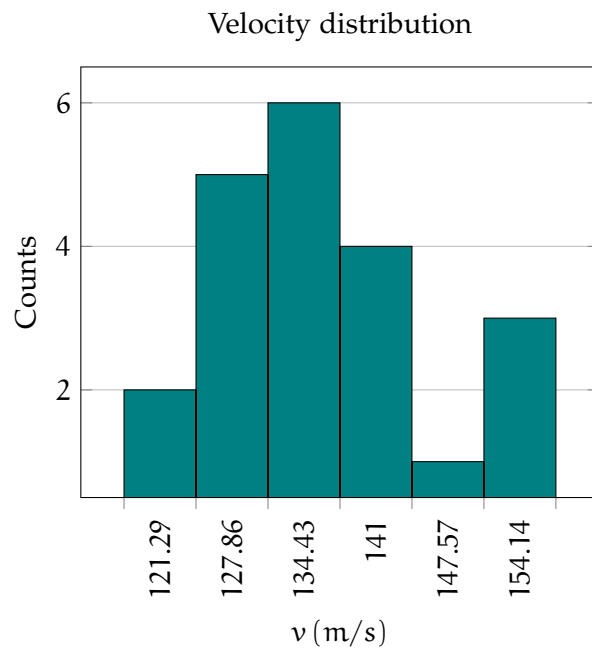stem did not observe either Aerosil or TiO_2 particles. Probably, this is due to a particle size too small to scatter a sufficient power to be detected by the system. Moreover, since the measurement volume is close to the rear plate, the received signal is noisy, and the signal from a particle is more difficult to observe. However, if the selection of the theoretically correct seeding particle is straightforward, finding a powder commercially available with the desired properties is tricky. Particle of the order of $150 - 250\,\mathrm{nm}$ or greater than $1.5 - 2\,\mathrm{nm}$ are common, but, as it has been shown in Section 5.2.1, for particle densities of the order of $2000 - 4000\,\mathrm{kg/m^3}$ particles with a diameter d_p smaller than $0.5\,\mathrm{\mu m}$ are needed. Another aspect related to the seeding powder is the material: solid seeding powder are frequently made of noble metals that are commonly used as chemical catalysts. In the laboratory, alumina (aluminum oxide - Al_2O_3) powder with a particle diameter $d_p \approx 500\,\mathrm{nm}$ is available. Tests with alumina will be carried out in the forthcoming future, but, after the test, the integrity of the fluid has to be assessed, since Al_2O_3 could catalyze decomposition reactions.

The second aspect that can influence the success and the data rate of LDV measurements is the type of atomizer. The tested nozzle is a hollow cone atomizer, with a cone angle of about 80° for MDM atomized in ambient air. With this configuration, it is possible that only a small fraction of the atomized droplets are entrained by the flow, while a great part impinges on the inner surface of the plenum, being the vast majority of the droplets confined on the surface of the cone. This leads to to a low data rate. There are three possible solutions to this issue:

- maintaining the actual atomizer and rotating it perpendicular to the flow;

- selecting an atomizer of the same series of the tested one, but with a narrower cone;

- selecting a full cone atomizer.

The rotation of the nozzle is the easiest one, and can possibly lead to a higher seeding flow rate in the axis of the flow. Regarding the selection of a narrower hollow cone atomizer, only the nozzle has to be replaced (the same manufacturer of the tested nozzle offers hollow cone atomizers with 30° cone angle for water). However, only data for nozzle working with air are available, and, based on the experience made with the atomizer used in this work suggests that

Some issues emerged from the tests: the atomizer, the seeding dimension, the cleaning of the optical window and the mixing pump must be improved. However, tests proved the complete evaporation of the spray.

with MDM the cone presents a wider angle with respect to water. Thus, the use of an hollow cone nozzle carries some uncertainties. Regarding the full cone nozzle, it works with high flow rates (the minimum flow rate is about $350\,\mathrm{ml/min}$) and much lower pressure differences Δp. The flow rate is not an issue, since the injected powder quantity depends also on the suspension concentration. However, the low pressure difference leads to the need of a second stage pressure regulator, to better control the seeding tank pressure.

The third aspect to be considered is the optical window fouling. It has been observed that, after the tests, the optical window was fouled by the seeding deposition, thus resulting in a lower light detected by the receiver (see Figure 52).

The fourth aspect to be considered is the mixing pump. As it has been mentioned in Section 5.7.2, the pump of the mixing system was a critical component, due to the low viscosity of the fluid. After some hours of functioning, the thermal protection switch on the pump motor intervened and the aforementioned powder was found in suspension in MDM (see Section 6.5.3.1). After this event, the pump was no longer able to realize the expected flow rate, thus mixing the suspension. Tests to assess the cause of this failure are under development. A solution to this problem may be to relax the flow rate constraint and adopt different pump types, such as small turbopumps. Obviously, the mixing nozzle has to be re-designed and a continuous by-pass has to be implemented. The pipe dimension has to be verified, in order to avoid an excessive fluid velocity and the cavitation possibility in the valves has to be verified. Also agitators can be further investigated (despite their higher cost).

Regardless these issues, it has been proven the correct evaporation of the spray (Test B) and that the designed system performs the task of seeding the flow (Tests C), even if the seeding powder showed some critical aspects.
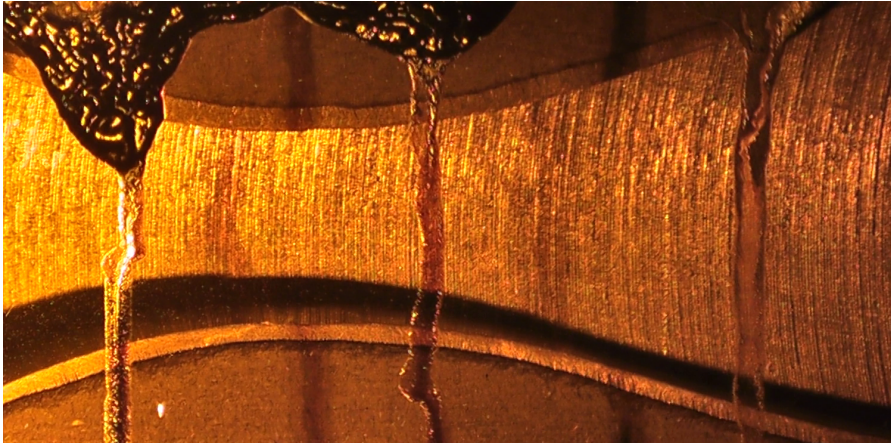
(a) *Clean optical window.*
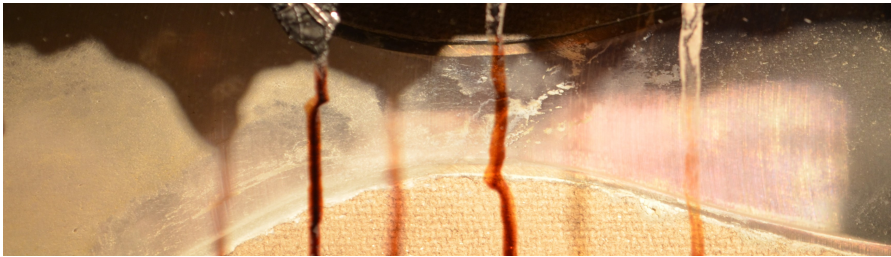
(b) *Full nozzle fouled by seeding particles.*

(c) *Particular of the throat fouled by seeding particles.*

Figure 52: Pictures of the clean optical window and the dirtied by the tracer one.

7

CONCLUSIONS AND FUTURE DEVELOPMENTS

7.1 CONCLUSIONS

A Laser Doppler Velocimetry seeding system has been designed to be applied for the measurement of velocity of an expanding flow in non-ideal conditions. Furthermore, the system has been constructed and its functioning has been investigated in its normal operation configuration, before running it on the TROVA. The seeding system has been tested during several TROVA tests, by means of LDV measurements.

The design procedure consisted of two main and interrelated parts:

- the selection of the suitable seeding particle;

- the design of a plant configuration able to introduce properly the tracker in the flow.

The type of tracker is strictly related to the conditions of the flow. Mainly due to the high temperature, liquid droplets cannot be used, thus solid particles have been selected. The seeding particle has to satisfy both dynamical and optical properties, to track adequately the flow and to be observed by the LDV system. From the dynamic point of view, the particle has to show a density and diameter that result in a low slip velocity between the particle and the flow. The purpose of velocity measurement in the TROVA is not to fully resolve the turbulence, so the particle has to properly follow the mean flow on the nozzle axis. Common solid seeding particle are metal oxide, with material density of the order of $1000 - 4500 \, \mathrm{kg/m^3}$. With these particle densities, the particle diameter of $0.5 \, \mathrm{\mu m}$ resulted in an acceptable tracking of the MDM vapor flow within the nozzle of the TROVA. On the optical side, the particle should exhibit a good refractive index and a dimension suitable to scatter a sufficient light power to permit the detection by the receiving optics of the LDV system. The selected particles, that satisfy the mentioned constraints, are titanium dioxide and Aerosil 200.

The design of the seeding plant requires as an input the total volume to be injected and the flow rates involved. These parameters have been calculated as a function of the LDV optics and flow requirements. Due to the high temperature and pressure involved and the necessity to avoid assisting fluids other than the working one, a system based on the atomization of a liquid suspension of MDM and the tracer particles has been designed. Different layouts have been examined, and the one featuring a pressurized and mixed seeding

tank has been selected. The designed system is composed by a seeding tank, a mixing system, a pressurizing device, a vacuum system, a level measurement and a atomizing line. The system is designed to be fully automated, even though the controlling software has not been implemented yet.

In the last part of the work, the system has been tested, verifying its behavior during the performance of all normal operations for which it was designed. Furthermore, it was tested during several TROVA tests leading to the conclusion that the evaporation is complete. Some measurements have been carried out, with the particles resulted from the failure of the mixing pump.

The present work is the initial part of an optimization process. The presented tests provided useful information about the functioning of the system and about the developments that have to be completed to perform a reliable LDV measurement.

Although some issues are present so far, this work proves the suitability of the designed system in performing LDV measurements in the TROVA, in non-ideal fluid flows and in all those high pressure and temperature applications, where the use of auxiliary fluids different from the working one is not feasible. Concerning the activity on the TROVA, the designed system represent the solid basis for future work, since only a few adjustment are required to solve emerged issues.

7.2   FUTURE DEVELOPMENTS

The work at the CREALab is continuing and further tests are going to be performed in the forthcoming future. The control software of the LDV seeding system has to be written. A seeding powder with greater diameter than those that have been currently used has to be tested. The rotation of the actual nozzle and the substitution of the atomizer with an hollow cone nozzle with a smaller cone angle or with a full cone nozzle has to be analyzed, in order to increase the data rate of the measurements. Furthermore, the reason of the pump failure has to be assessed, a new pump has to be selected and the functioning of the system with the new machine has to be verified.

Further tests at the TROVA are now under way, bringing to the first reliable LDV measurements in a MDM supersonic expansion flow field that will lead, along with independent pressure and temperature measurements and Schlieren visualizations, to the validation of the non-ideal thermo-fluid dynamic models of the flow.

Part IV

APPENDIX

THERMODYNAMIC PROPERTIES OF FLUIDS

This appendix is a short summary of the peculiarities associated with the thermodynamic properties of organic compounds, that are the object of study of the TROVA.

The particular behavior of organic compounds is due mainly to their molecular complexity and their high molecular mass. Thermodynamic properties can, in general, be seen as the sum of an ideal gas term and a term that accounts for the deviation from ideality.

Molecule degrees of freedom play a fundamental role in defining fluid properties. They are related to possible variation in position and configuration of a molecule. The maximum number of degrees of freedom is the sum of all possible vibrational, translational, rotational and electronic configurations. Each degree of freedom can be activated or not, depending on the thermodynamic state considered. Increasing the temperature may lead to the activation of degrees of freedom, if specific activation threshold are crossed. Therefore, the number of degrees of freedom can be used as an indication of the molecular complexity.

A.1 SPECIFIC HEATS

A formulation for the specific heats per unit mass is

$$c_v(T,v) = c_v^0(T) + \Delta c_v(T,v) = c_v^0(T) + \int_\infty^v \left(\frac{\partial^2 p}{\partial T^2}\right)_v dv, \quad \text{(63a)}$$

$$c_p(T,v) = c_v(T,v) - \frac{T\left(\frac{\partial p}{\partial T}\right)_v^2}{\left(\frac{\partial p}{\partial v}\right)_T}, \quad \text{(63b)}$$

where

c_v is the specific heat at constant volume;

c_p is the specific heat at constant pressure.

As previously mentioned, they are composed by an ideal gas term (for $p \to 0$ or $v \to \infty$) and a non-ideal behavior term. The real gas correction $\Delta c_v(T,v)$ is positive for pressures and temperatures of our interest, so specific heats of a real fluid are higher than an ideal one.

In the ideal gas limit, molar specific heats are related to the number of degrees of freedom, since they are different ways for the molecule to store energy. Each degree of freedom brings $R/2$ to c_v^0, so the

molecular complexity increases the ideal gas state specific heat. This contribution is so high that the real gas one is less important, unless we are in the vicinity of the critical point.

A.2 TEMPERATURE DROP ACROSS EXPANSIONS

The temperature drop across expansions experienced by organic compounds is lower than for a simpler fluid. This is due to their high specific heats (see Section A.1). For an isentropic expansion, by considering an ideal gas (we mentioned that the ideal gas term was predominant, except in the critical point region) we obtain

$$\left(\frac{T_1}{T_2}\right)^{\frac{c_{p,m}}{R_m}} = \frac{p_1}{p_2},\tag{64}$$

where $c_{p,m}$ and R_m are the molar specific heat at constant pressure and the molar ideal gas constant respectively. If the pressure ratio remains unaltered, we see that an increase in the specific heat leads to a decrease in the temperature ratio, thus in the temperature difference.

A.3 ENTHALPY OF VAPORIZATION

For a given reduced state point, the Clausius-Clapeyron equation gives the enthalpy of phase transition. In general, it could be written as

$$\Delta h_{ev}\left(T_r, v_r\right) = \frac{T_c}{M_m} f\left(T_r, v_r\right),\tag{65}$$

where

T_r is the reduced temperature T/T_c;

v_r is the reduced volume v/v_c;

$f\left(T_r, v_r\right)$ is a function of T_r and v_r.

In the approximation of the correspondent state principle, $f\left(T_r, v_r\right)$ is not function of the considered fluid, thus Δh_{ev} depends only on the T_c/M_m ratio. For fluid of the same class, the effect of the molecular mass is predominant, so heavier fluids tend to have a lower enthalpy of vaporization. In comparing fluids from different classes, this no longer holds, since the critical temperature can significantly change.

A.4 ENTHALPY DROP ACROSS EXPANSIONS

For a fixed expansion ratio and reduced state, the enthalpy drop across isentropic expansions (that can be either total-to-total or total-to-static) reduces significantly with the molecular mass and only slightly

increases with the molecular complexity. Also the critical temperature influences the enthalpy drop, but plays a secondary role since its restricted variability between different compounds.

A.5   SLOPE OF THE VAPOR SATURATION LINE

The slope of the vapor saturation line depends on the molecular complexity. In the reduced plane $T_r - s_r$ (with $T_r = T/T_c$ and $s_r = s/R$), for $T_r \leqslant 0.6$ (region in which the ideal gas model is a good approximation), the slope takes the form of

$$\left(\frac{dT_r}{ds_r}\right)_{vap} = \frac{2T_r^2}{(2+N)\,T_r - 2B},$$ (66)

where B is a constant that can be obtained from the following relation resulting from the correspondent state principle:

$$\frac{dp_{r,sat}}{p_{r,sat}} = B\frac{dT_{r,sat}}{T_{r,sat}^2}.$$ (67)

For fluid of a certain complexity, the denominator of Equation 66 is positive and the saturation curve slope is positive. For simple fluids the slope is negative, such as for water. T_r also plays a role: the considered denominator becomes negative for low reduced temperature values, that are, however, below the temperature of interest for power cycles.

A.6   FUNDAMENTAL DERIVATIVE OF GASDYNAMICS

The *fundamental derivative of gasdynamics* is defined as [26]

$$\Gamma = 1 - \frac{v}{c}\left(\frac{\partial c}{\partial v}\right)_s = 1 + \frac{\rho}{c}\left(\frac{\partial c}{\partial \rho}\right)_s = \frac{v^3}{2c^2}\left(\frac{\partial^2 p}{\partial v^2}\right)_s.$$ (68)

It is clear that values assumed by Γ depend on the curvature of isentropes in the $p - v$ plane. If $\left(\partial^2 p/\partial v^2\right)_s > 0$, $\Gamma > 0$ and the corresponding gasdynamic regime is called *classical*. This is the case of common gases such as ideal gases. On the other side, if $\Gamma < 0$, the gasdynamic regime is called *non-classical*. Many thermodynamic models predict a $\Gamma < 0$ region close to the saturation curve, in the vicinity of the critical point, for complex enough fluids. For an ideal gas, $\Gamma = (\gamma + 1)/2$, so $1 \leqslant \Gamma \leqslant 4/3$. Region with $\Gamma < 1$ or $\Gamma < 0$ appear for sufficiently complex fluid, with an increase in the dimension of this region with the molecular complexity. Therefore, the possible Γ value in the vapor region has been taken as an index for the classification of fluids:

$\Gamma \geqslant 1$ low molecular complexity fluids, LMC;

$0 \leqslant \Gamma < 1$ high molecular complexity fluids, HMC;

$\Gamma < 0$ Bethe, Zel'dovich and Thompson fluids, BZT.

The Γ value defines different gasdynamic behavior of fluids during the expansion. Concerning the Mach number M along an expansion, it could be demonstrated that

$$\left(\frac{\partial M}{\partial \rho} \right)_s = -\frac{1}{\rho M} \left[1 + (\Gamma - 1) M^2 \right]. \tag{69}$$

Equation 69 shows that three different cases are possible:

$\Gamma > 1$ the Mach number M increases monotonically along the expansion;

$0 \leqslant \Gamma < 1$ the Mach number M can decrease, but only in supersonic flows;

$\Gamma < 0$ the Mach number M can decrease, either in supersonic or subsonic flows, so the $M = 1$ limit can be crossed and more than one throat can exist.

Regarding the shape of the throat, it can be showed that

$$\left(\frac{\partial M}{\partial x} \right)^2 = \frac{\Gamma}{2A} \frac{d^2 A}{dx^2}, \tag{70}$$

thus, also in this case there is a different behavior depending on the Γ value:

$\Gamma > 0$ the throat is the connection of a converging region to a diverging one;

$\Gamma < 0$ the throat is the connection of a diverging region to a converging one.

In the throat, $dA/dx = 0$.

Concerning the shock wave formation, it depends on the dependency of the velocity of propagation of a wave v_w on the wave variation of amplitude dp:

$$dv_w = \frac{\Gamma}{\rho c} dp. \tag{71}$$

For

$\Gamma > 0$ a rarefaction $dp < 0$ flattens and spreads in an isentropic fan, due to the resulting decrease in wave velocity $dv_w < 0$ and a compression $dp > 0$ collapses leading to a compression shock;

$\Gamma < 0$ a rarefaction $dp < 0$ steepens and leads to a shock wave, due to the resulting increase in wave velocity $dw > 0$ and a compression $dp > 0$ flattens leading to a compression fan.

If interested in negative shock waves see [27].

B

THERMODYNAMIC MODELS

Specific thermodynamic models are required, in order to predict the behavior of non-ideal fluid flows. Organic fluid expantions in ORCs belong to this category of flows, since non negligible liquid compressibility or high vapor inter-molecular forces region are commonly crossed.

Thermodynamic models for a homogeneous fluid of constant composition are expressed through the functional form of the *fundamental relation*, in one of its forms

$$E = E\,(S, V) \qquad \textit{Energy form} \tag{72a}$$

$$S = S\,(E, V) \qquad \textit{Entropy form} \tag{72b}$$

$$H = H\,(E, V) \qquad \textit{Enthalpy form} \tag{72c}$$

$$A = A\,(E, S) \qquad \textit{Helmholtz energy form} \tag{72d}$$

$$G = G\,(H, S) \qquad \textit{Gibbs energy form} \tag{72e}$$

where

E is the internal energy;

S is the entropy;

V is the volume;

H is the enthalpy;

A is the Helmoltz energy;

G is the Gibbs energy.

Another way to give a thermodynamic model is through *equations of state* (EoS), that are relations between fundamental relation derivatves:

$$p = p\,(T, v) \qquad \textit{Thermal equation of state} \tag{73a}$$

$$e = e\,(T, v) \qquad \textit{Caloric equation of state} \tag{73b}$$

where

P is the pressure;

T is the temperature;

V is the specific volume per unit mass;

E is the specific internal energy per unit mass.

There are many different models, that provide different accuracies depending on the single case. Some of the most common are:

- ideal gas model;

- van der Waals model;

- multi-parameter equations of state (e. g. the Span Wagner model);

- cubic equations of state (e. g. the Redlich-Kwong and Peng-Robinson EoS).

B.1 THE SPAN-WAGNER MODEL

The Span-Wagner model is a multi-parameter equation of state (see [21], [22] and [23]), highly accurate for technical applications. This model is implemented in RefProp, the thermodynamic library used for property calculation in this work. A functional form of the reduced Helmoltz free energy α_r as a function of the critical temperature T_r and reduced density ρ_r is given:

$$\alpha_r = \frac{a}{RT} \tag{74a}$$

$$T_r = \frac{T}{T_c} \tag{74b}$$

$$\rho_r = \frac{\rho}{\rho_c} \tag{74c}$$

where T_c and ρ_c are the critical temperature and density. The reduced Helmoltz free energy is given from the sum of a dilute ideal gas term α_r^0 and a real gas term α_r^{res}:

$$\alpha_r = \alpha_r^0 \left(T_r, \rho_r\right) + \alpha_r^{res} \left(T_r, \rho_r\right) \tag{75}$$

The first term is obtainable by integration of a specific heat at constant pressure for the ideal gas. For the second term, are available expression in the case of non-polar and weakly polar fluids or for polar fluids.

This model is not calibrated on a single fluid, but can be used for each fluid for which the required coefficients are available.

BIBLIOGRAPHY

[1] MDM data. URL http://ttm.tugraz.at/edu/downloads/stoffdaten_mdm.pdf.

[2] H.E. Albrecht, M. Borys, N. Damaschke, and C. Tropea. *Laser Doppler and Phase Doppler Measurements Techniques*. Springer-Verlag Berlin Heidelberg, New York, 1st edition, 2003.

[3] *API Recommended Practice 520, Sizing, Selection, and Installation of Pressure-Relieving Devices in Refineries, Part I - Sizing and Selection*. API, seventh edition, January 2000.

[4] *API Recommended Practice 520, Sizing, Selection, and Installation of Pressure-Relieving Devices in Refineries, Part II - Installation*. API, fifth edition, August 2003.

[5] M. M. C. Carmine and R. C. D. Cheli. Studio di Correnti Comprimibili Non-ideali in Ugelli Convergenti-Divergenti Mediante Misure di Pressione e Visualizzazioni Schlieren. Master's thesis, Politecnico di Milano, 2013/2014.

[6] R. Clift and W.H. Gauvin. Motion of Entrained Particles in Gas Streams. *The Canadian Journal of Chemical Engineering*, 49:439–448, August 1971.

[7] P. Colonna, E. Casati, C. Trapp, T. Mathijssen, J. Larjola, T. Turunen-Saaresti, and A. Uusitalo. Organic Rankine Cycle Power Systems: From the Concept to Current Technology, Applications, and an Outlook to the Future. *Journal of Engineering for Gas Turbines and Power*, 137, October 2015.

[8] *Crosby Pressure Relief Valve Engineering Handbook*. Crosby Valve Inc., May 1997.

[9] R. C. Doane. Designing for Pressure Safety Valves in Supercritical Service. *Hydrocarbon Processing*, pages 63–67, January 2010.

[10] A. Guardone, A. Spinelli, and V. Dossena. Influence of Molecular Complexity on Nozzle Design for an Organic Vapor Wind Tunnel. *Journal of Engineering for Gas Turbines and Power*, 135, April 2013.

[11] S. P. Lin and D. J. Kang. Atomization of a Liquid Jet. *Physics of Fluids*, 30(7):2000–2006, July 1987.

[12] Y. Liu and P.H. Daum. Relationship of Refractive Index to Mass Density and Self-consistency of Mixing Rules for Multicomponent Mixtures Like Ambient Aerosols. *Journal of Aerosol Science*, (39):974–986, 2008.

[13] R. Mei. Velocity Fidelity of Flow Tracer Particles. *Experiments in fluids*, 22:1–13, 1996.

[14] A. Melling. Tracer Particles and Seeding for Particle Image Velocimetry. *Measurement Science and Technology*, 8:1406–1416, 1997.

[15] R. Ouderkirk. Rigorously Size Relief Valves for Supercritical Fluids. *Cep*, August 2002.

[16] E. L. Paul, V. A. Atiemo-Obeng, and S. M. Kresta. *Handbook of Industrial Mixing, Science and Practice*. Wiley and sons, 2004.

[17] R. D. Reitz and F. V. Bracco. Mechanism of Atomization of a Liquid Jet. *Physics of Fluids*, 25(10):1730–1742, October 1982.

[18] A. Schroeder and C. E. Willert. Selected Applications of Planar Imaging Velocimetry in Combustion Test Facilities. In *Particle Image Velocimetry, Topics in Applied Physics 112*, pages 283–309. Springer-Verlag Berlin Heidelberg, 2008.

[19] A. Schuster, S. Karellas, E. Kakaras, and H. Spliethoff. Energetic and Economic Investigation of Organic Rankine Cycle Applications. *Applied Thermal Engineering*, 29(8-9):1809–1817, 2009.

[20] M. Spampatti. Start-up di un Banco Prova per Fluidi Organici. Master's thesis, Politecnico di Milano, 2011/2012.

[21] R. Span and W. Wagner. Equations of State for Technical Applications. I. Simultaneously Optimized Functional Forms for Nonpolar and Polar Fluids. *International Journal of Thermophysics*, 24 (1):1–39, January 2003.

[22] R. Span and W. Wagner. Equations of State for Technical Applications. II. Results for Nonpolar Fluids. *International Journal of Thermophysics*, 24(1):41–109, January 2003.

[23] R. Span and W. Wagner. Equations of State for Technical Applications. III. Results for Polar Fluids. *International Journal of Thermophysics*, 24(1):111–162, January 2003.

[24] A. Spinelli. *Design and Construction of a Test Rig for Organic Vapours*. PhD thesis, Politecnico di Milano, December 2010.

[25] A. Spinelli, M. Pini, V. Dossena, P. Gaetani, and F. Casella. Design, Simulation, and Construction of a Test Rig for Organic Vapors. *Journal of Engineering for Gas Turbines and Power*, 135, April 2013.

[26] P. A. Thompson. A Fundamental Derivative in Gasdynamics. *The physics of fluids*, 14(9):1843–1849, September 1971.

[27] P. A. Thompson and K.C. Lambrakis. Negative Shock Waves. *Journal of fluid mechanics*, 60, part 1:187–208, 1973.

[28] G. Tomasoni. Prove Preliminari su un Banco Prova per Fluidi Organici. Master's thesis, Politecnico di Milano, 2012/2013.

[29] C. Tropea, A. L. Yarin, and J. F. Foss. *Springer Handbook of Experimental Fluid Mechanics*. Springer-Verlag Berlin Heidelberg, 2007.

[30] TSI. Solid Seed Particle Generator Model 9309, Application Note 9309-001 (US).

[31] S. R. Turns. *An Introduction to Combustion, Concept and Applications*. McGraw-Hill, second edition, 2000.

[32] K. L. Wasewar. A Design of Jet Mixed Tank. *Chemical and Biochemical Engineering Quarterly*, 20(1):31–46, 2006.

[33] R. W. Whitesides. *Selection and Sizing of Pressure Relief Valves*. PDH, 2012.